

2007

Multifunctionalized mesoporous silica nanoparticles for selective catalysis

Hung-Ting Chen
Iowa State University

Follow this and additional works at: <https://lib.dr.iastate.edu/rtd>

 Part of the [Organic Chemistry Commons](#)

Recommended Citation

Chen, Hung-Ting, "Multifunctionalized mesoporous silica nanoparticles for selective catalysis" (2007). *Retrospective Theses and Dissertations*. 15523.
<https://lib.dr.iastate.edu/rtd/15523>

This Dissertation is brought to you for free and open access by the Iowa State University Capstones, Theses and Dissertations at Iowa State University Digital Repository. It has been accepted for inclusion in Retrospective Theses and Dissertations by an authorized administrator of Iowa State University Digital Repository. For more information, please contact digirep@iastate.edu.

Multifunctionalized mesoporous silica nanoparticles for selective catalysis

by

Hung-Ting Chen

A dissertation submitted to the graduate faculty
in partial fulfillment of the requirements for the degree of

DOCTOR OF PHILOSOPHY

Major: Chemistry

Program of Study Committee:
Victor S.-Y. Lin, Major Professor
Robert J. Angelici
William S. Jenks
Aaron D. Sadow
Malika Jeffries-EL

Iowa State University

Ames, Iowa

2007

Copyright © Hung-Ting Chen, 2007. All rights reserved.

UMI Number: 3259465

UMI[®]

UMI Microform 3259465

Copyright 2007 by ProQuest Information and Learning Company.
All rights reserved. This microform edition is protected against
unauthorized copying under Title 17, United States Code.

ProQuest Information and Learning Company
300 North Zeeb Road
P.O. Box 1346
Ann Arbor, MI 48106-1346

TABLE OF CONTENTS

ACKNOWLEDGMENTS	iv
ABSTRACT	v
CHAPTER 1. GENERAL INTRODUCTION	1
Dissertation Organization	2
Introduction	2
Conventional Functionalization Method	7
Recent Development of Functionalized Mesoporous Silica Material	9
References	16
CHAPTER 2. DIALKYLAMINOPYRIDINE-FUNCTIONALIZED MESOPOROUS SILICA NANOSPHERE AS AN EFFICIENT AND HIGHLY STABLE HETEROGENEOUS NUCLEOPHILIC CATALYST	21
Abstract	21
Introduction	21
Experimental Section	23
Result and Discussion	26
Conclusion	38
Acknowledgements	39
References	39
CHAPTER 3. ENHANCING CATALYTIC ACTIVITY BY SURFACE FUNCTIONAL GROUP ACTIVATION THROUGH HYDROGEN BOND – A NEW CONCEPT TO DEVELOP HETEROGENEOUS UREA OR THIOUREA FUNCTIONALIZED MESOPOROUS SILICA NANOPARTICLE CATALYSTS APPLIED FOR DIELS-ALDER REACTION	42
Abstract	42
Introduction	43
Result and Discussion	44
Conclusion	50
References	50
Appendix	53
CHAPTER 4. FINE-TUNING REACTIVITY OF COOPERATIVE GENERAL ACID AND BASE BIFUNCTIONALIZED MESOPOROUS SILICA NANOPARTICLE CATALYSTS	64
Abstract	64
Introduction	65
Result and Discussion	65
Conclusion	70

References	70
Appendix	72
CHAPTER 5. SYNTHESIS AND CHARACTERIZATION OF CONJUGATED POLY(<i>p</i>-PHENYLENE ETHYNYLENE)- ENCAPSULATED MESOPOROUS SILICA NANOCOMPOSITE MATERIALS (PPE-MSN)	75
Abstract	75
Introduction	76
Experimental Section	77
Results and Discussion	79
Conclusion	88
References	88
Appendix	91
CHAPTER 6. TEMPLATE REMOVAL AND THERMAL STABILITY OF ORGANICALLY FUNCTIONALIZED MESOPOROUS SILICA NANOPARTICLES	100
Abstract	100
Introduction	101
Experimental Section	103
Results and Discussion	108
Conclusion	123
Acknowledgements	123
References	124
Appendix	128
CHAPTER 7. GENERAL CONCLUSION	133

ACKNOWLEDGMENTS

First and foremost, I would like to thank my major advisor, Professor Victor S.-Y. Lin, for all his guideline and help in my entire PhD study in Iowa State University. Without his assistance and scientific discussion, I could not finish those projects and have current achievement. From him, I have been learned more than just chemistry. His enthusiasm of science, broadness of knowledge inspires me and drives me to success.

I also would like to thank all my past and current POS committee members, Professor Angelici, Professor Jenks, Professor Sadow, Professor Jefferies-EL, and Professor Larock for their guidance and suggestion.

Also I would like to thank our past and current group members, especially Dr. Seong Huh, Dr, Brian Trewyn, Dr. Daniela Radu, and Dr. Jennifer Nieweg. They made Ames a joyful place for learning and working.

I would like to thank Professor Marek Pruski and his group members, Dr. Jerzy W. Wiench and Dr. Rajeev Kumar. They help me to learn a lot of knowledge in the solid state NMR study.

I also would like to express thank to my family and friends both in Taiwan and in USA. For my entire PhD study in Ames, they delighted my life and supported me with their friendship. I will not forget you all.

ABSTRACT

The research presented and discussed within this dissertation involves the development of multifunctional mesoporous silica nanoparticles (MSN), and an investigation of performance of those MSN materials for heterogeneous catalysis.

A heterogeneous Lewis base MSN catalyst with an immobilized 4-dimethylaminopyridine functionality (DMAP-MSN) was synthesized, and have been demonstrated the catalytic activities of several nucleophilic reactions, such as acylation, silylation, and Baylis-Hillman reactions, and recyclable at least up to ten times. An unprecedented selectivity of Baylis-Hillman catalyzed by DMAP-MSN has also been observed, which could be attributed to size-discriminating effect induced by the 3-D cavity of regular mesoporous structure.

To take advantage of the double hydrogen bonding ability of urea and thiourea functionalities, I have synthesized a series of organically functionalized Lewis acid MSN catalysts with several urea or thioiurea functional groups. These heterogonous Lewis acid MSN materials have been demonstrated a capability to be serve as highly efficient catalysts for carbonyl activation of dienophiles in Diels-Alder reaction. I have discovered that the reactivity of the MSN catalysts is higher than those of the homogeneous analogs.

Multifunctionalization of mesoporous silica materials could be achieved with precise control the composition of each functionality as well as the particle morphologies. A variety of bifunctionalized MSN catalysts with one catalytic functional group, and another gatekeeper group to regulate diffusion of reactants. Fine-tuning local chemical mesoporous environment by different gatekeeper groups enabled to control the diffusion of substrates by hydrophilic/hydrophobic interactions, giving rise a selectivity in a competitive Henry reaction. The same strategy was also applied to yield several bifunctionalized MSN catalysts, comprised

of acid and base functionalities inside the mesopores. These acid and base bifunctional MSNs exhibited a cooperative behavior by activation of nucleophile and electrophile.

A palladium (II) complex was also successfully immobilized on the mesoporous silica surface by a radical coupling reaction to yield the Pd(II) functionalized MSN(Pd-MSN) catalyst. The well-aligned mesoporous channels of Pd-MSN material allowed the encapsulation of conducting poly(*p*-phenylene ethynylene) (PPE) polymer by the Sonogashira coupling reaction. The resulting PPE-MSN nanocomposite exhibited interesting photophysical and electronic properties, which could lead to further developments of new optical and electronic nanodevices.

CHAPTER 1. GENERAL INTRODUCTION

Dissertation Organization

This dissertation begins with a general introduction on the synthesis and characterization of surface-functionalized mesoporous silica materials. The recent progress and current challenge in utilizing this kind of organic and inorganic hybrid materials for catalysis applications is outlined. Our efforts in developing this class of heterogeneous catalysts are described in the following chapters of this thesis. Specifically, Chapter 2 describes the synthesis of a 4-dimethylaminopyridine functionalized mesoporous silica nanoparticle (DMAP-MSN) material as a heterogeneous Lewis base catalyst for various nucleophilic reactions, such as Baylis-Hillman reaction, acylation, and silylation reactions.¹ Chapter 3 entails a new concept for catalyst design. We have demonstrated that the catalytic performance of a urea or thiourea functionalized MSN material could be significantly improved for a series of Diels-Alder reactions by taking advantage of the hydrogen bonding between the silicate and the pore-anchored organic groups of these functionalized mesoporous silicas. Chapter 4 highlights our recent success in developing a bifunctional MSN-based cooperative catalytic system, which is capable of activating both nucleophile and electrophile in Michael addition reaction by various bifunctional MSNs with both Lewis acid and base functionalities. Chapter 5 outlines a synthetic method of incorporating a transition metal palladium (II) complex into the pore surface as a structure-directing catalytic system for the fabrication of a light-harvesting composite material with an arrays of π -conjugated conducting polymers encapsulated inside the parallel channels of MSNs. Chapter 6 narrates

a new pyrolysis method for selective removal of pore-embedded surfactant while preserving the integrity of the covalently immobilized organic functional groups on the mesoporous silica framework. This method could serve as an economical yet environmentally benign way for template removal on an industrial scale.² The last chapter gives a conclusion and outlines several future research directions.

Introduction

Design and synthesis of materials with well-defined particle size, morphology, and ordered mesoporosity (2 to 10 nm in pore diameter) is a burgeoning area of current research in materials chemistry. These materials have two different surfaces, the *interior pore surface* and the *exterior particle surface*, which offer many advantages over solid particle materials. The mesoporous structure provides a size and functional group selective microenvironment that allows encapsulation of various molecular moieties, and shelters these molecules from exposure to the external environment. The unique structural features of these mesoporous materials are important prerequisites for diverse applications, such as catalysis, chromatographic supports, controlled release of drugs and/or agrochemicals, development of medical implants, miniaturization of electronic devices, sensor design, and formation of semiconductor nanostructures.³⁻¹⁷ To realize these applications, the desired mesoporous material should also have the following features:

1. *Chemically, thermally, and mechanically stable structure.*
2. *Ordered particle and pore morphology.*
3. *Large surface area and tunable pore size.*

4. *The ability of selective functionalization of the interior and exterior surfaces.*

A major breakthrough in fabrication of mesoporous material was the development at Mobil corporation of the MCM family of mesostructured silicas by utilizing surfactants as structure-directing templates to generate a range of MCM-type mesoporous silica structures with tunable pore size and pore morphology, such as MCM-41 and MCM-48 silicas, consisting of hexagonal channels and cubic pores, respectively.^{18,19} Over the past decade, several other mesoporous silica materials with ordered porous structures, such as SBA-^{20,21} MSU-^{22,23} and FSM-type²⁴ of mesoporous silicas, have also been developed. As depicted in Figure 1, the typical synthesis of these structurally well-defined mesoporous silicas is based on a surfactant micelle templating approach. In an acidic or basic aqueous solution, organic surfactants, such as Pluronic 123 triblock copolymer^{20,21} and cetyltrimethylammonium bromide (CTAB),^{18,19} first form self-assembled micelles. These micelles serve as a structure-directing template that can interact with oligomeric silicate anions via hydrogen bonding or electrostatic interaction during the condensation reaction of tetraethoxysilane (TEOS). By either calcination or acid extraction, the organic surfactants are removed, leaving an inorganic mesoporous silica framework. Depending on the specific synthetic condition, a disordered, hexagonal, or cubic pore structure of mesoporous silica can be obtained.

The mechanism of mesostructure formation was first postulated by Mobil researchers based on the similarity between liquid crystalline surfactant assemblies (lyotropic phase) and the MCM family.^{18,19} This “liquid crystal templating (LCT) mechanism” postulates that cationic surfactants tend to self-assemble into hexagonal lyotropic liquid crystal phase in solution, even without the presence of silicate. Later on, the inorganic silicate precursor is

filled in the space between each pre-assembled micellar rod through electrostatic interactions, then further condensed and solidified to form inorganic-organic composite structures.

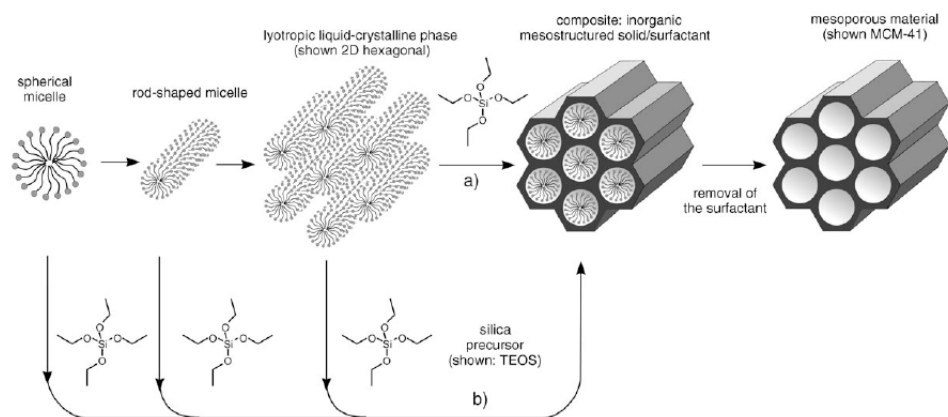


Figure 1. Formation of Mesoporous Silica Materials by structuring directing agents: (a) true liquid crystal template mechanism, (b) cooperative liquid crystal template.

Although the truly LCT synthetic condition involved large amounts of surfactants, it has been applied for material preparation by Attard et al.,²⁵ where in most cases, the surfactant concentration used was far below the critical micelle concentration (CMC) required for hexagonal LC formation. Further spectroscopic studies conducted simultaneously by the Davis,²⁶ Steel,²⁷ and Stucky groups²⁸⁻³¹ concluded that this hexagonal phase transformed from the micelle solution of CTAB is indeed triggered by the assistance of oligomeric polydentate silicate anion, not pre-assembled in the solution. The multi-charged silicate anions are preferentially bonded with ammonium head groups by ion exchanging with surfactant halide counterions, inducing a hexagonal silicate coated LC phase in the very low surfactant concentration. Also, the interaction between head groups and silicate oligomer is so strong that an alkyltrimethylammonium surfactant solution such as CTAB could drive the equilibrium of a silicate solution to form oligomeric silicate anions.^{30,31} The resulting “silicatropic liquid crystal” assembly could either form a lamellar or hexagonal

structure, depending on the reaction condition. The phase transition from lamellar to hexagonal phase was also observed in the X-ray diffraction (XRD) studies by Monnier et al.²⁸ and Stucky et al.²⁹ This phase transformation was rationalized by the “charge density matching” theory. As the reaction progresses, the charge density of the silicate assembly is reduced due to further condensation, which led to the silica frameworks curving in order to maintain the charge density balance with cationic surfactants.

A fundamental key point of this self-assembling templating synthetic strategy is regarding an attractive interaction between the structure directing agent (surfactant) *S* and inorganic precursor *I*, to avoid phase separation taking place. The specific interaction could be classified into two major categories, such as electrostatic interaction and hydrogen bonding, according to the suggestion of Huo et al.,^{32,33} as shown in Figure 2.

(1) *Electrostatic interaction:* Under basic conditions with cationic quaternary ammonium surfactants, the synthetic pathway is denoted as S^+I^- , representing an electrostatic interaction of positively charged surfactant head groups and negatively charged silicate anions, while a reversed electrostatic interaction (SI^+) is principally attainable for mesoporous silica material preparation. Tasumi and co-workers adapted this synthetic approach (SI^+) by using an anionic surfactant, sodium dodecyl sulfate (SDS), with a co-structural directing agent, aminopropyltrimethoxysilane (APTMS), and tetraethoxysilane (TEOS) to form a periodic ordered anionic-surfactant-templated mesoporous silica (AMS).³⁴⁻³⁶ Tasumi further applied this strategy for the fabrication of helical chiral mesoporous silica nanorods by introducing chiral amino acid segments into the anionic surfactant structure.^{37,38} The mesoporous silica preparation can also take place under the acidic conditions below the isoelectric point of silanol, $pH = 2$. In such case, the silicate

species are presented as protonated forms, resulting in positive charge. For this cationic silicate species, it is possible to work with an anionic surfactant via the S^+I^- pathway; however, a negatively charged mediator ion should be added to bridge with the quaternary ammonium surfactant (S^+XI^- pathway).

(2) *Hydrogen bonding interaction:* The attracted interaction could be also mediated through hydrogen bonds, whereby the material is synthesized in neutral conditions with the presence of a non-ionic surfactant (S^0 for a long-chained

amine or N^0 for a polyethylene oxide).²³ Due to the absence of strong interaction, critical for controlling the packing of the micellar rod, the materials prepared by this route usually lack long-range ordering of pores and have high amounts of interparticle mesoporosity. Although the materials prepared from the neutral pathway are less ordered than ones prepared through an ionic route, the materials show much thicker walls, giving rise to higher thermal stability,

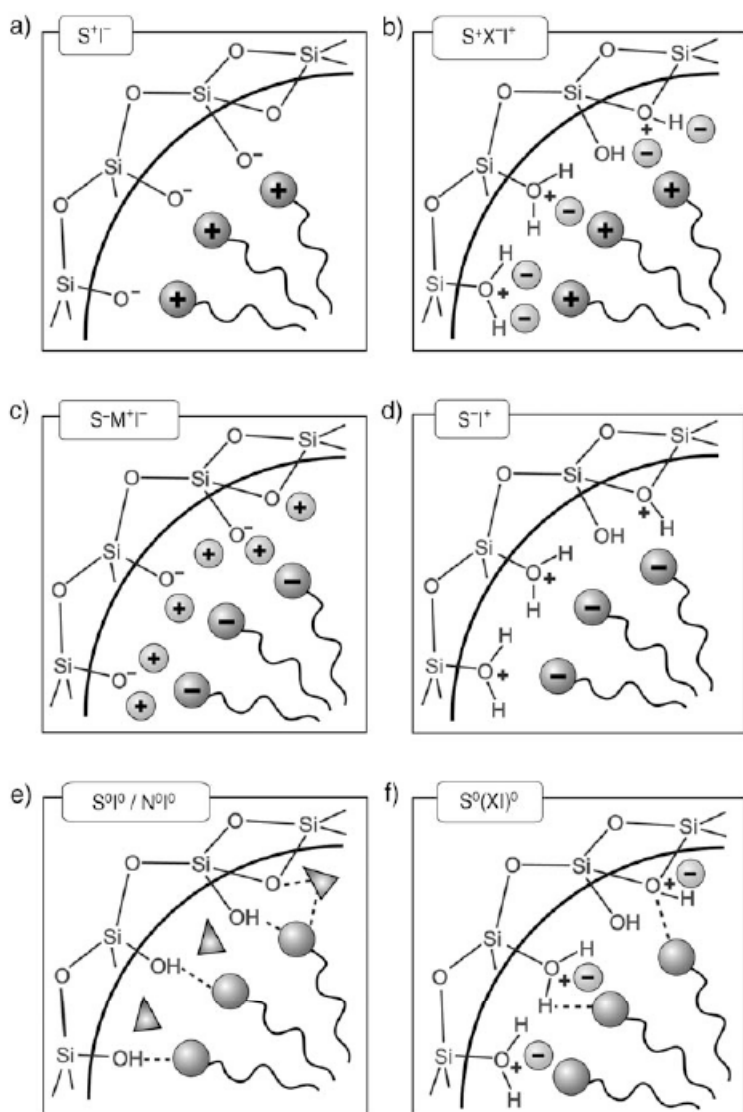


Figure 2. Interaction between inorganic species and the surfactants through electrostatic (S^+I^- , S^+XI^- , $S^-M^+I^-$, S^+I^+) or hydrogen bonds (S^0I^0/N^0I^0 , $S^0(XI)^0$)

and surfactant removal can also be done in the neutral extraction without the assistance of acid.

Conventional Functionalization Method

To utilize these mesoporous silica materials for the aforementioned applications, it is important to develop methods for controlling the degree of organic functionalization, so that the physical and chemical properties of the mesoporous silicas can be fine-tuned. Generally, organic functional groups can be immobilized onto the silica surface through covalent or noncovalent interactions between the organic moiety and the surface silanol group. For most applications, functionalization through covalent bonding is preferred, in order to circumvent undesired leaching problems.

Among various surface functionalization methods, the post-synthesis grafting method is the most popular approach for covalently incorporating organic functionalities into mesoporous silica materials. As shown in Figure 3, this method is based on a condensation reaction between a given organosilane, such as $\text{RSi}(\text{OR}')_3$, chlorosilanes RSiCl_3 or silazanes $\text{HN}(\text{SiR}_3)_2$, and the surface free silanol ($\equiv\text{Si-OH}$) and geminal silanol ($=\text{Si}(\text{OH})_2$) groups of the surfactant-removed mesoporous silica in dry nonpolar solvent, such as toluene and benzene. This functionalization method is advantageous in that the mesostructure of the starting silica phase is usually preserved after reaction. Even though a wide variety of organic functionalities have been introduced to the mesoporous silica surface via this straightforward approach, it has been studied that most materials functionalized via the grafting method contain an inhomogeneous surface coverage of organic functional groups.³⁹

This result has been attributed to the diffusion dependent mass transport issue associated with

these three-dimensional mesoporous materials. Given that the silanols located on the external surface and the pore opening are kinetically more accessible than those of the interior pore surface, most organic functional groups introduced by the grafting method have been shown to be located on the external surface and/or congregated at the mesopore opening. In extreme cases, the mesopores of grafted silica materials can be completely blocked, indicated by low measured surface areas of functionalized samples.

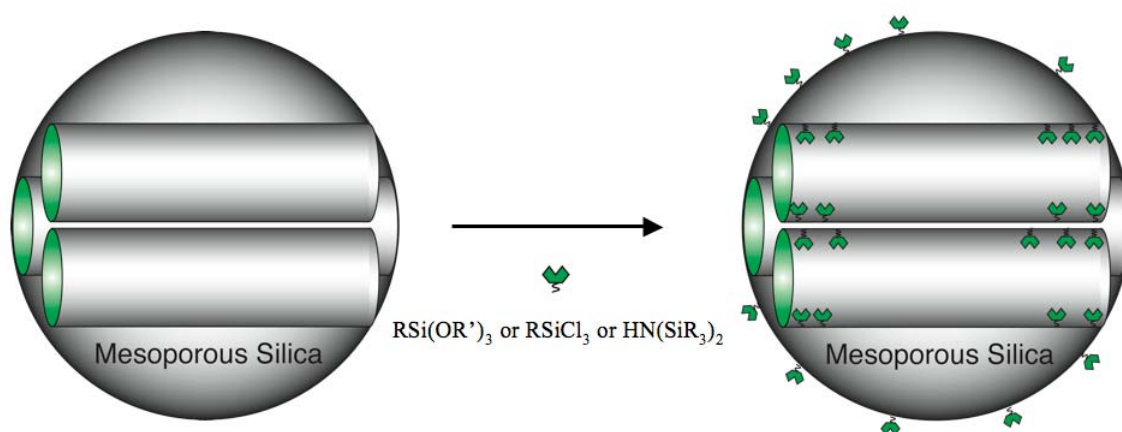


Figure 3. Schematic representation of functionalization of mesoporous silicas by the post synthesis grafting method.

Another common approach for preparing organically functionalized mesoporous silica materials is called the co-condensation method, which is a direct synthesis method where a given organoalkoxysilane is introduced to the aqueous solution of CTAB and TEOS during the condensation reaction (Figure 4). In order to efficiently incorporate organic functional groups to the mesoporous silica surface, the organosilane precursors need to compete with silicate anions to interact favorably with the surfactant micelles, by either electrostatic or other non-covalent interactions during the acid- or base-catalyzed condensation of silicate. Therefore, the choice of the organosilane precursors for the co-

condensation reaction is limited to those with organic functional groups that would be soluble in water and could tolerate the extreme pH conditions that are required for the synthesis of mesoporous silicas, and the subsequent removal of surfactants. Furthermore, the amount of functional groups introduced by the co-condensation method often cannot exceed 25% surface coverage without destroying the structural integrity and the long-range periodicity of the synthesized materials.¹⁵ Despite these limitations, it has been studied that the spatial distribution of the pore surface-immobilized organic groups in the mesoporous silica materials functionalized by the co-condensation method are more homogeneous than those of the post synthesis grafting method, as recently reviewed by Stein and co-workers.^{15,39}

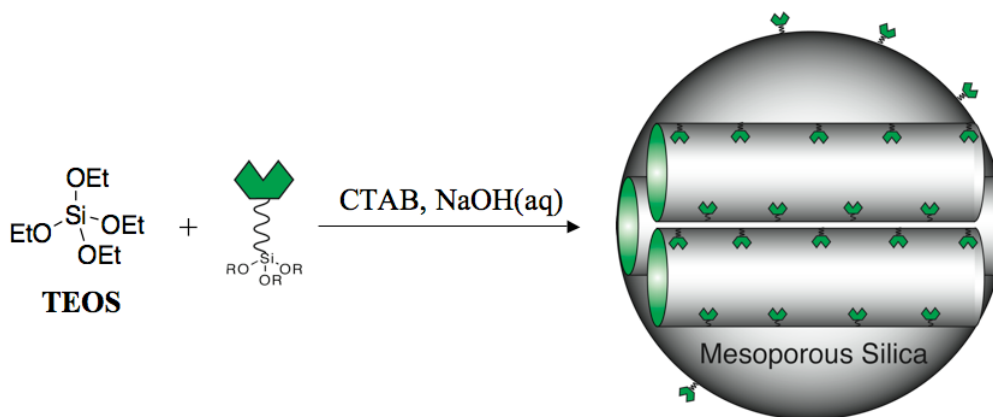


Figure 4. Schematic representation of functionalization of mesoporous silicas by the co-condensation method.

Recent Development of Functionalized Mesoporous Silica Materials

Several groups have developed strategies for selectively functionalizing external and internal surfaces, allowing controlled spatial distribution of catalytic sites. Shephard *et al.* demonstrated that multiple grafting steps of mesoporous silica with different organic

functionalities could be achieved by a kinetic control approach.⁴⁰ The calcined MCM-41 was first modified with Ph_2SiCl_2 at room temperature within a short time to passivate the external surface, and then the internal channels were decorated with aminopropyl trimethoxysilane (APTMS). To visualize distribution of organic functional groups, tethered aminopropyl group is employed as an anchor point for a ruthenium cluster, which serves a stain in the high-resolution transmission electronic microscopy (HRTEM). The author concluded that the aminopropyl groups are almost entirely located on the internal surface. De Juan *et al.* utilized an alternative approach to address this problem.⁴¹ The first grafting step is carried out on as-synthesized MCM-41, with surfactant template-filled mesopores. Due to the steric restrictions in the surfactant filled inner channels, the first grafted organosilane is mainly deposited on the exterior surface. After surfactant removal by extraction, the interior mesochannel surface is restored and ready for sequential immobilizations of a second functionality. However, caution needs to be taken in assuming that silylation agents are excluded from the channels of as-made MCM-41, in particular when high concentration of less hindered silylation reagents are used.^{42,43} Johnson *et al.* applied a similar sequential grafting method to immobilize a Pd-1,1'-bis(diphenylphosphino)ferrocene complex on the inner mesochannels of MCM-41.⁴⁴ The selectivity of the resulting Pd functionalized MCM-41 is investigated by allylic amination of cinnamyl acetate and benzylamine. Unlike the homogenous analog or Pd immobilized amorphous silica solid particle, which yields a majority of linear product, a branched amination product with 51% selectivity is produced by Pd functionalized MCM-41. Meanwhile, the enantioselectivity of a branched product is also dramatically changed from 43% by amorphous silica solid support to close to 100% by porous MCM-41 support. This result with MCM-41 supported catalysts shows that a

significant enhancement in terms of regio- and enantioselectivity could be accomplished, which is attributed to the spatial restrictions imposed by the mesopores. Precise control of spatial distribution of catalytic site is demanded for this special pore confinement effect. Fujiwara and co-workers utilized De Juan's approach to construct a photochemically controllable uptake and release system by gating pore openings with coumarin derivatives.^{45,46} Again, selective functionalization was achieved by grafting coumarin silanes onto an as-synthesized MCM-41 with surfactant present inside the channel, followed by acid extraction for surfactant removal to yield photo-responsive coumarin derivatives loaded on the exterior surface and pore opening. Upon irradiation of UV-light at 250 nm, the coumarin dye dimerized to block pore entrances and "turn off" diffusion of encapsulated molecules loaded before gate closure. The gate of coumarin dimers could be turned back "on" by irradiating with UV-light at wavelengths larger than 310 nm, cleaving the coumarin dimer into the original monomers. This sophisticated transport MCM-41 system allows reversible controlled uptake or release of loaded chemical molecules, or perhaps pharmaceutical drugs.

The functionalization of mesoporous silica phase is not restricted to small organic functional groups. Co-condensation method allows constructing more complex organic or transition metal complex functionality in certain conditions with preservation of chemical structure integrity. Also, tethered simple organic functional groups could serve as an anchoring point for further chemical transformation. Huq *et al.* successfully synthesized cyclodextrin-modified silicas by the co-condensation method with TEOS.⁴⁷ This material showed an adsorption capability of *p*-nitrophenol from aqueous solution. Corriu *et al.* anchored 1,4,8,11-tetraazacyclotetradecane (cyclam) molecules by substitution of chloropropyl groups on pre-synthesized chloropropyl functionalized silicas.⁴⁸ The cyclam

was found mostly located inside the channel, freely accessible for complexation with Cu (II) and Co (II) ions. Corma and co-workers reported a chiral Cu (II)-bis(oxazoline) (BOX) immobilized onto the silica surface by a radical coupling reaction with thiol tethered MCM-41 for Friedel-Crafts chemistry.⁴⁹ The residual surface silanol groups of the material were further capped with hexamethyldisilazane (HMDS) to eliminate possible undesirable interactions with catalytic sites. This Cu (II)-BOX modified heterogeneous catalyst exhibited higher conversion of Friedel-Crafts product than the homogeneous analog, and enabled catalysts recycling with essentially no loss in conversion or enantio excess. However, the result of *e.e.* was slightly lower than corresponding grafted amorphous silica, due to the presence of free silanol groups. An impressive work done by Acosta *et al.* has demonstrated that it is possible to grow uniform melamine-based dendrimers of various generations starting from an aminopropyl functionalized SBA-15 support.⁵⁰ The grown yield of each generation ranged from 75-80%, on the basis of thermogravimetric analysis (TGA) and element analysis (EA). Simultaneously, Reynhardt *et al.* reported the synthesis of PAMAM dendrimers grown in large-pore MCM-41.^{51,52} The author proved the material to be catalytically active for olefin formylation after dendrimers were phosphinomethylated and complexed with rhodium. Their work also showed that lower generation dendrimers were more easily phosphinomethylated, and subsequently more active catalysts. The aforementioned dendrimer functionalization provided a systematic way to fine-tune surface polarity of local physicochemical environments, which was able to manipulate diffusion of substrate. Furthermore, it increased loading of organic functionalities as dendrimer generation built up, which could not be obtained by silylation, on the basis of limited surface silanols. However, a mesoporous silicas support with larger pores, like SBA-15, is necessary to perform such

functionalization to eliminate the possibility of pore blocking resulting from the development of dendrimers.

As mentioned in the section 1.3.1, the post-grafting approach is a straightforward functionalization method, but usually results in multiple catalytic sites due to undesired intermolecular interactions. It has been reported that even grafting a simple APTMS on the silica surface creates ill-defined amine sites with potentially different chemical reactivities, due to the hydrogen bonds between basic amine sites and acidic surface silanols, as well as the amine by itself in close proximity. When attempting to further functionalize the surface-immobilized amine group, the steric hinderance or hydrogen bonding from proximal amine sites can prevent high conversion. Wulff *et al.* introduced a protection concept to circumvent this issue by placing a spacer via hydrolyzable linkage with two amines.^{53,54} After immobilization of whole organosilanes on the surface, the spacer could be removed by hydrolysis, leaving the amine site within a precisely controlled distance. This protection-deprotection concept indeed provides well-defined catalytic sites on the surface, at low loading of functional groups. Despite the success of this strategy, the closeness of amine sites is inevitable, in particular at higher loading of functional groups. Jones and co-workers reported a clever design which utilized a bulky 3,3,3-triphenylpropanal to protect APTMS by forming an imine linkage.⁵⁵⁻⁵⁸ The steric constraint of resulting tritylimine organosilanes forced individual amino functional group apart when grafting on SBA-15, even at high loadings. Furthermore, the residual silanols were capped with trimethylsilyl (TMS) group to diminish possible problematic hydrogen bonds between isolated amino groups and the silica surface. The author demonstrated that isolated single amine sites could be attained by examining the chemical reactivity of the amine group with chlorodimethyl(2,3,4,5-

tetramethyl-2,4-cyclopentadiene-1yl)silane (Cp-silane). The resulting site-isolated Cp-amino functionalized SBA-15 material was subjected to coordinate with Ti metal to yield a heterogeneous Ti functionalized mesoporous silica catalyst for ethylene polymerization. This catalyst showed higher reactivity than the similar material prepared by the traditional grafting method.

Since ordered mesoporous silicas possess exceptionally high surface areas and narrow pore size distributions, heterogenization of structurally and functionally well-defined molecular catalysts on such solid supports is desirable since the catalyst becomes considerably easier to handle, retrieve, and recycle. Although the immobilization of the molecule usually suffers from reduced activity compared to their homogeneous analog, some unique physiochemical properties of mesoporous silica might benefit the catalytic performance of the resultant heterogeneous catalysts. An impregnated Mn (bpy)₂²⁺ (bpy = 2,2'-bipyridine) MCM-41 reported by Knops-Gerrits *et al.* exhibited a higher catalytic activity in terms of oxidation reactivity and selectivity for styrene than the corresponding homogeneous catalysts.⁵⁹ The author attributed this enhancement to the fact that dimerization of homogeneous Mn (bpy)₂ happened easily in the solution, and the dimer form of the Mn (II) complex preferred to decompose peroxide rather than oxidize styrene. Heterogenization of Mn(II) complex on the surface isolated the catalytic species, and prohibited dimer formation. Anwender and co-workers developed a particularly useful silylamidation route for surface modification of the metal complex, which allowed simultaneous immobilization of metal complex and passivation of the silica surface.⁶⁰⁻⁶³ A metal silylamide complex was first introduced on the surface by coordination with silanols forming a stable Si-O-metal linkage, followed by ligand exchange of the resultant silylamide-

MCM complex with fod (1,1,1,2,2,3,3-heptafluoro-7,7'-dimethyl-4,6-octanedionate). The replaced HDMS in the solution capped the rest of surface silanols. An improved diastereoselectivity of Diels-Alder reaction catalyzed by yttrium-fod MCM-41 was observed, which is due to the steric hinderance between the pore wall and bulky fod ligand. Immobilized dichloro-(*S*)-6,6'-dimethyl-2,2'-diaminobiphenyl-ruthenium complex on MCM-41 has been reported by Corma and co-workers. This supported catalyst gave an excellent performance in the enantioselectivity of hydrogenation. The enantioselectivity in heterogeneous and homogeneous catalysts were 96.8 and 69.8%, respectively. The author proposed that this enhancement of enantioselectivity was caused by the increased rigidity of the tethered structure, in which the anchored structure would hamper the rotation of the transition state during the insertion of hydrogen atoms to the double bond. Jones *et al.* also observed enhancement of enantioselectivity in the hydrogenation reaction catalyzed by Rh (I) or Pd (II) functionalized MCM-41 catalysts.⁶⁴ In their further comprehensive studies, they perceived that this enhancement occurred only in the MCM-41 supported catalyst, but not with either homogeneous or silica supported catalysts with convex silica surface. The author claimed this improved performance could be attributed to the immobilization of active sites on a concave inner surface of mesoporous materials, where the access of bulky substrates to the active site was restricted to diffuse along the pore axis.

This review of recent development of functional mesoporous silicas expresses enormous interest to utilize such mesoporous materials as solid support for catalysis application. By precisely controlling the spatial distribution of catalytic sites,²⁸ adjusting sterically confined nanospaces, and fine-tuning physicochemical properties of local

environments created by the concave geometry of the silica framework, these approaches can serve as new concepts of designing more efficient heterogeneous catalysts.

References

- (1) Chen, H.-T.; Huh, S.; Wiench, J. W.; Pruski, M.; Lin, V. S.-Y. *J. Am. Chem. Soc.* **2005**, *127*, 13305-13311.
- (2) Kumar, R.; Chen, H.-T.; Escoto, J. L. V.; Lin, V. S. Y.; Pruski, M. *Chem. Mater.* **2006**, *18*, 4319-4327.
- (3) Ciesla, U.; Schuth, F. *Micropor. Mesopor. Mater.* **1999**, *27*, 131-149.
- (4) Corma, A. *Chem. Rev.* **1997**, *97*, 2373-2419.
- (5) Davis, M. E. *Nature* **2002**, *417*, 813-821.
- (6) Descalzo, A. B.; Martinez-Manez, R.; Sancenon, F.; Hoffmann, K.; Rurack, K. *Angew. Chem. Int. Ed.* **2006**, *45*, 5924-5948.
- (7) Ford, D. M.; Simanek, E. E.; Shantz, D. F. *Nanotechnology* **2005**, *16*, 458-475.
- (8) Giri, S.; Trewyn, B. G.; Stellmaker, M. P.; Lin, V. S. Y. *Angew. Chem. Int. Ed.* **2005**, *44*, 5038-5044.
- (9) Hoffmann, F.; Cornelius, M.; Morell, J.; Froeba, M. *Angew. Chem. Int. Ed.* **2006**, *45*, 3216-3251.
- (10) Lai, C.-Y.; Trewyn, B. G.; Jeftinija, D. M.; Jeftinija, K.; Xu, S.; Jeftinija, S.; Lin, V. S.-Y. *J. Am. Chem. Soc.* **2003**, *125*, 4451-4459.
- (11) Lin, V. S.-Y.; Lai, C.-Y.; Huang, J.; Song, S.-A.; Xu, S. *J. Am. Chem. Soc.* **2001**, *123*, 11510-11511.

- (12) Radu, D. R.; Lai, C.-Y.; Wiench, J. W.; Pruski, M.; Lin, V. S.-Y. *J. Am. Chem. Soc.* **2004**, *126*, 1640-1641.
- (13) Schuth, F.; Schmidt, W. *Adv. Mater.* **2002**, *14*, 629-638.
- (14) Stein, A. *Adv. Mater.* **2003**, *15*, 763-775.
- (15) Stein, A.; Melde, B. J.; Schroden, R. C. *Adv. Mater.* **2000**, *12*, 1403-1419.
- (16) Taguchi, A.; Schueth, F. *Micropor. Mesopor. Mater.* **2004**, *77*, 1-45.
- (17) Ying, J. Y.; Mehnert, C. P.; Wong, M. S. *Angew. Chem. Int. Ed.* **1999**, *38*, 56-77.
- (18) Beck, J. S.; Vartuli, J. C.; Roth, W. J.; Leonowicz, M. E.; Kresge, C. T.; Schmitt, K. D.; Chu, C. T. W.; Olson, D. H.; Sheppard, E. W. *J. Am. Chem. Soc.* **1992**, *114*, 10834-10843.
- (19) Kresge, C. T.; Leonowicz, M. E.; Roth, W. J.; Vartuli, J. C.; Beck, J. S. *Nature* **1992**, *359*, 710-712.
- (20) Zhao, D.; Feng, J.; Huo, Q.; Melosh, N.; Frederickson, G. H.; Chmelka, B. F.; Stucky, G. D. *Science* **1998**, *279*, 548-552.
- (21) Zhao, D.; Huo, Q.; Feng, J.; Chmelka, B. F.; Stucky, G. D. *J. Am. Chem. Soc.* **1998**, *120*, 6024-6036.
- (22) Bagshaw, S. A.; Prouzet, E.; Pinnavaia, T. J. *Science* **1995**, *269*, 1242-1244.
- (23) Tanev, P. T.; Pinnavaia, T. J. *Science* **1995**, *267*, 865-867.
- (24) Inagaki, S.; Fukushima, Y.; Kuroda, K. *J. Chem. Soc., Chem. Commun.* **1993**, 680-682.
- (25) Attard, G. S.; Glyde, J. C.; Goltner, C. G. *Nature* **1995**, *378*, 366-368.
- (26) Chen, C. Y.; Burkett, S. L.; Li, H. X.; Davis, M. E. *Microporous Mater.* **1993**, *2*, 27-34.

- (27) Steel, A.; Carr, S. W.; Anderson, M. W. *J. Chem. Soc., Chem. Commun.* **1994**, 1571-1572.
- (28) Monnier, A.; Schuth, F.; Huo, Q.; Kumar, D.; Margolese, D.; Maxwell, R. S.; Stucky, G. D.; Krishnamurty, M.; Petroff, P. *Science* **1993**, *261*, 1299-1303.
- (29) Stucky, G. D.; Monnier, A.; Schueth, F.; Huo, Q.; Margolese, D.; Kumar, D.; Krishnamurty, M.; Petroff, P.; Firouzi, A. *Mol. Cryst. Liq. Cryst.* **1994**, *240*, 187-200.
- (30) Firouzi, A.; Kumar, D.; Bull, L. M.; Besier, T.; Sieger, P.; Huo, Q.; Walker, S. A.; Zasadzinski, J. A.; Glinka, C. *Science* **1995**, *267*, 1138-1143.
- (31) Firouzi, A.; Atef, F.; Oertli, A. G.; Stucky, G. D.; Chmelka, B. F. *J. Am. Chem. Soc.* **1997**, *119*, 3596-3610.
- (32) Huo, Q.; Margolese, D. I.; Ciesla, U.; Feng, P.; Gier, T. E.; Sieger, P.; Leon, R.; Petroff, P. M.; Schueth, F.; Stucky, G. D. *Nature* **1994**, *368*, 317-321.
- (33) Huo, Q.; Margolese, D. I.; Ciesla, U.; Demuth, D. G.; Feng, P.; Gier, T. E.; Sieger, P.; Firouzi, A.; Chmelka, B. F. *Chem. Mater.* **1994**, *6*, 1176-1191.
- (34) Che, S.; Garcia-Bennett, A. E.; Yokoi, T.; Sakamoto, K.; Kunieda, H.; Terasaki, O.; Tatsumi, T. *Nature Materials* **2003**, *2*, 801-805.
- (35) Yokoi, T.; Yoshitake, H.; Yamada, T.; Kubota, Y.; Tatsumi, T. *J. Mater. Chem.* **2006**, *16*, 1125-1135.
- (36) Gao, C.; Qiu, H.; Zeng, W.; Sakamoto, Y.; Terasaki, O.; Sakamoto, K.; Chen, Q.; Che, S. *Chem. Mater.* **2006**, *18*, 3904-3914.
- (37) Che, S.; Liu, Z.; Ohsuna, T.; Sakamoto, K.; Terasaki, O.; Tatsumi, T. *Nature* **2004**, *429*, 281-284.
- (38) Ohsuna, T.; Liu, Z.; Che, S.; Terasaki, O. *Small* **2005**, *1*, 233-237.

- (39) Lim, M. H.; Stein, A. *Chem. Mater.* **1999**, *11*, 3285-3295.
- (40) Shephard, D. S.; Zhou, W.; Maschmeyer, T.; Matters, J. M.; Roper, C. L.; Parsons, S.; Johnson, B. F. G.; Duer, M. J. *Angew. Chem. Int. Ed.* **1998**, *37*, 2719-2723.
- (41) De Juan, F.; Ruiz-Hitzky, E. *Adv. Mater.* **2000**, *12*, 430-432.
- (42) Aronson, B. J.; Blanford, C. F.; Stein, A. *Chem. Mater.* **1997**, *9*, 2842-2851.
- (43) Antochshuk, V.; Jaroniec, M. *Chem. Commun.* **1999**, 2373-2374.
- (44) Johnson, B. F. G.; Raynor, S. A.; Shephard, D. S.; Mashmeyer, T.; Mashmeyer, T.; Thomas, J. M.; Sankar, G.; Bromley, S.; Oldroyd, R.; Gladden, L.; Mantle, M. D. *Chem. Commun.* **1999**, 1167-1168.
- (45) Mal, N. K.; Fujiwara, M.; Tanaka, Y.; Taguchi, T.; Matsukata, M. *Chem. Mater.* **2003**, *15*, 3385-3394.
- (46) Mal, N. K.; Fujiwara, M.; Tanaka, Y. *Nature* **2003**, *421*, 350-353.
- (47) Huq, R.; Mercier, L.; Kooyman, P. J. *Chem. Mater.* **2001**, *13*, 4512-4519.
- (48) Corriu, R. J. P.; Mehdi, A.; Reye, C.; Thieuleux, C. *Chem. Mater.* **2004**, *16*, 159-166.
- (49) Corma, A.; Garcia, H.; Moussaif, A.; Sabater, M. J.; Zniber, R.; Redouane, A. *Chem. Commun.* **2002**, 1058-1059.
- (50) Acosta, E. J.; Carr, C. S.; Simanek, E. E.; Shantz, D. F. *Adv. Mater.* **2004**, *16*, 985-989.
- (51) Reynhardt, J. P. K.; Yang, Y.; Sayari, A.; Alper, H. *Adv. Funct. Mater.* **2005**, *15*, 1641-1646.
- (52) Reynhardt, J. P. K.; Yang, Y.; Sayari, A.; Alper, H. *Chem. Mater.* **2004**, *16*, 4095-4102.
- (53) Wulff, G.; Heide, B.; Helfmeier, G. *J. Am. Chem. Soc.* **1986**, *108*, 1089-1091.

- (54) Wulff, G.; Heide, B.; Helfmeier, G. *React. Polym.* **1987**, *6*, 299-310.
- (55) McKittrick, M. W.; Jones, C. W. *Chem. Mater.* **2003**, *15*, 1132-1139.
- (56) McKittrick, M. W.; Jones, C. W. *J. Am. Chem. Soc.* **2004**, *126*, 3052-3053.
- (57) McKittrick, M. W.; Jones, C. W. *Chem. Mater.* **2005**, *17*, 4758-4761.
- (58) Jones, C. W.; McKittrick, M. W.; Nguyen, J. V.; Yu, K. *Top. Catal.* **2005**, *34*, 67-76.
- (59) Knops-Gerrits, P.-P.; De Vos, D.; Thibault-Starzyk, F.; Jacobs, P. A. *Nature* **1994**, *369*, 543-546.
- (60) Anwander, R.; Gerstberger, G.; Palm, C.; Groeger, O.; Engelhardt, G. *Chem. Commun.* **1998**, 1811-1812.
- (61) Gerstberger, G.; Palm, C.; Anwander, R. *Chem. Eur. J.* **1999**, *5*, 997-1005.
- (62) Nagl, I.; Widenmeyer, M.; Grasser, S.; Koehler, K.; Anwander, R. *J. Am. Chem. Soc.* **2000**, *122*, 1544-1545.
- (63) Gerstberger, G.; Anwander, R. *Micropor. Mesopor. Mater.* **2001**, *44-45*, 303-310.
- (64) Jones, M. D.; Raja, R.; Thomas, J. M.; Johnson, B. F. G.; Lewis, D. W.; Rouzaud, J.; Harris, K. D. M. *Angew. Chem. Int. Ed.* **2003**, *42*, 4326-4331.

CHAPTER 2. DIALKYLAMINOPYRIDINE-FUNCTIONALIZED MESOPOROUS SILICA NANOSPHERE AS AN EFFICIENT AND HIGHLY STABLE HETEROGENEOUS NUCLEOPHILIC CATALYST

A paper published in *Journal of the American Chemical Society* **2005**, *127*, 13305-13311

Hung-Ting Chen, Seong Huh, Jerzy W. Wiench, Marek Pruski, and Victor S.-Y. Lin

Abstracts

A new nucleophilic catalytic system comprised of dialkylaminopyridine-functionalized mesoporous silica nanosphere (DMAP-MSN) has been synthesized and characterized. We have demonstrated that this material is an efficient heterogeneous catalyst for Baylis-Hillman, acylation, and silylation reactions with good reactivity, product selectivity, and recyclability. We envision that this DMAP-functionalized mesoporous silica material can also serve as an effective heterogeneous catalyst for many other catalytic nucleophilic reactions.

Introduction

Due to its high nucleophilicity, 4-(dimethylamino)pyridine (DMAP) has been widely utilized as an efficient catalyst for many important reactions,¹⁻⁵ such as acylation, silylation, tritylation, ester rearrangement, polymerization, Darkin-West reaction, and Baylis-Hillman

reaction. Several approaches for immobilization of this remarkable homogeneous catalyst on various organic and inorganic solid supports, such as polymers⁶⁻¹⁶ and sol-gel silica-based materials,^{17,18} have been reported in the literature. However, the catalytic reactivities of most of these systems have been shown to be lower than that of the DMAP molecule in homogeneous solution reactions. The decrease in catalytic reactivity has been attributed to the difficulty of controlling the degree of functionalization and the complication due to the mass transport of reactants and products in-and-out of the catalytic sites within the solid matrices. For example, the catalytic reactivity of DMAP-functionalized polymers has been shown to be solvent dependent due to the swelling and contraction of the polymer matrices in different solvent environments.¹⁹

The MCM- and SBA-type silicas, with their regular structural characteristics, high surface areas and tunable pore diameters, represent a promising support for DMAP immobilization. However, to the best of our knowledge, successful functionalization of DMAP on mesoporous silica surfaces has not yet been reported. This can be attributed to the undesired protonation of the pyridyl group of various trialkoxysilyl-derivatized dialkylamino pyridines by the surface silanol group during the conventional post-synthesis grafting reaction.

Recently, we have developed a co-condensation-based synthetic method that provides control of the degree of organic functionalization and particle morphology.^{20,21} By utilizing this method, we report herein the synthesis, characterization, and catalytic reactivity study of a 4-(dialkylamino)pyridine-functionalized mesoporous silica nanosphere (DMAP-MSN) material. Our synthetic approach allows us to circumvent the undesired protonation of DMAP and produce a heterogeneous catalyst for Baylis-Hillman, acylation, and silylation reactions with superb reactivity, product selectivity, and recyclability.

Experimental Section

All reagents were purchased from commercial sources and used as received without further purification. Benzene was dried by calcium hydride and used after distillation. Dichloromethane was dried by aluminum oxide column. All catalytic reactions were performed in a screw-capped vial.

Preparation of 4-[N-[3-(triethoxysilyl)propyl]-N-methyl-amino]pyridine (DMAP-*TES*). A solution of 4-(*N*-methylamino)pyridine (5.00 g, 46.2 mmol) in 70 mL of dry tetrahydrofuran (THF) was added dropwise to a suspension of sodium hydride (1.77 g, 73.9 mmol) in 30 mL of dry THF under N₂ atmosphere at 0°C ice bath. The solution was stirred for additional 2 h at room temperature. A solution of chloropropyltriethoxysilane (11.1 mL, 46.2 mmol) in 10 mL of dry THF was introduced to the mixture at 0°C ice bath via injection. After injection, the solution was stirred further for 15 h at 70 °C. The solution was filtered, evaporated in vacuo, and chromatographed on silica gel with eluent (MeOH/CHCl₃ = 1/9 with 5% NEt₃), to give pure DMAP-*TES* as a liquid (8.85g, yield = 61.3%). The ¹H and ¹³C NMR spectra of the product were found identical with reported data.^{17,18}

Synthesis of dialkylaminopyridine-functionalized mesoporous silica nanosphere catalyst (DMAP-MSN). The mixture of cetyltrimethylammonium bromide surfactant (CH₃(CH₂)₁₅N(CH₃)₃Br, referred to as CTAB) (2.0 g, 5.49 mmol), 2.0 M of NaOH (aq) (7.0 mL, 14.0 mmol) and H₂O (480 g, 26.67 mol) was heated to 80 °C for 30 min. To this clear solution, tetraethoxysilane (9.34 g, 44.8 mmol), DMAP-*TES* (1.80 mL, 5.74 mmol) was added sequentially and rapidly via injection. White solids were observed within 85 sec upon mixing of the initial opaque emulsion. The reaction was stirred vigorously at 80 °C for 2 h followed by a hot filtration of the solution to yield the crude DMAP-MSN product (white

solid). The as-made material was washed with copious amount of water and methanol and then dried under vacuum. An acid extraction was performed with a methanolic solution (100 mL) of concentrated hydrochloric acid (0.6 mL) and the as-made DMAP-MSN material (1.0 g) at 60 °C for 3 h. The resulting surfactant-removed DMAP-MSN was filtered, washed with water and methanol, and dried under vacuum. The neutralization was conducted in saturated sodium carbonate methanol solution (100 mL) of extracted DMAP-MSN (1.0 g) at room temperature for 3 h. The neutralized DMAP-MSN material was isolated by filtration, washed by water and methanol, and dried under vacuum.

NMR spectroscopy. The ^1H and ^{13}C NMR spectra of products in solution were acquired on a Varian VRX 300 spectrometer. Solid-state ^{13}C and ^{29}Si NMR on DMAP-MSN utilized a Chemagnetics Infinity 400 MHz spectrometer equipped with 5 mm (Chemagnetics) and 1.8 mm (A. Samoson²²) double tuned probes capable of MAS at 10 and 40 kHz, respectively. The fast MAS probe was used to carry out the two-dimensional (2D) heteronuclear ^1H - ^{13}C correlation (HETCOR) experiment, where a spinning rate of 40 kHz provided sufficient homonuclear ^1H - ^1H decoupling during proton evolution without any additional RF irradiation in the ^1H channel, as previously described.²³ Instead of RF decoupling, a single π pulse at the ^{13}C spin frequency was introduced in the middle of the ^1H evolution period to refocus the $J_{\text{C-H}}$ coupling. One of the additional advantages of using the fast MAS is that low power decoupling could be efficiently used during the acquisition of ^{13}C signal.^{23,24} Other experimental details are given in section 3 and in the figure captions, where ν_{R} is the MAS rate and $\nu_{\text{RF}}^{\text{X}}$ denotes the magnitude of radiofrequency field applied to X nuclei (X = ^1H and ^{13}C). The ^1H and ^{13}C chemical shifts are referenced to TMS at 0 ppm.

General procedure for DMAP-MSN-catalyzed Baylis-Hillman reactions. An enone of choice (0.5 mmol), aldehyde of choice (0.25 mmol), and DMAP-MSN (50 mg, 30 mol%) were added to a mixture solution of tetrahydrofuran and water (2 mL, volume ratio = 3/1) in a screw-capped vial at 50°C for 24 h. After the reaction, the crude reaction mixture was filtered and washed by copious amount of acetone. The filtrate was concentrated under vacuum. The corresponding products were isolated by column chromatography with ethyl acetate/hexane as eluent.

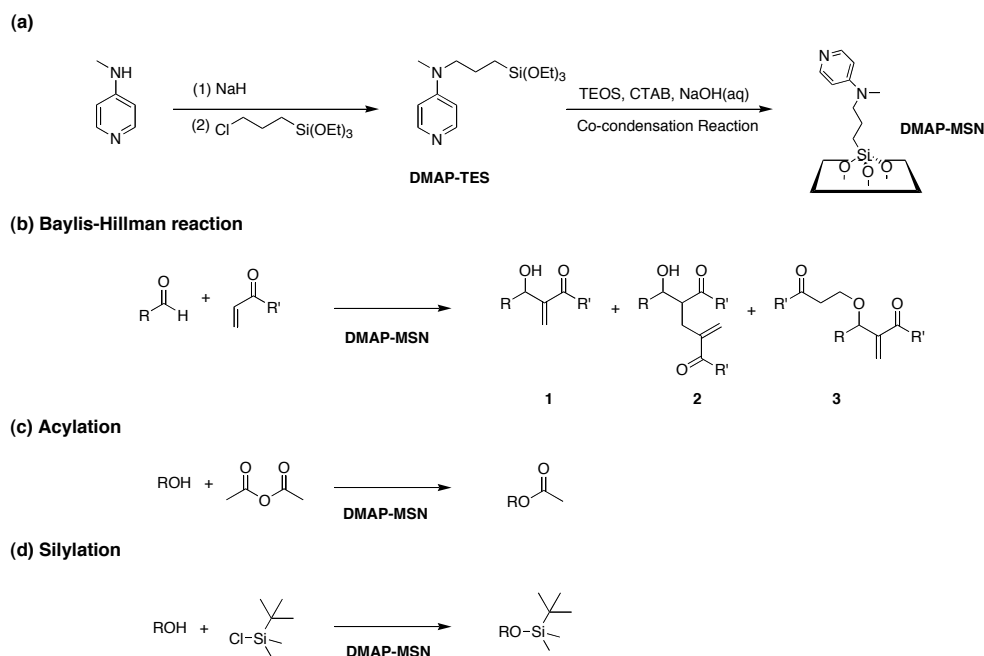
General procedure for DMAP-MSN-catalyzed acylation reactions. The mixture of DMAP-MSN (50 mg, 7.5 mol%), an alcohol of choice (1 mmol), triethylamine (1.5 mmol), and dry benzene (2 mL) were charged to a screw-capped vial and heated to 60°C for 20 min. Acetic anhydride (2 mmol) was added to the solution mixture via injection. After 2.5 to 24 h, the crude reaction mixture was filtered on a glass frit and the catalyst was thoroughly washed with copious amount of chloroform. The resulting filtrate was evaporated under vacuum. The corresponding acetates were obtained by column chromatography with ethyl acetate/hexane as eluent.

General procedure for DMAP-MSN-catalyzed silylation reactions. An alcohol of choice (0.5 mmol), *t*-butyldimethylsilyl chloride (0.55 mmol), DMAP-MSN (20 mg, 6 mol%), and triethylamine (0.55 mmol) were added to a dichloromethane solution (2 mL) in a screw-capped vial. The solution mixture was stirred at room temperature for 24 h. After the reaction, the reaction mixture was filtered and washed by copious amount of chloroform. The filtrate was concentrated under vacuum. The corresponding silyl ether products were isolated by column chromatography with ethyl acetate/hexane as eluent.

Results and Discussion

Synthesis and characterization of DMAP-MSN catalyst. We first synthesized an organosilane, 4-[N-[3-(triethoxysilyl)propyl]-N-methyl-amino]pyridine (DMAP-TES), via a procedure described in the experimental section (Scheme 1). To prepare the DMAP-functionalized mesoporous silica nanosphere (DMAP-MSN) material, DMAP-TES and tetraethoxysilane (TEOS) were introduced to a sodium hydroxide aqueous solution with low concentration of cetyltrimethylammonium bromide (CTAB) under a reaction condition that we have reported previously.^{20,21} After an acid extraction of the CTAB surfactant from the as-made material, the DMAP-MSN material was neutralized by submerging in a saturated sodium carbonate methanolic solution at room temperature for 3 h. The resulting solid was isolated by filtration, washed by water and methanol, and dried under vacuum.

Scheme 1 (Reprinted from *J. Am. Chem. Soc.* Copyright **2005** American Chemical Society)



The XRD measurement of DMAP-MSN showed a large (100) peak and a weak broad peak representing a higher-order diffraction (Figure 1a). The observed d_{100} value was 32.2 Å. The observed low-intensity broad peak (2θ) at $\sim 4.5^\circ$ could be attributed to the overlapping (110) and (200) diffraction peaks, typical of a disordered pore structure as we investigated and reported previously.²¹ The TEM micrograph of the material also confirmed its disordered pore structure (Figure 1b). The DMAP-MSN material exhibited a spherical particle shape with an average particle diameter of 400 nm as depicted in the SEM micrograph (Figure 1c). The N₂ surface sorption analysis of this mono-functionalized MSN exhibited a typical type IV isotherm without any significant hysteresis. The measured BET surface area of DMAP-MSN is 835 m²/g and the BJH average pore diameter is around 20 Å.

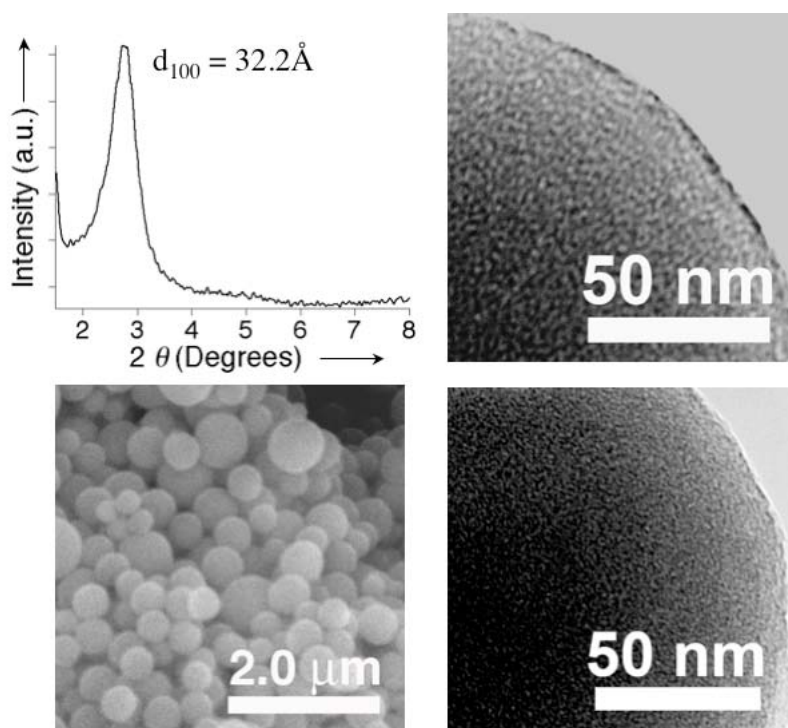


Figure 1. (a) XRD spectrum of DMAP-MSN. (b) TEM micrograph of DMAP-MSN, Scale bar = 50 nm, (c) SEM micrograph of DMAP-MSN, Scale bar = 2.0 μm , (d) TEM micrograph of DMAP-MSN after 10 runs of acylations, Scale bar = 50 nm. (Reprinted from *J. Am. Chem. Soc.* Copyright 2005 American Chemical Society)

Solid-state NMR studies of DMAP-MSN catalyst. The structure of the organic functionality was detailed by comparing the ^{13}C liquid spectrum of DMAP-TES (Figure 2a) with the ^{13}C MAS spectrum of DMAP-MSN (Figure 2b) acquired using ramped-amplitude cross polarization (CP)²⁵ and with the ^1H - ^{13}C HETCOR spectrum of the same sample (Figure 3). The assignments of ^{13}C resonances in solution DMAP-TES were based on the observed chemical shifts (see Table 1). The shifts obtained in solid-state NMR spectra of DMAP-MSN, which are also listed in Table 1, match well with the solution data, and thus confirm the presence of a DMAP ligand on the silica surface. The additional peak observed at around 48 ppm in Figure 2b most likely represents the methanol molecules adsorbed on the surface during the synthesis. The changes in peak intensities between solution and solid-state spectra reflect the differences in CP dynamics for individual carbon sites.

The concentration of functional groups in DMAP-MSN was measured from the relative intensities of T^n and Q^n silicon groups observed by ^{29}Si MAS NMR under direct polarization (DP), (Figure 2c). T^n and Q^n denote silicon sites $(\equiv\text{SiO})_n\text{Si}(\text{OH})_{4-n-m}\text{R}_m$ with $m = 1$ and $m = 0$, respectively. In order to improve the sensitivity, the ^{29}Si DPMAS spectrum was acquired using the Carr-Purcell-Meiboom-Gill (CPMG) train of echoes during the acquisition period.²³ By co-adding 10 echoes to construct the enhanced spectrum, a sensitivity gain of approximately 3 was achieved without any distortions due to transverse relaxation. We first note that the presence of resonances representing T^2 and T^3 sites at around -60 and -66 ppm confirms that covalent bonds exist between DMAP and the surface in this sample. By deconvolution and integration of the ^{29}Si spectrum, the following molecular formula was obtained for DMAP-MSN: $(\text{SiO}_2)_{100}(\text{H}_2\text{O})_8(\text{C}_9\text{H}_{14}\text{N}_2)_{13}$. From this formula, the amount of

organic groups can be estimated at $1.2 (\pm 0.1)$ molecules per nm^2 ($1.6 \pm 0.15 \text{ mmol}\cdot\text{g}^{-1}$) and the number of silanol groups at $2.6 (\pm 0.2)$ per nm^2 .

The NMR spectra also show that the pyridine and amine nitrogen atoms in DMAP-MSN are not protonated. In Table 1, we compare the chemical shifts of carbons of 4-(dimethylamino)pyridine in CDCl_3 solution with the corresponding shifts observed in mono- and di-protonated species observed in the presence of trifluoroacetic acid and trifluoromethanesulfonic acid, respectively.²⁶ After a prolonged exposure (3 weeks) of the DMAP-MSN sample to ambient humidity, an upfield shift of about 10 ppm was observed for C8 and C10 resonances in the 1D and 2D ^{13}C spectra (not shown), which demonstrates that the pyridine nitrogen is susceptible to protonation under such conditions.

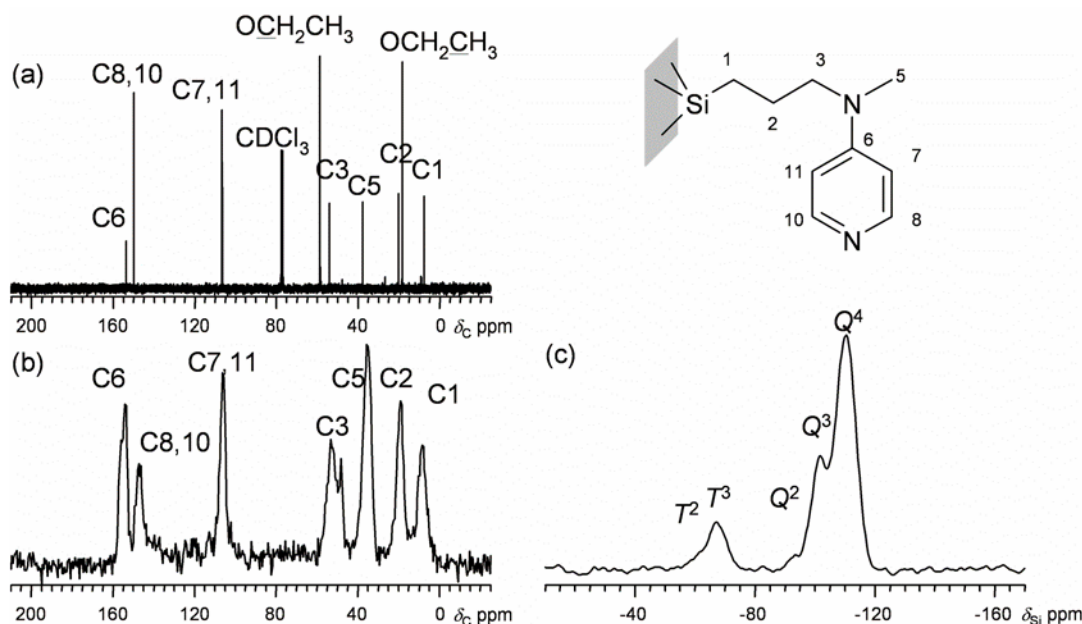


Figure 2. (a) ^{13}C NMR spectrum of DMAP-TES in CDCl_3 solution. (b) ^{13}C CP/MAS spectrum of DMAP-MSN resulting from 12,000 scans acquired with a delay of 1 s in a 5 mm probe ($\nu_{\text{R}} = 10 \text{ kHz}$). During each CP period of 1.5 ms, $\nu_{\text{RF}}^{\text{H}}$ was ramped between 16 and 40 kHz (in 11 steps), while $\nu_{\text{RF}}^{\text{H}}$ was set to 36 kHz. The $\nu_{\text{RF}}^{\text{H}}$ fields of 83 kHz and 65 kHz were applied to protons during initial excitation and high power decoupling, respectively. (c) ^{29}Si DPMAS spectrum of DMAP-MSN obtained with the same probe using CPMG acquisition (10 echoes). A total of 600 scans were collected with a delay of 300 s to allow the complete relaxation of ^{29}Si nuclei. (Reprinted from *J. Am. Chem. Soc.* Copyright 2005 American Chemical Society)

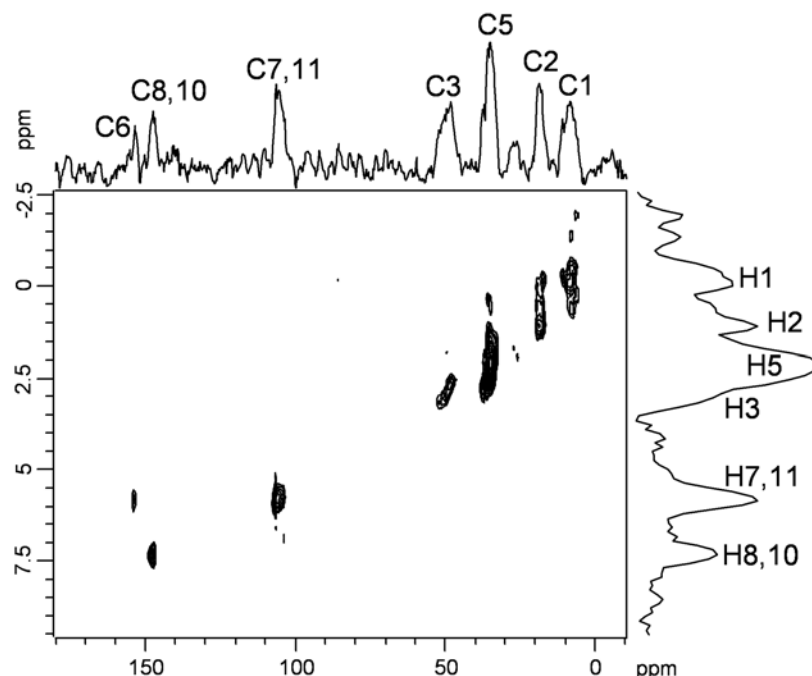


Figure 3. ^1H - ^{13}C HETCOR spectrum of DMAP-MSN measured under MAS at 40 kHz. During the CP period of 1.5 ms, the $\nu_{\text{RF}}^{\text{H}}$ field was ramped between 100 and 140 kHz (in 15 steps) and $\nu_{\text{RF}}^{\text{H}}$ was set to 80 kHz. TPPM decoupling with $\nu_{\text{RF}}^{\text{H}} = 10$ kHz was used during the detection of ^{13}C signals, which were accumulated using a delay of 1 s between scans. The hypercomplex method was employed to discriminate the sine and cosine parts in the ^1H dimension. The experiment was completed in approximately 80 h, using 10 mg of natural abundance sample. (Reprinted from *J. Am. Chem. Soc.* Copyright 2005 American Chemical Society)

Table 1. ^{13}C chemical shifts observed in DMAP-MSN and in the reference compounds (DMAP-TES and 4NMe₂-Py). (Reprinted from *J. Am. Chem. Soc.* Copyright 2005 American Chemical Society)

Sample	Solvent	C1	C2	C3	C5	C6	C7,C11	C8,C10
DMAP-TES	CDCl_3	7.8	20.1	54.0	37.5	153.5	106.6	149.8
DMAP-MSN	Solid-state	8.8	19.3	53.0	35.8	153.8	106.1	147.8
4NMe ₂ -Py ^[a]	CDCl_3				38.4	153.6	106.0	149.1
	CF_3COOH in CDCl_3				40.1	153.6	105.6	139.9
	$\text{CF}_3\text{SO}_3\text{H}$ in CD_3NO_2				47.3	157.8	120.6	145.6

^[a] Data taken from ref. 26.

DMAP-MSN catalyzed Baylis-Hillman reaction. Baylis-Hillman reaction is one of the most useful synthetic ways for forming carbon-carbon bonds between aldehydes and α,β -unsaturated ketones or esters. This reaction can be catalyzed by organic bases, such as amines, pyridines, and phosphines, without any assistance of metal.^{27,28} It typically requires stoichiometric or overstoichiometric amounts of catalysts and is usually performed in homogeneous solutions. Among various ketone substrates, cycloalkenones are known for their low reactivities for undergoing the Baylis-Hillman reaction catalyzed by nucleophilic molecules, such as DABCO (1,4-diazabicyclo [2,2,2]-octane).²⁹ Furthermore, in the homogeneous reaction of aryl aldehydes with methyl vinyl ketone (MVK) catalyzed by DABCO, the formation of undesired products, such as diadduct (compound **2** in Scheme 1) and Michael adduct (compound **3**), have been reported in the literature.³⁰

DMAP, on the other hand, is able to efficiently catalyze the Baylis-Hillman reaction of cycloalkenones in homogeneous solutions.³¹ To construct a recyclable DMAP catalysts, Corma and co-workers¹⁶ have recently reported on the synthesis of a DMAP-functionalized, Merrifield-type polystyrene resin that could serve as an active catalyst for the Baylis-Hillman reaction. However, this polymer-based DMAP catalyst showed a lower reactivity in protic solvents in comparison with those of DMAP-catalyzed homogeneous reactions.^{32,33} The low reactivity was attributed to the contraction of polymer matrix in protic solvents.¹⁶ Furthermore, a stoichiometric amount of the polymer-based DMAP catalyst was needed to obtain decent yields within reasonable reaction times. In some cases, the undesired diadduct and Michael adduct were also observed.

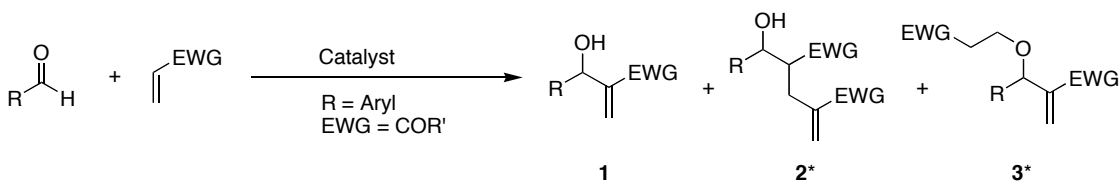
In contrast, our DMAP-MSN material showed an excellent catalytic performance (Table 2) for the Baylis-Hillman reaction of aryl aldehydes and various α,β -unsaturated

ketones. Only a catalytic amount (30 mol%) of DMAP-MSN was needed for the complete conversion of cyclic and aliphatic enones to the corresponding Baylis-Hillman products (entry 1-3 in Table 2). In the case of methyl vinyl ketone (MVK), the desired product was obtained in quantitative yield (entry 3 in Table 2) within 24 h. No undesired diadduct and Michael adduct were detected even at relatively high reaction temperature (50°C). Conversely, the same reaction catalyzed by DMAP in homogeneous solution gave rise to a mixture of products under the same reaction condition (Scheme 2a). In addition to the diadduct and Michael addition side products, the formation of insoluble brown precipitates was also observed, which could be attributed to products of the oligomerization of MVK and compound **1** catalyzed by DMAP at the elevated temperature. Using a physical mixture of DMAP and fumed silica gel as catalysts yielded a mixture of product as well. Based on these results, the high yield and good product selectivity of DMAP-MSN catalyzed reactions could not be due to the silanol groups on the silica surface. Given the fact that the DMAP catalytic groups are mainly located in the mesopores of MSN, we suspect that the observed product selectivity could be attributed to the difference in the rate of diffusion to the “active sites” located inside the pores between the aldehyde reactant and compound **1**, which would serve as the reactant for the undesired side reactions. To investigate this supposed “matrix effect”, we carried out two DMAP- and DMAP-MSN-catalyzed Baylis-Hillman reactions by using compound **1** (1.0 e.q.) as reactant to interact with MVK (2.0 e.q.) in the aforementioned THF/H₂O solution at 50 °C for 24 h. Indeed, the reaction catalyzed by homogeneous DMAP catalyst gave rise to a mixture of products. On the contrary, no reaction was observed in the case of DMAP-MSN. The results support the hypothesis that the MSN matrix could regulate

the reaction selectivity by preferentially allowing certain reactants to access the catalytic sites.

The intrinsic steric and electronic properties of the aldehyde reactants also strongly affect the product yields of the Baylis-Hillman reaction catalyzed by our DMAP-MSN. In the case of sterically hindered aryl aldehydes, e.g. *o*-nitrobenzaldehyde, a lower product yield of 49% was observed (entry 4 in Table 2). Compared to the case of *p*-nitrobenzaldehyde, the reactions of the less activated or non-activated aldehydes, such as *p*-chlorobenzaldehyde and benzaldehyde, respectively, required more methyl vinyl ketones and extended reaction time to obtain the desired products (entry 6,7 in Table 2). In contrast to the reactivities of other reported, surface-supported DMAP catalysts, the DMAP-MSN-catalyzed Baylis-Hillman reaction of a non-activated aryl aldehyde (benzaldehyde) with MVK gave rise to a high yield of the desired product with less catalyst loading (0.3 e.q. vs. 1.0 e.q.) and shorter reaction time (4 days vs. 10 days).¹⁶ Therefore, our heterogeneous DMAP-MSN catalyst exhibits higher reactivity than polymer-based DMAP catalyst (entry 7 in Table 2). Among the examined substrates, the reactivity of α,β unsaturated ketones follows the order: methyl vinyl ketone > cyclopentenone > cyclohexenone. To further compare the catalytic performance of DMAP-MSN with other silica-immobilized tertiary amines, we have examined a Baylis-Hillman reaction catalyzed by 3-(dimethylamino)propyl-functionalized silica gel (DMA-SiO₂). A 20 % yield (entry 8 in Table 2) was observed, which indicated that the reactivity of DMAP-MSN (99% yield, entry 3 in Table 2) was indeed superior. Unlike DMAP-MSN, pure MCM-41 silica showed no reactivity in catalyzing the Baylis-Hillman reaction (entry 3, 9 in Table 2).

Table 2. DMAP-MSN catalyzed Baylis-Hillman reaction.^[a] (Reprinted from *J. Am. Chem. Soc.* Copyright 2005 American Chemical Society)

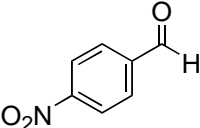
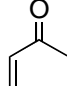
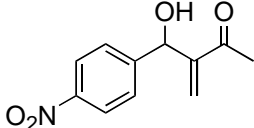
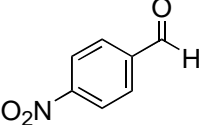
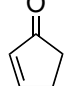
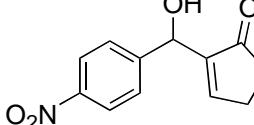


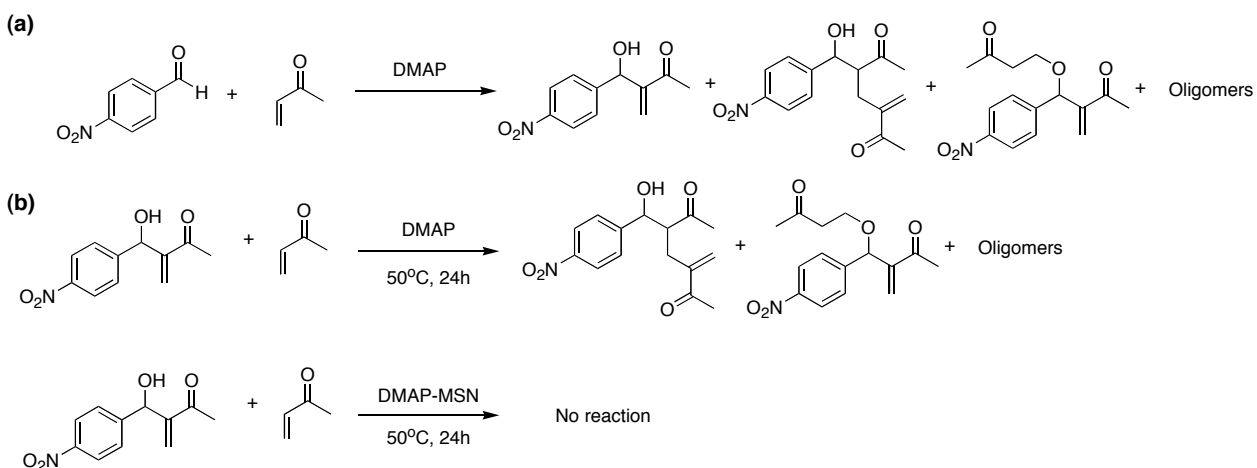
* Side products **2** and **3** are not observed in all reactions.

Entry	Aldehyde	Ketone	Catalyst	Product	Yield [%] ^[b]
1			DMAP-MSN		86
2			DMAP-MSN		49
3			DMAP-MSN		99
4			DMAP-MSN		49
5			DMAP-MSN		25
6 ^[c]			DMAP-MSN		50
7 ^[c]			DMAP-MSN		25

^[a] Reaction condition: *p*-nitrobenzaldehyde (0.25 mmol), α,β -unsaturated ketone (0.5 mmol), and catalyst (50 mg, 30 mol%) in THF/H₂O = 3:1 (2 mL) at 50°C for 24 h; ^[b] isolated yield; ^[c] aldehyde/ketone = 1:4 at 50°C for 3 d; ^[d] 3-(dimethylamino)propyl-functionalized silica gel; ^[e] no reaction.

Table 2. (continued)

Entry	Aldehyde	Ketone	Catalyst	Product	Yield [%] ^[b]
8			DMA-SiO ₂ ^[d]		20
9			MCM-41		NR ^[e]

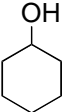
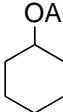
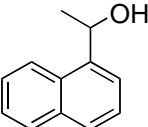
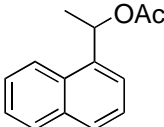
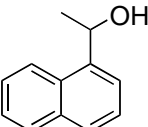
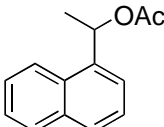
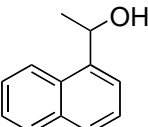
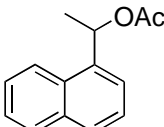
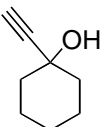
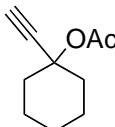
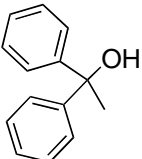
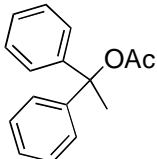
Scheme 2. (Reprinted from *J. Am. Chem. Soc.* Copyright 2005 American Chemical Society)

DMAP-MSN catalyzed acylation reaction. Catalytic acylations of various alcohols by DMAP-MSN were investigated, and the results are outlined in Table 3. As shown in entry 1 and 2, the acylations of secondary alcohols proceeded rapidly and completed within 2.5 h under our reaction condition. In the absence of DMAP-MSN catalyst, however, only a small amount of product (33 %) was obtained under the same reaction condition. As a control, pure inorganic MCM-41 silica, prepared by a similar procedure, was also used as a catalyst for the acylations. As shown in Table 3 (entry 3, 4), pure MCM-41 silica does not catalyze acylation. These results clearly indicated that DMAP-MSN could efficiently catalyze

acylation reactions of various secondary alcohols. Contrary to the reactions with secondary alcohols, lower yields and longer reaction times were found in the cases of various tertiary alcohols (entry 5, 6 in Table 3). Such a pronounced difference could be attributed to the steric hindrance of carbinol as observed in homogeneous reactions.³⁴

Table 3. DMAP-MSN catalyzed acylation of alcohols.^[a] (Reprinted from *J. Am. Chem. Soc.* Copyright 2005 American Chemical Society)

$$\text{ROH} \xrightarrow[\text{Catalyst}]{\text{Ac}_2\text{O, NEt}_3} \text{ROAc}$$

Entry	Alcohol	Catalyst	t [h]	Product	Yield [%] ^[b]
1		DMAP-MSN	2.5		90
2		DMAP-MSN	2.5		93
3		MCM-41	2.5		32
4		Without catalyst	2.5		33
5		DMAP-MSN	6		54
6		DMAP-MSN	24		13

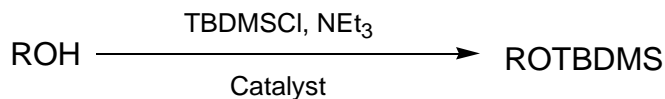
^[a] Reaction condition: alcohol (1mmol), catalyst (50 mg, 7.5 mol%), Ac₂O (2 mmol), and NEt₃ (1.5 mmol) in dry benzene (2 mL) at 60°C; ^[b] isolated yield.

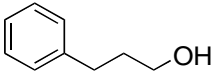
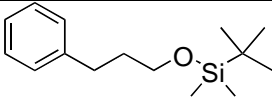
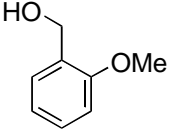
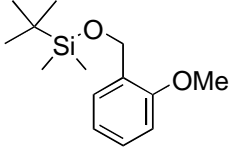
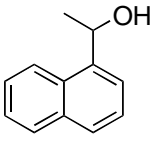
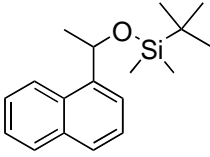
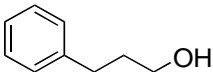
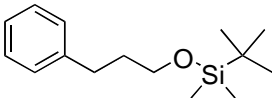
Recyclability and stability studies of DMAP-MSN catalyst. To investigate the recyclability of DMAP-MSN catalyst, 1-(1-naphthyl)ethanol was chosen as a substrate because the chemical shift of the α -proton of this molecule could be clearly resolved from other peaks in the ^1H NMR spectrum. After the reaction reached completion, the catalyst was reused in 10 consecutive cycles, which included recovery by decanting the aliquots after centrifuge and drying in air followed by the reaction. No change in reaction yield was observed. The TEM micrograph of the recovered DMAP-MSN catalyst (Figure 1d) showed the same clear structure as the freshly synthesized material. The result indicated that the mesopores of DMAP-MSN were not destroyed by chemical or thermal decompositions during the repeated use as a catalyst. To further evaluate the stability of DMAP-MSN, cyclohexanol (100.2 mmol) was introduced to a 200 mL benzene solution with acetic anhydride (200.4 mmol) and DMAP-MSN (20 mg). The reaction was stirred vigorously at 60°C for 24 days. The resulting cyclohexyl acetate product was obtained in 100 % yield based on the ^1H NMR spectrum, which gave rise to a turnover number (TON) of 3340 for 24 days. This result suggested that the catalytic reactivity of DMAP-MSN could be maintained for an extended period of time.

DMAP-MSN catalyzed silylation reaction. We also carried out several silylation reactions of alcohols by using DMAP-MSN as catalyst (Table 4).³⁵ The reaction yield of these DMAP-MSN-catalyzed silylations appeared to be sensitive to the steric hindrance of the alcohols. In the case of sterically hindered alcohols, lower yields (entry 1-3 in Table 4) were observed in comparison with those of less sterically demanding alcohols. It is interesting to note that pure MCM-41 silica also catalyzed the silylation reactions and gave

rise to certain amounts of silyl ethers. The result suggested that the acidic surface silanol groups of MCM-41 could be responsible for catalyzing the silylation reactions.

Table 4. DMAP-MSN catalyzed silylation of alcohols.^[a] (Reprinted from *J. Am. Chem. Soc.* Copyright 2005 American Chemical Society)



Entry	Alcohol	Catalyst	Product	Yield [%] ^[b]
1		DMAP-MSN		96
2		DMAP-MSN		52
3		DMAP-MSN		35
4		MCM-41		64

^[a] Reaction condition: alcohol (0.5 mmol), catalyst (20 mg, 6 mol%), *t*-butyldimethylsilyl chloride (0.55 mmol), and NEt₃ (0.55 mmol) in dry CH₂Cl₂ (2 mL) at room temperature for 24 h; ^[b] isolated yield.

Conclusion

We have successfully synthesized and characterized DMAP immobilized mesoporous silica catalyst, which showed high recyclability and high turnover number for Baylis-Hillman, acylation, and silylation reaction. We expect that this DMAP-functionalized

mesoporous silica material also can serve as an efficient heterogeneous catalyst for many other catalytic nucleophilic reactions.

Acknowledgments

This research was supported at Ames Laboratory by the U.S. Department of Energy, Office of Basic Energy Sciences, through the Catalysis Science Grant No. AL-03-380-011 and under Contract W-7405-Eng-82

References

- (1) Hoefle, G.; Steglich, W.; Vorbrueggen, H. *Angew. Chem.* **1978**, *90*, 602-615.
- (2) Heinrich, M. R.; Klisa, H. S.; Mayr, H.; Steglich, W.; Zipse, H. *Angew. Chem., Int. Ed. Engl.* **2003**, *42*, 4826-4828.
- (3) Scriven, E. F. V. *Chem. Soc. Rev.* **1983**, *12*, 129-161.
- (4) Spivey, A. C.; Arseniyadis, S. *Angew. Chem., Int. Ed. Engl.* **2004**, *43*, 5436-5441.
- (5) Murugan, R.; Scriven, E. F. V. *Aldrichimica Acta* **2003**, *36*, 21-27.
- (6) Hierl, M. A.; Gamson, E. P.; Klotz, I. M. *J. Am. Chem. Soc.* **1979**, *101*, 6020-6022.
- (7) Delaney, E. J.; Wood, L. E.; Klotz, I. M. *J. Am. Chem. Soc.* **1982**, *104*, 799-807.
- (8) Shinkai, S.; Tsuji, H.; Hara, Y.; Manabe, O. *Bull. Chem. Soc. Jpn.* **1981**, *54*, 631-632.

- (9) Tomoi, M.; Akada, Y.; Kakiuchi, H. *Makromol. Chem., Rapid Commun.* **1982**, *3*, 537-542.
- (10) Menger, F. M.; McCann, D. J. *J. Org. Chem.* **1985**, *50*, 3928-3930.
- (11) Deratani, A.; Darling, G. D.; Frechet, J. M. J. *Polymer* **1987**, *28*, 825-830.
- (12) Deratani, A.; Darling, G. D.; Horak, D.; Frechet, J. M. J. *Macromolecules* **1987**, *20*, 767-772.
- (13) Guendouz, F.; Jacquier, R.; Verducci, J. *Tetrahedron* **1988**, *44*, 7095-7108.
- (14) Bergbreiter, D. E.; Li, C. *Org. Lett.* **2003**, *5*, 2445-2447.
- (15) Bergbreiter, D. E.; Osburn, P. L.; Li, C. *Org. Lett.* **2002**, *4*, 737-740.
- (16) Corma, A.; Garcia, H.; Leyva, A. *Chem. Commun.* **2003**, 2806-2807.
- (17) Rubinsztajn, S.; Zeldin, M.; Fife, W. K. *Macromolecules* **1990**, *23*, 4026-4027.
- (18) Rubinsztajn, S.; Zeldin, M.; Fife, W. K. *Macromolecules* **1991**, *24*, 2682-2688.
- (19) Benaglia, M.; Puglisi, A.; Cozzi, F. *Chem. Rev.* **2003**, *103*, 3401-3429.
- (20) Huh, S.; Wiench, J. W.; Trewyn, B. G.; Song, S.; Pruski, M.; Lin, V. S. Y. *Chem. Commun.* **2003**, 2364-2365.
- (21) Huh, S.; Wiench, J. W.; Yoo, J.-C.; Pruski, M.; Lin, V. S. Y. *Chem. Mater.* **2003**, *15*, 4247-4256.

- (22) Samoson, A. In *Encyclopedia of Nuclear Magnetic Resonance*; Grant, D. M., Harris, R. K., Ed.; John Wiley & Sons: Chichester, 2002; Vol. 9, pp 59-64.
- (23) Trebosc, J.; Wiench, J. W.; Huh, S.; Lin, V. S. Y.; Pruski, M. *J. Am. Chem. Soc.* **2005**, *127*, 3057-3068.
- (24) Ernst, M.; Samoson, A.; Meier, B. H. *Chem. Phys. Lett.* **2001**, *348*, 293-302.
- (25) Metz, G.; Wu, X.; Smith, S. O. *J. Magnetic Resonance, Series A* **1994**, *110*, 219-227.
- (26) Dega-Szafran, Z.; Kania, A.; Nowak-Wydra, B.; Szafran, M. *J. Mol. Struct.* **1994**, *322*, 223-232.
- (27) Basavaiah, D.; Rao, A. J.; Satyanarayana, T. *Chem. Rev.* **2003**, *103*, 811-891.
- (28) Basavaiah, D.; Rao, P. D.; Hyma, R. S. *Tetrahedron* **1996**, *52*, 8001-8062.
- (29) Rezgui, F.; El Gaied, M. M. *Tetrahedron Lett.* **1998**, *39*, 5965-5966.
- (30) Shi, M.; Li, C.-Q.; Jiang, J.-K. *Chem. Commun.* **2001**, 833-834.
- (31) Lee, K. Y.; Gong, J. H.; Kim, J. N. *Bull. Korean Chem. Soc.* **2002**, *23*, 659-660.
- (32) Aggarwal, V. K.; Dean, D. K.; Mereu, A.; Williams, R. *J. Org. Chem.* **2002**, *67*, 510-514.
- (33) Yu, C.; Liu, B.; Hu, L. *J. Org. Chem.* **2001**, *66*, 5413-5418.
- (34) Hassner, A.; Krepski, L. R.; Alexanian, V. *Tetrahedron* **1978**, *34*, 2069-2076.
- (35) Chaudhary, S. K.; Hernandez, O. *Tetrahedron Lett.* **1979**, 99-102.

CHAPTER 3. ENHANCING CATALYTIC ACTIVITY BY SURFACE FUNCTIONAL GROUP ACTIVATION THROUGH HYDROGEN BOND – A NEW CONCEPT TO DEVELOP HETEROGENEOUS UREA OR THIOUREA FUNCTIONALIZED MESOPOROUS SILICA NANOPARTICLE CATALYSTS APPLIED FOR DIELS-ALDER REACTION

A manuscript in preparation and to be submitted to *Journal of the American Chemical Society*

Hung-Ting Chen, Brian G. Trewyn, Rajeev Kumar, Jerzy W. Wiench, Marek Pruski, and

Victor S.-Y. Lin

Abstract

A series of urea or thiourea functionalized mesoporous silica nanoparticle catalysts has been successfully synthesized and fully characterized. These materials showed a catalytic activity of the Diels-Alder reaction through carbonyl activation of dienophiles by double hydrogen bonding capability of the surface-immobilized urea or thiourea organic functionalities. Incorporation of strong electron-withdrawing groups (trifluoromethyl) into the urea or thiourea structures, resulted in increasing Lewis acidity of MSN materials, further enhanced the catalytic activity of the Diels-Alder. The catalytic performance of these heterogeneous catalysts was found to be significantly superior to their homogeneous analogs by a factor ranging from 2 to 6. This unprecedented reactivity could be attributed to an isolation effect induced by the heterogenization of the individual catalytic groups on the surface, so that the undesired aggregation could be avoided. Also, the hydrogen bonding between tethered urea or thiourea functionalities and the silanol groups could also elevate the activity of the catalytic sites.

Introduction

The utilization of structurally ordered mesoporous silicas with high surface area, tunable pore size, and well-defined particle and pore morphology¹⁻⁴ as solid support for the preparation of single-site heterogeneous catalysts recently attracts a large research effort worldwide. Although several obstacles have been overcome, such as selective functionalization of silica wall,⁵⁻⁷ controlled spatial distribution of functional groups,^{8,9} and material hydrothermal stability,¹⁰⁻¹⁴ there are still a few key challenges yet to be circumvented. For example, the reactivity and selectivity of many efficient homogeneous catalysts were found to be degraded upon surface immobilization. Many have attributed this phenomenon to the undesirable molecular interaction between the catalysts and the surface groups of the solid matrix. For example, we and others have found that the basicity of primary amino functionality decreased upon immobilization on silicate surface caused by the hydrogen bonding with the acidic silanols on surface.¹⁵⁻¹⁷ In contrast to the conventional approach of pacifying the support, we would like to take advantage of the interactions between the catalytic functional groups and the support to enhance the overall reactivity. Herein, we report on a new concept of catalyst design by taking advantage of strong affinity between surface silanol and amide functionality.¹⁸⁻²¹ As a proof of principle, we immobilized urea and thiourea functionalities on the mesoporous silica surface to serve as a catalyst for carbonyl activation through double hydrogen bonding mechanism. These hydrogen bond donors have been demonstrated to be successful catalysts for many homogeneous reactions, such as Diels-Alder reaction, Michael addition, Henry reaction, and cyanosilylation.²²⁻³⁰ We demonstrated in this study that the catalytic reactivity of the surface anchored urea and thiourea functional groups for carbonyl activation could be magnified by the presence of

surface hydrogen bonding between these groups and the silanol groups on the mesopore surface.

Results and Discussion

Three urea/or thiourea organotrialkoxysilanes, 3-(3-phenyl ureido) propyl trimethoxysilane (**PUP-TMS**), 3-[3-(3,5-ditrifluoromethyl phenyl)-ureido]-propyl triethoxysilane (**FPUP-TES**), and 3-(3-phenyl thioureido)-propyl trimethoxysilane (**TUP-TMS**), were prepared by reacting an amine with corresponding isocyanate/or thioisocyanate reagents (see Appendix). The urea/ or thiourea functionalized mesoporous silica nanoparticles (MSN) catalysts, **PUP-**, **FPUP-**, and **TUP-MSN**, were synthesized by our previous reported co-condensation method.³¹⁻³⁵ The 3-[3-(3,5-ditrifluoromethyl phenyl)-thioureido]-propyl functionalized mesoporous silica nanoparticle catalyst (**FTUP-MSN**) was synthesized by further reaction of 3-amino propyl functionalized MSN (AP-MSN) with 3,5-bistrifluoromethyl phenyl isothiocyanate. As depicted in Figure 1, powder X-ray diffraction (XRD) spectra of the first three MSNs showed a similar diffraction pattern with a large (100) peak and broad and overlapped higher diffraction peaks, indicated the presence of a disordered mesoporous structure. In contrast, FTUP-MSN, prepared by further functionalization, exhibited three distinct (100), (110), and (200) diffraction peaks, typical of MCM-41 type hexagonally packed mesopore structure. The TEM micrographs of these four catalysts further confirmed the aforementioned porous structures as showed in Figure 2. The N₂ sorption analysis of all MSN materials revealed typical type IV BET isotherm without significant hysteresis and narrow BJH pore size distribution. The measured BET surface areas of PUP-, FPUP-, TUP-, and FTUP-MSN are 1029.1, 803.1, 881.0, and 593.0 m²/g,

respectively. The corresponding BJH average pore diameters are 2.5, 2.6, 2.6, and 2.8 nm. The ^{13}C and ^{29}Si solid-state NMR spectra of these MSN materials confirmed the covalently bonded organic functional group on the surface. The amounts of functional groups of PUP-, FPUP-, TUP-, and FTUP-MSN, quantified from ^{29}Si DPMAS spectra, were 0.9, 0.7, 1.0, and 0.5 mmol/g, respectively.

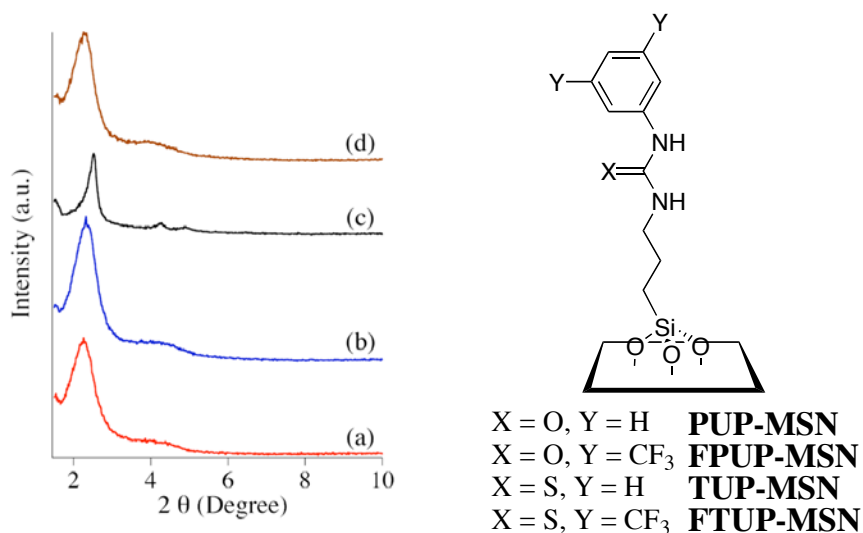


Figure 1. Powder X-ray diffraction (XRD) pattern (left) of FPUP-MSN(a), PUP-MSN(b), FTUP-MSN(c), and TUP-MSN(d) and chemical structure of surface functional group (right).

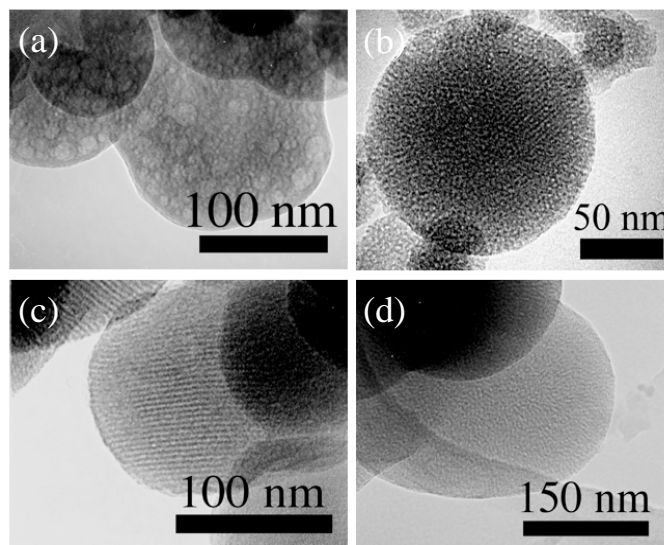
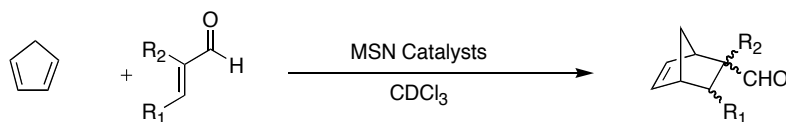


Figure 2. Transmission electron microscopy (TEM) micrographs of FPUP-MSN(a), PUP-MSN(b), FTUP-MSN(c), and TUP-MSN(d). Scale bars are indicated inside the pictures.

To investigate catalytic activity of urea- and thiourea-functionalized MSNs, a series of Diels-Alder reactions were investigated and the results are summarized in Table 1. In general, the Diels-Alder reactions catalyzed by the organically functionalized MSNs showed higher reactivity as well as selectivity than those without catalyst, which indicated surface-anchored urea and thiourea functional groups are indeed catalytically active. Also, the incorporation of strong electron-withdrawing substituents, such as bis-trifluoromethyl groups, into the meta-position of aromatic rings further enhanced the reactivity of these heterogeneous MSN catalysts as demonstrated by the higher reactivity of FPUP-MSN and FTUP-MSN in comparison with those of PUP- and TUP-MSN. Six-fold enhancement in reactivity was observed when methyl methacrolein was employed as the dienophile. Given that the nature of the catalytic ability stems from dienophile activation through double hydrogen bonding with urea or thiourea group, the Lewis acidity of urea or thiourea center dictates the catalytic reactivity. Therefore, the introduction of bis-trifluoromethyl group into the catalytic system makes aromatic ring more electron deficient, resulted in an increase of the Lewis acidity of the catalysts. It is noteworthy that non-functionalized MCM-41 silica, synthesized by the same method, also displayed a low catalytic activity for the reaction, which can be attributed to the presence of weakly acidic surface silanol groups inside the hexagonal mesopores. PUP- and TUP-MSN catalysts only give rise to a minor improvement of reactivity with respect to pure MCM-41.

Table 1. Diels-Alder reaction catalyzed by MSN catalysts.

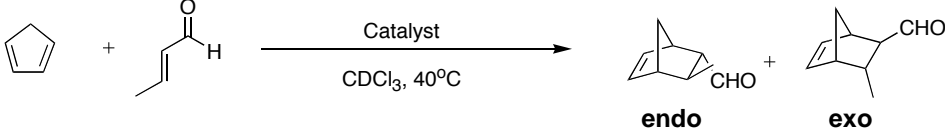
R ₁	R ₂	MSN catalyst	Yield (%) ^a	Selectivity (endo/exo) ^a	TON ^b
H	H	FPUP	93.1	83:17	51.8
		FTUP	82.2	80:20	64.0
		PUP	84.9	80:20	36.7
		TUP	86.9	79:21	33.8
		NC ^c	62.5	77:23	-
H	CH ₃	FPUP	95.3	17:83	5.3
		FTUP	98.4	17:83	7.6
		PUP	81.6	17:83	3.5
		TUP	96.7	16:84	3.8
		NC ^c	45.5	17:83	-
CH ₃	H	FPUP	67.2	83:17	3.7
		FTUP	74.7	70:30	5.8
		PUP	23.0	77:23	1.0
		TUP	34.0	79:21	1.3
		MCM-41 ^d	23.4	77:23	-
		NC ^c	7.7	63:37	-

^a. Yield and selectivity are calculated from ¹H-NMR spectra of supernatant. ^b. TON = mmol product/mmol catalyst during 2 h of reaction time for acrolein and 20 h for other dienophiles. ^c. No catalyst. ^d. Pure MCM-41 silica prepared under the same method without any addition of organotrialkoxysilane.

To study the recyclability of these urea- and thiourea- functionalized MSN catalysts, Diels-Alder reaction of methyl vinyl ketone and cyclopentadiene catalyzed by FPUP-MSN was performed in ten consecutive cycles. The results demonstrated that FPUP-MSN catalyst could be recycled and reused for at least up to ten times without losing the original reactivity as well as selectivity. To examine the difference in the catalytic performance of our heterogeneous materials versus their homogeneous counter part, several reactions with the least reactive dienophile, crotonaldehyde, were conducted, and the results are outlined in

Table 2. We found that the heterogeneous MSN catalysts exhibited a superior catalytic activity than those of homogeneous analogue. Although both physical mixture of homogeneous catalyst and MCM-41 showed some reaction yield, the conversions were much lower than those of the heterogeneous MSN catalysts. It is interesting to note that the mixture of TUP and MCM-41 showed large improvement of reactivity, which was even higher than sum of yield obtained by individual catalyst; whereas PUP and MCM-41 only had similar catalytic activity.

Table 2. Comparison of heterogeneous and homogeneous urea or thiourea catalysts.

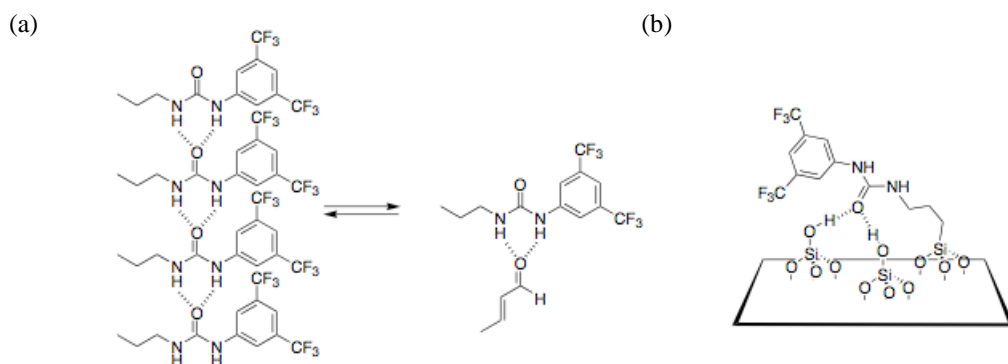


Catalysts	Yield (%)	Selectivity (endo/exo)
FTUP-MSN	74.7	70:30
FTUP+MCM-41 ^a	58.7	81:19
FTUP ^b	12.3	78:22
FPUP-MSN	67.2	83:17
FPUP+MCM-41 ^a	26.5	77:23
FPUP ^b	16.0	68:32
FPUP-MSN(cal) ^c	28.1	74:26

^a. Physical mixture of corresponding homogeneous catalyst and 50.0 mg MCM-41. ^b. Corresponding homogeneous catalyst. ^c. FPUP-TES grafted calcined MSN.

The observed superior reactivity of our heterogeneous catalysts could be rationalized by following two factors: First, the urea compounds are known for their low solubility due to a self-assembled supramolecular structure through hydrogen bonding. A pre-equilibrium of dissociated free urea and urea aggregates was presence in the system as depicted in Scheme 1. Given that only free urea or thiourea can function as catalyst, the equilibrium constant has a profound effect in terms of reactivity, whereas heterogenized urea or thiourea functional

group on the silica wall would prevent the aggregation, which would lead to the observed high reactivity of heterogeneous catalysts. Second, immobilized urea or thiourea functional group might adopt a spatial orientation, in which carbonyl group could point toward the surface and thereby forming two hydrogen bonds with the surface silanol groups. This surface hydrogen bonding between ureido or thioureido and silanol groups increases the Lewis acidity of the catalytic center.



Scheme 1. Pre-equilibrium of urea (or thiourea) network (a) and surface hydrogen bonding between urea or thiourea and silanol group (b).

To find evidence to support this hypothesis, a series of FT-IR studies of heterogeneous MSN catalysts was conducted (see appendix). The observed C=O stretching band of FPUP-TES diluted in CCl_4 (5×10^{-3} M) and in KBr, which represent free urea and urea network, respectively, are 1714.3 and 1657.7 cm^{-1} . The measured C=O stretching band of FPUP-MSN material is 1668.1 cm^{-1} , agreed with our hypothesis of surface hydrogen bonding model. Moreover, given that surface silanol groups transformed to siloxane during the heating process of calcinations, a urea or thiourea grafted MSN catalyst, prepared after calcinations, suppose lose some catalytic activity due to deficit of surface hydrogen bonding

effect. Indeed, the yield obtained from FPUP-MSN(cal) dropped to 28.1 % as showed in Table 2. Both experimental results clearly prove that the profound reactivity of heterogeneous catalysts was originated from surface activation of catalytic site through hydrogen bonding with silica wall.

Conclusion

In conclusion, we have demonstrated that the catalytic activity of urea- and thiourea-functionalized mesoporous silica catalysts can be fine-tuned through surface hydrogen bonding with the silanol groups of the solid support. We envision that this new concept for catalyst design can be applied to other inorganic based heterogeneous catalysts.

References

- (1) Corma, A. *Chem. Rev.* **1997**, *97*, 2373-2419.
- (2) Lim, M. H.; Stein, A. *Chem. Mater.* **1999**, *11*, 3285-3295.
- (3) Stein, A. *Adv. Mater.* **2003**, *15*, 763-775.
- (4) Stein, A.; Melde, B. J.; Schroden, R. C. *Adv. Mater.* **2000**, *12*, 1403-1419.
- (5) De Juan, F.; Ruiz-Hitzky, E. *Adv. Mater.* **2000**, *12*, 430-432.
- (6) Johnson, B. F. G.; Raynor, S. A.; Shephard, D. S.; Mashmeyer, T.; Mashmeyer, T.; Thomas, J. M.; Sankar, G.; Bromley, S.; Oldroyd, R.; Gladden, L.; Mantle, M. D. *Chem. Commun.* **1999**, 1167-1168.
- (7) Mal, N. K.; Fujiwara, M.; Tanaka, Y. *Nature* **2003**, *421*, 350-353.
- (8) Jones, C. W.; McKittrick, M. W.; Nguyen, J. V.; Yu, K. *Top. Catal.* **2005**, *34*, 67-76.

- (9) McKittrick, M. W.; Jones, C. W. *J. Am. Chem. Soc.* **2004**, *126*, 3052-3053.
- (10) Cassiers, K.; Linszen, T.; Mathieu, M.; Benjelloun, M.; Schrijnemakers, K.; Van Der Voort, P.; Cool, P.; Vansant, E. F. *Chem. Mater.* **2002**, *14*, 2317-2324.
- (11) Igarashi, N.; Hashimoto, K.; Tatsumi, T. *J. Mater. Chem.* **2002**, *12*, 3631-3636.
- (12) Igarashi, N.; Koyano, K. A.; Tanaka, Y.; Nakata, S.; Hashimoto, K.; Tatsumi, T. *Microporous Mesoporous Mater.* **2003**, *59*, 43-52.
- (13) Kruk, M.; Jaroniec, M.; Sayari, A. *Microporous Mesoporous Mater.* **1999**, *27*, 217-229.
- (14) Kumar, R.; Chen, H.-T.; Escoto, J. L. V.; Lin, V. S. Y.; Pruski, M. *Chem. Mater.* **2006**, *18*, 4319-4327.
- (15) Caravajal, G. S.; Leyden, D. E.; Quinting, G. R.; Maciel, G. E. *Anal. Chem.* **1988**, *60*, 1776-86.
- (16) Kanan, S. M.; Tze, W. T. Y.; Tripp, C. P. *Langmuir* **2002**, *18*, 6623-6627.
- (17) McKittrick, M. W.; Jones, C. W. *Chem. Mater.* **2003**, *15*, 1132-1139.
- (18) Bass, J. D.; Solovyov, A.; Pascall, A. J.; Katz, A. *J. Am. Chem. Soc.* **2006**, *128*, 3737-3747.
- (19) Defreese, J. L.; Hwang, S.-J.; Parra-Vasquez, A. N. G.; Katz, A. *J. Am. Chem. Soc.* **2006**, *128*, 5687-5694.
- (20) Notestein, J. M.; Iglesia, E.; Katz, A. *J. Am. Chem. Soc.* **2004**, *126*, 16478-16486.
- (21) Notestein, J. M.; Katz, A. *Chem. Eur. J.* **2006**, *12*, 3954-3965.
- (22) Dalko, P. I.; Moisan, L. *Angew. Chem. Int. Ed.* **2001**, *40*, 3726-3748.
- (23) McCooey, S. H.; Connon, S. J. *Angew. Chem. Int. Ed.* **2005**, *44*, 6367-6370.
- (24) Okino, T.; Hoashi, Y.; Takemoto, Y. *J. Am. Chem. Soc.* **2003**, *125*, 12672-12673.

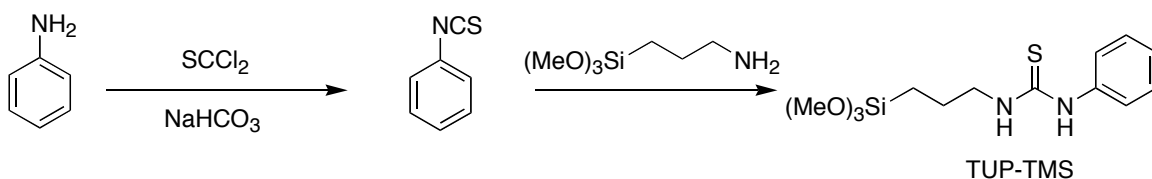
- (25) Okino, T.; Hoashi, Y.; Takemoto, Y. *Tetrahedron Lett.* **2003**, *44*, 2817-2821.
- (26) Schreiner, P. R. *Chem. Soc. Rev.* **2003**, *32*, 289-296.
- (27) Schreiner, P. R.; Wittkopp, A. *Org. Lett.* **2002**, *4*, 217-220.
- (28) Schuster, T.; Bauch, M.; Duerner, G.; Goebel, M. W. *Org. Lett.* **2000**, *2*, 179-181.
- (29) Taylor, M. S.; Jacobsen, E. N. *Angew. Chem. Int. Ed.* **2006**, *45*, 1520-1543.
- (30) Wittkopp, A.; Schreiner, P. R. *Chem. Eur. J.* **2003**, *9*, 407-414.
- (31) Chen, H.-T.; Huh, S.; Wiench, J. W.; Pruski, M.; Lin, V. S. Y. *J. Am. Chem. Soc.* **2005**, *127*, 13305-13311.
- (32) Huh, S.; Chen, H.-T.; Wiench, J. W.; Pruski, M.; Lin, V. S. Y. *J. Am. Chem. Soc.* **2004**, *126*, 1010-1011.
- (33) Huh, S.; Chen, H.-T.; Wiench, J. W.; Pruski, M.; Lin, V. S. Y. *Angew. Chem. Int. Ed.* **2005**, *44*, 1826-1830.
- (34) Huh, S.; Wiench, J. W.; Trewyn, B. G.; Song, S.; Pruski, M.; Lin, V. S. Y. *Chem. Commun.* **2003**, 2364-2365.
- (35) Huh, S.; Wiench, J. W.; Yoo, J.-C.; Pruski, M.; Lin, V. S. Y. *Chem. Mater.* **2003**, *15*, 4247-4256.

Appendix

Experimental section

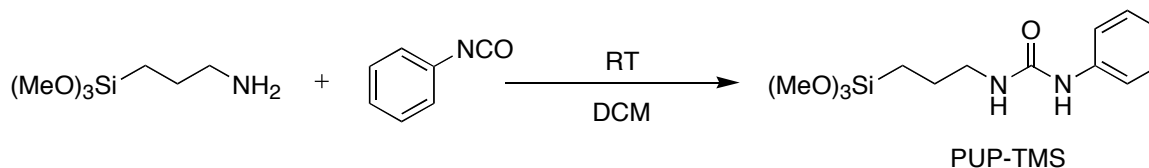
General procedure for urea/thiourea organosilane formation

3-(3-phenyl thioureido) propyl trimethoxysilane (TUP-TMS):



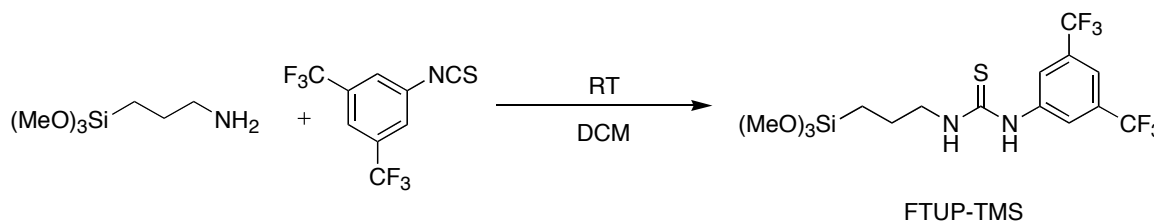
Phenyl amine (2.6 ml, 28.35 mmol) was added to a mixture of saturated sodium bicarbonate aqueous solution (100 ml) and dichloromethane (100 ml) at 0°C and stirred for 20 min. After stop stirring, thiophosgene (2.4 ml, 31.15 mmol) was added to dichloromethane layer in one portion. The resulting solution was stirred vigorously for 1.5 h at 0°C. The reaction was transferred to a separation funnel and extracted by dichloromethane (20 ml x 3). The organic layer was combined and dried by MgSO₄. Solvent removal in vacuo afforded crude phenyl thioisocyanate. The crude thioisocyanate was further added to a solution of 3-aminopropyl trimethoxysilane (5 ml, 28.35 mmol) in dichloromethane (20 ml), followed by stirring at 25°C for 30 min. Extra solvent was removed in vacuo. The resulting yellow oil was loaded to a silica gel column and chromatographed (CH₂Cl₂: CH₃COCH₃ = 10:1) to afford light yellow solid (4.4 g, 25% yield). IR spectrum (KBr, cm⁻¹) 3258.0, 3162.1, 1596.5, 1536.5, 1194.2, 1081.5, 813.5; ¹H NMR spectrum (400 MHz, CD₃COCD₃) δ 8.80 (br s, 1H), 7.50~7.30 (m, 4H), 7.21 (br s, 1H), 7.16 (m, 1H), 3.59 (m, 2H), 3.52 (s, 9H), 1.71 (m, 2H), 0.63 (m, 2H); ¹³C NMR spectrum (100 MHz, CD₃COCD₃) δ 182.3, 139.7, 130.0, 126.0, 125.0, 50.7, 48.0, 23.1, 7.2; LRMS (EI) *m/z*: 314 [M⁺].

3-(3-phenyl ureido) propyl trimethoxysilane (PUP-TMS):



Phenyl isocyanate (6.2 ml, 56.7 mmol) was added dropwise to a solution of 3-aminopropyl trimethoxysilane (10 ml, 56.7 mmol) in dichloromethane (200 mL) at 25°C. The resulting solution was stirred at 25°C for 30 min, then concentrated in vacuo. The product was purified through column chromatography (CH_2Cl_2 : CH_3COCH_3 = 7:1) to obtain white waxy solid (5.1 g, 30% yield). IR spectrum (KBr, cm^{-1}) 3342.6, 3044.5, 1648.7, 1597.9, 1563.0, 1442.8, 1085.8, 820.1; ^1H NMR spectrum (400 MHz, CD_3COCD_3) δ 7.84 (br s, 1H), 7.47 (d, $J=8.0\text{Hz}$, 2H), 7.20(m, 2H), 6.90 (m, 1H), 5.78 (br s, 1H), 3.53 (s, 9H), 3.18 (m, 2H), 1.59 (m, 2H), 0.63 (m, 2H); ^{13}C NMR spectrum (100 MHz, CD_3COCD_3) δ 156.2, 141.8, 129.5, 122.1, 118.9, 50.7, 43.1, 24.4, 7.1; LRMS (EI) m/z : 298 [M^+].

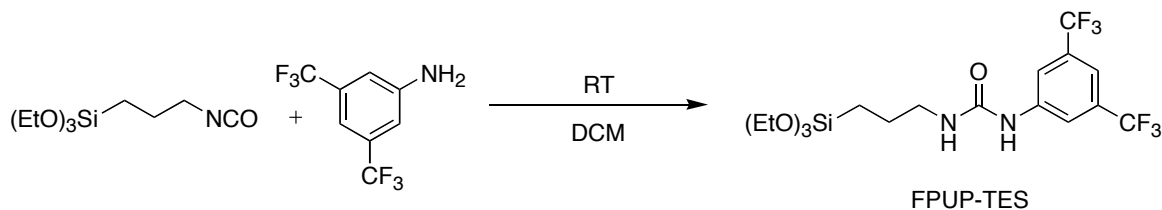
3-[3-(3,5-ditrifluoromethyl phenyl)-thioureido)]-propyl trimethoxysilane (FTUP-TMS):



The general procedure described above was performed on 11.33 mmol scale, using 1.0 equivalent 3,5-ditrifluoromethyl phenyl amine. After 30min the resulting solution was concentrated in vacuo to afford an analytically pure white solid product (5.0 g, 98% yield). IR spectrum (KBr, cm^{-1}) 3204.8, 3036.4, 1548.6, 1134.7, 1074.6, 892.7; ^1H NMR spectrum (400 MHz, CD_3COCD_3) δ 8.32 (s, 2H), 7.70 (s, 1H), 3.62 (m, 2H), 3.54 (s, 9H), 1.75 (m,

2H), 0.67 (m, 2H); ^{13}C NMR spectrum (100 MHz, CD_3COCD_3) δ 181.4, 142.1, 131.1 (q, $J = 33.2\text{Hz}$), 123.5 (q, $J = 270.3\text{Hz}$), 122.5, 116.5, 49.8, 46.8, 22.0, 6.3; LRMS (EI) m/z : 450 $[\text{M}^+]$.

3-[3-(3,5-ditrifluoromethyl phenyl)-ureido)]-propyl triethoxysilane (FPUP-TES):



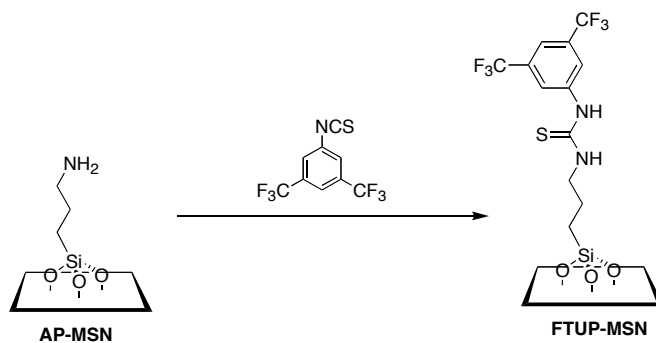
3,5-Ditrifluoromethyl phenyl amine (0.69 ml, 4.44 mmol) was added dropwise to a solution of 3-triethoxysilyl propyl isocyanate (1.10 ml, 4.44 mmol) in dichloromethane (20 ml) at 25°C. The resulting solution was refluxed overnight. After cooling to ambient temperature, the solution was concentrated in vacuo, followed by the addition of hexane (20 ml) to precipitate product. The white tiny crystal was isolated by filtration to obtain a pure compound (1.13 g, 53.4% yield). IR spectrum (KBr, cm^{-1}) 3337.6, 3121.5, 1657.7, 1588.9, 1130.3, 956.4; ^1H NMR spectrum (400 MHz, CD_3COCD_3) δ 8.54 (br s, 1H), 8.16 (s, 2H), 7.51 (s, 1H), 6.12 (br s, 1H), 3.81 (q, $J=7.2$ Hz, 6H), 3.22 (m, 2H), 1.62 (m, 2H), 1.18 (t, $J=7.2$ Hz, 9H), 0.67 (m, 2H); ^{13}C NMR spectrum (100 MHz, CD_3COCD_3) δ 154.7, 142.9, 131.46 (q, $J = 32.5\text{Hz}$), 123.7 (q, $J = 270.3\text{Hz}$), 117.5, 113.7, 57.6, 42.3, 23.5, 17.8, 7.5; LRMS (EI) m/z : 476 $[\text{M}^+]$.

General procedure for MSN material preparation

A solution of cetyltrimethylammonium bromide (CTAB) (1.0 g, 2.75 mmol), 2.0M NaOH(aq) (3.5 ml, 7.0 mmol) in 480 ml H_2O was stirred at 80°C for 30 min. A solution of

organic trialkoxysilane (1.435 mmol) in 2 ml MeOH and tetraethoxysilane (TEOS) (5 ml, 22.42 mmol) were added to the surfactant solution sequentially via syringes. The resulting mixture was stirred at 80°C for 2 h to yield a white solid as synthesized MSN. The as synthesized material was isolated by filtration, washed by copious amounts of H₂O and MeOH, and then drying in vacuo. The surfactant removal was performed by acid extraction. In a typical method, as-made MSN (1.0 g) was stirred in a 100 ml methanolic solution of concentrated hydrochloric acid (0.6 ml) at 60°C for 3 h. The resulting extracted MSN was obtained by filtration, washing by H₂O and MeOH, and dried in vacuo.

Synthesis of FTUP-MSN material



A solution of 3,5-bis(trifluoromethyl)phenyl isothiocyanate (0.24 ml, 1.305 mmol) was added dropwise to the aminopropyl functionalized MSN material (0.58g), prepared according to our previous paper, in 50 ml dichloromethane at 25 °C and stirred for 24 h. The resulting FTUP-MSN material was filtered out, washed thoroughly by acetone, and dried in vacuo.

Synthesis of FPUP grafted calcined MSN [FPUP-MSN(cal)] material.

FPUP-TEOS (76.7 mg, 0.161 mmol) was added to a solution of calcined pure silica MSN material (161 mg) in 10 ml dry toluene solution. The resulting mixture was refluxed for 20 h to graft FPUP functional group on the silica surface. The final FPUP functionalized calcined MSN catalyst was filtered out, washed thoroughly by acetone, and dried in vacuo.

General procedure for Diels-Alder reaction

The kinetic study was carried out in a solution of methyl vinyl ketone (15.5 μ l, 0.189 mmol), fresh distilled cyclopentadiene (0.16 ml, 1.928 mmol), and respective MSN catalyst (5.0 mg) in 2 ml CDCl_3 , stirred at 25°C. The reaction conversion was calculated from the ^1H NMR spectra of supernatants.

Figure Caption

Figure S1. SEM micrographs of FPUP-MSN(a), PUP-MSN(b), FTUP-MSN(c), and TUP-MSN(d). Scale bar = 2.0 μ m.

Figure S2. N_2 adsorption/desorption isotherms of FPUP-MSN(a), PUP-MSN(b), FTUP-MSN(c), and TUP-MSN(d). Insets are BJH pore size distributions of pertinent MSN catalysts.

Figure S3. Recycling test of FPUP-MSN catalyst.

Tables

Table S1. Textual properties of urea or thiourea functionalized MSN catalysts.

Materials	S_{BET} (m ² /g) ^a	V_p (cm ³ /g) ^a	W_{BJH} (nm) ^a
FPUP-MSN	803.1	0.72	2.6
FTUP-MSN	593.0	0.43	2.8
PUP-MSN	1029.1	1.03	2.5
TUP-MSN	881.0	0.86	2.6
FPUP-MSN(cal) ^b	961.9	0.48	2.4

^a The BET surface area (S_{BET}), the mesopore volume (V_p), and the mean mesopore width (W_{BJH}) were obtained from the nitrogen adsorption/desorption data. ^b FPUP-TES grafted MSN material, prepared after calcination.

Table S2. FT-IR carbonyl stretching frequencies of FPUP-MSN and its corresponding organic triethoxysilane.

Sample	C=O stretch (cm ⁻¹)
FPUP-TES in CCl ₄ ^a	1714.3
FPUP-TES ^b	1657.7
FPUP-MSN ^b	1668.1

^a. 5×10⁻³ M of FPUP-TES in CCl₄. ^b. measured in KBr.

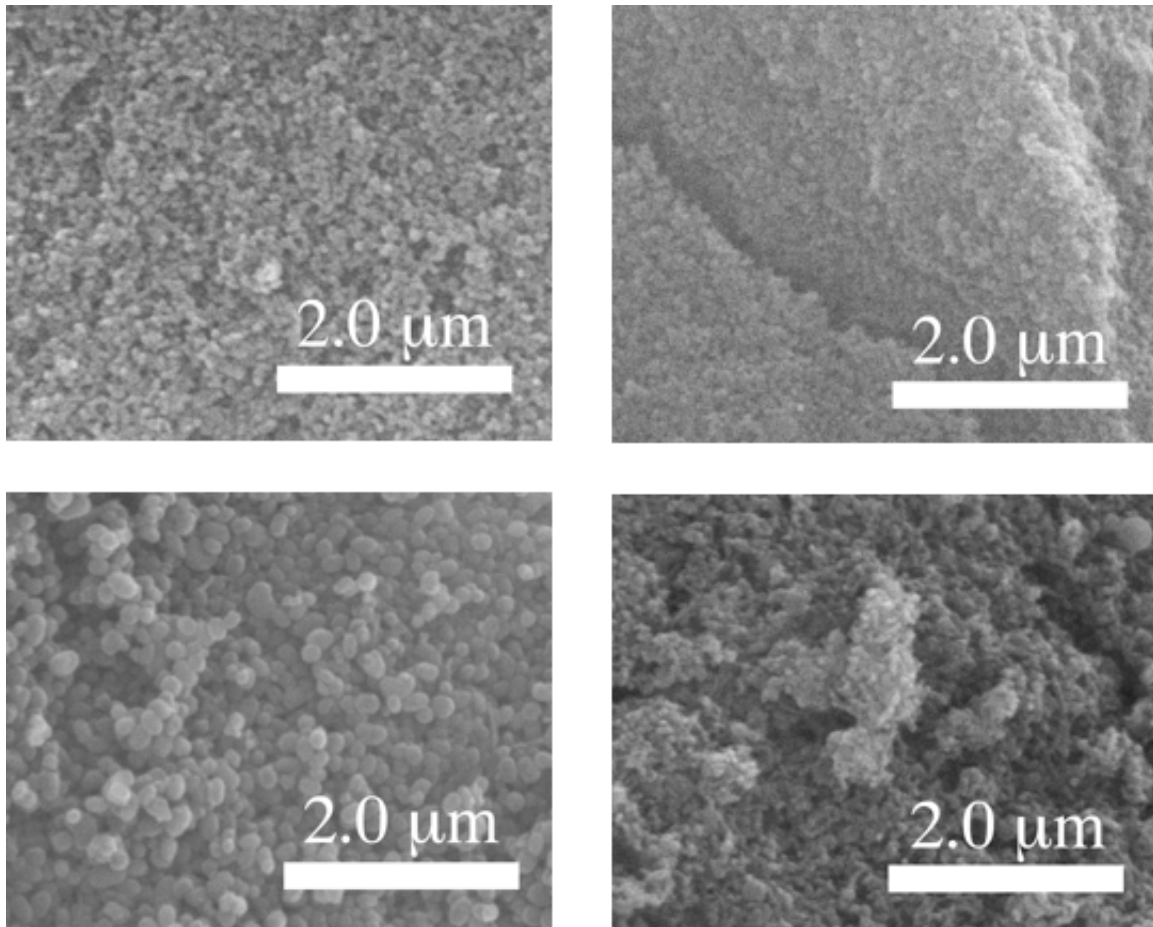
Figure S1.

Figure S2.

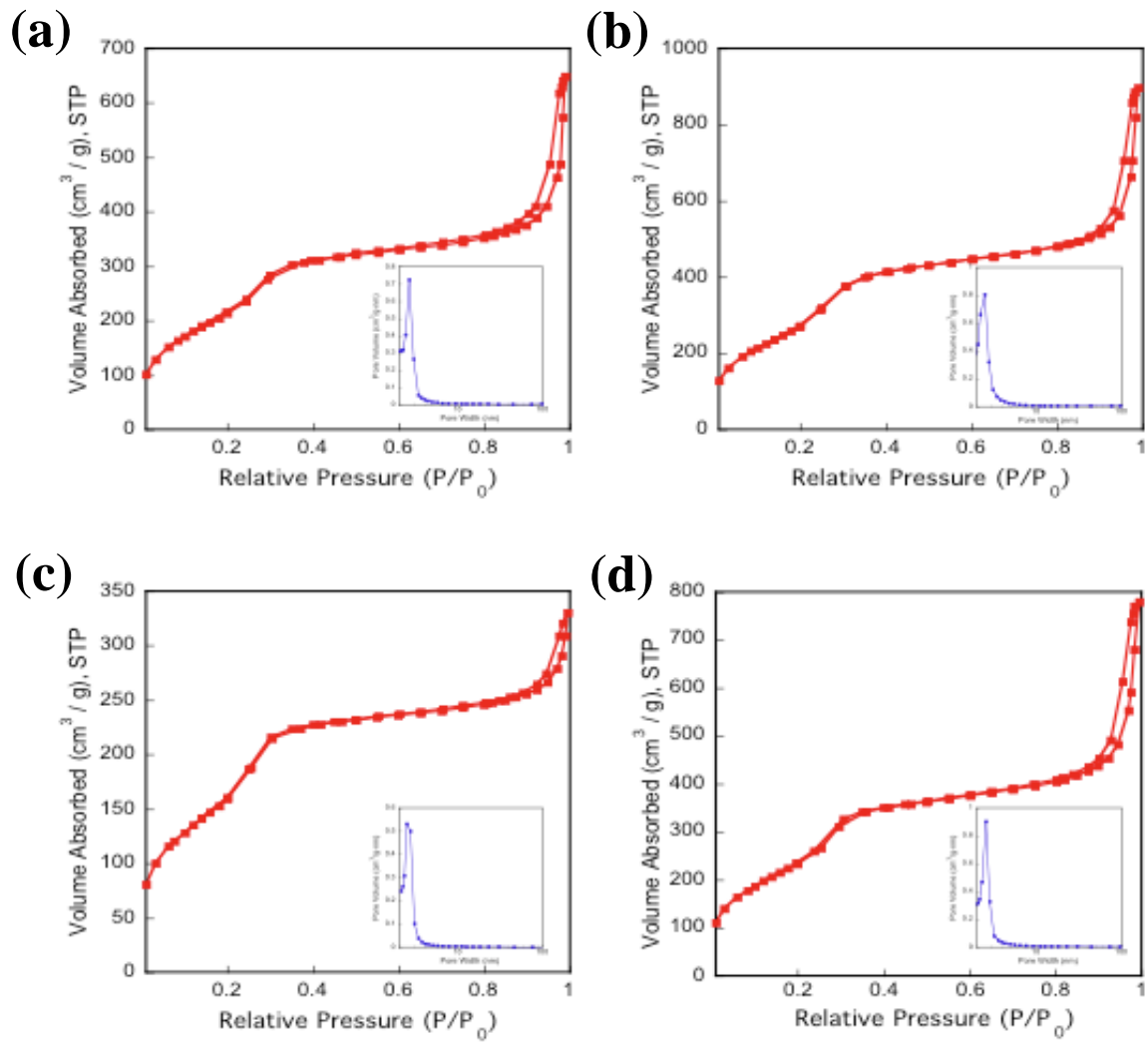
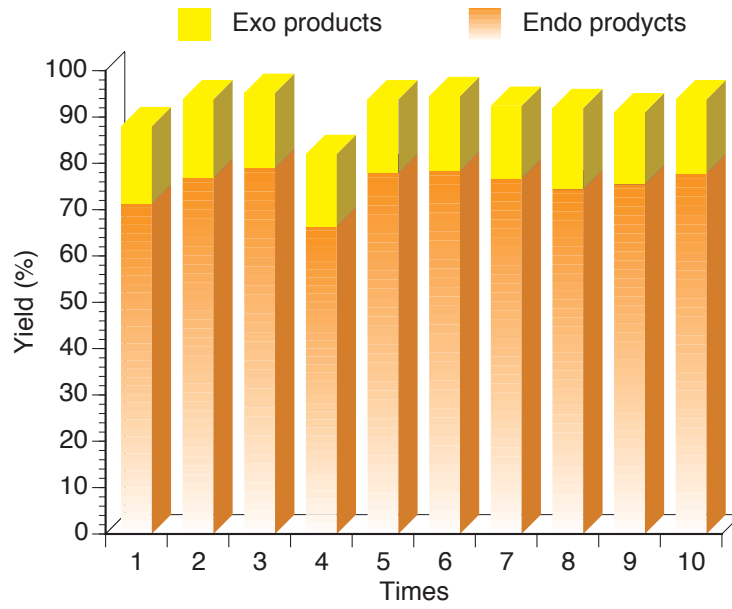


Figure S3.

CHAPTER 4. FINE-TUNING REACTIVITY OF COOPERATIVE GENERAL ACID AND BASE BIFUNCTIONALIZED MESOPOROUS SILICA NANOPARTICLE CATALYSTS

A manuscript in preparation and to be submitted to *Journal of the American Chemical Society*

Hung-Ting Chen, Brian G. Trewyn, Rajeev Kumar, Jerzy W. Wiench, Marek Pruski, and
Victor S.-Y. Lin

Abstract

A series of three general acid and base bifunctional mesoporous silica nanoparticles (MSNs) for reactions involving carbonyl activation has been synthesized. A common 4-dimethylaminopyridine (DMAP) base group and three different urea acid functionalities, 3-[3-(3,5-dinitrofluoromethyl phenyl)-ureido]-propyl (FPUP), 3-(3-phenyl ureido) propyl (PUP), and ureido propyl (UP), have been successfully incorporated into mesoporous silica material by the co-condensation method. The textural properties and relative concentration of organic loading for all bifunctional MSN were investigated by various techniques, including XRD, SEM, TEM, N₂ sorption analysis, and solid-state NMR spectroscopy. By varying three different urea functional groups, we examine the reactivity of these heterogeneous catalysts by a Michael addition of β -nitrostyrene and diethyl malonate. The results indicated that the reactivity of bifunctional MSN catalysts could be fine-tuned by simply manipulating the combination of bifunctionalities on the silica surface.

Introduction

Natural enzyme achieved its superior reactivity and selectivity by utilizing both acid and base segments inside a confined enzymatic pocket to activate substrates and stabilize the transition state in preference to either starting material or product by multiple non-covalent catalytic-substrate interactions.^{1,2} Learning from mother nature, multifunctionalization of solid support with properly spatial arrangement of functionalities in the confined space was pre-required for construction of a perfect heterogeneous catalytic system.³⁻⁵ We recently reported a heterogeneous multifunctionalized mesoporous silica nanoparticle (MSN) catalysis system, which exhibited an enzyme-liked cooperative effect.³ This bifunctional MSN catalysis system involved both general acid and base functionalities within the confined nanospace, which simultaneously activated nucleophile and electrophile of the reaction. By varying the relative concentration of acid and base sites in the bifunctional MSN material, the reactivity of the heterogeneous catalyst could be optimized. In principle, the reactivity and selectivity of such kinds of heterogeneous catalytic system depended on the combination of each functional group because both acid and base groups functioned orthogonally. Herein, we reported a variety of bifunctional MSN catalysts with different acid functional groups to demonstrate that fine-tuning reactivity of these heterogeneous catalysts can be achieved by simply manipulating the combination of immobilized acid and base functionalities.

Result and Discussion

To examine the influence of general acid groups in terms of catalytic activity, we prepared several bifunctional acid and base MSN catalysts with one common base functional

group, 4-dimethylaminopyridine (DMAP), and three different general acid functionalities, 3-[3-(3,5-difluoromethyl phenyl)-ureido]-propyl (FPUP), 3-(3-phenyl ureido) propyl (PUP), and ureido propyl (UP) groups, respectively.^{6,7} These urea groups were chosen based on the order of the double hydrogen bonding ability (FPUP > PUP > UP).^{8,9} All bifunctional MSN catalysts were synthesized via the co-condensation route according to our previous reported method.^{3,6,10-12} The powder X-ray diffraction (XRD) pattern of three bifunctional MSNs exhibited different mesoporous structures as shown in Figure 1. The DMAP/FPUP-MSN showed a disordered mesoporous structure, indicated by a large (100) and weak broad peaks, representing a higher-order diffraction; whereas DMAP/PUP- and DMAP/UP-MSN revealed a hexagonally packed MCM-41 typed mesopores, indicated by three distinct (100), (110), and (200) peaks observed in XRD spectra. The TEM micrographs of bifunctional MSN materials further confirmed the mesoporous structure agreed with the result of XRD spectrum, and also displayed a variety of particle morphology as depicted in Figure 2. The DMAP/FPUP-MSN material showed an agglomeration of tiny round shaped particles. In contrast, the DMAP/PUP-MSN and DMAP/UP-MSN unveiled the elongated curved rod and the oval shaped morphology, respectively. This result implied that particle morphology of MSN catalysts was mainly controlled by ureas rather than the DMAP functional group. The nitrogen sorption analysis of all bifunctionalized MSNs was summarized in the Table S1 of appendix. All three bifunctional MSNs showed a typical type IV BET isotherm without significant hysteresis. The measured BET surfaces of DMAP/FPUP-MSN, DMAP/PUP-MSN, and DMAP/UP-MSN materials were 619.0, 929.1, and 738.4 m²/g, respectively. The mean pore diameters calculated from BJH method were 2.3, 2.7, and 2.6 nm for DMAP/FPUP-, DMAP/PUP-, and DMAP/UP-MSN materials. The structure of organic

functional groups on the silica surface, their relative concentration, and total amount of organic groups loading in each bifunctional MSN were inspected by ^{13}C CPMAS and ^{29}Si DPMAS solid-state NMR spectroscopy. The presence of resonance representing T^2 and T^3 sites indicated the covalent bonds exist between organic functional group and silica surface. The resonance peaks in the ^{13}C CPMAS NMR spectra, assigned on the basis of the solution spectra of the corresponding precursors, also confirmed the successful functionalization of MSNs. The total amount of functional group loading in the DMAP/FPUP-, DMAP/PUP-, and DMAP/UP-MSN materials evaluated from ^{29}Si solid-state NMR studies were 1.49, 1.53, and 0.97 mmol/g. Furthermore, the relative concentration of DMAP functional group in each sample was 0.72, 0.56, and 0.75 mmol/g for DMAP/FPUP-, DMAP/PUP-, and DMAP/UP-MSN, respectively.

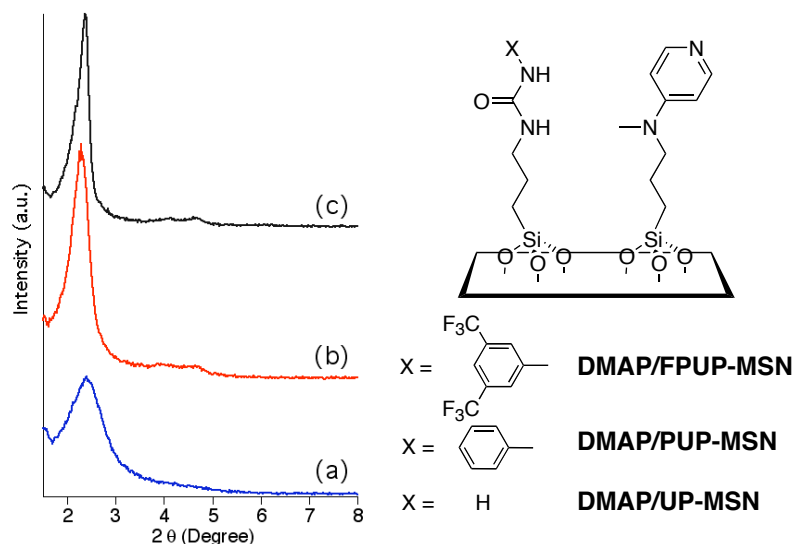


Figure 1. Powder X-ray diffraction (XRD) pattern (left) of DMAP/FPUP-MSN (a), DMAP/PUP-MSN (b), DMAP/UP-MSN (c), and chemical structure of bifunctional DMAP/Urea-MSN materials (right).

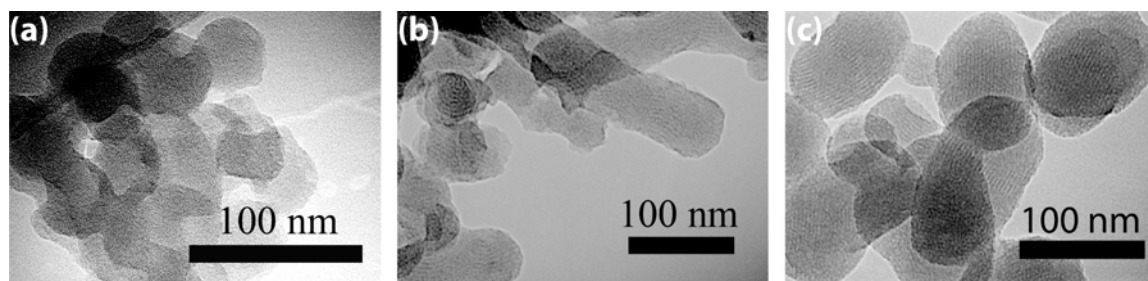


Figure 2. TEM micrographs of DMAP/FPUP-MSN (a), DMAP/PUP-MSN (b), and DMAP/UP-MSN (c); scale bar = 100 nm.

To investigate the reactivity performance of each heterogeneous bifunctional MSN catalyst, a Michael addition reaction of β -nitrostyrene and diethyl malonate was conducted, and the result was outlined in the Table 1.¹³⁻¹⁷ The twofold to sixth fold reactivity enhancement was observed in all bifunctionalized MSN catalysts compared to their mono-functionalized MSN. Moreover, the reactivity of all bifunctionalized MSNs was higher than their physical mixture of DMAP-MSN and coresponding urea functionalized MSN, which implied a cooperative effect of both functionalities, resulting in dual activation of the nucleophile by DMAP through deprotonation and the electrophile by urea through double hydrogen bonding as depicted in Figure 3. Comparing the catalytic performance of three urea functional groups, the reactivity of bifunctionalized MSN catalysts were following the order: DMAP/FPUP-MSN \approx DMAP/PUP-MSN>DMAP/UP-MSN. Given the fact that three catalysts contained similar amount of urea groups, the enhanced reactivity of bifunctional MSNs could not be rationalized by the “dilution effect” of secondary group. Indeed, this result strongly supported the cooperative effect due to the proximity of general acid and base functional groups in the confined mesoporous nanospace. Although FPUP functional group possessed stronger ability of hydrogen bonding than PUP group, the DMAP/FPUP- and DMAP/PUP-MSNs still exhibited similar reactivity. This contradict result might be

attributed to the different spatial orientation of bifunctionalities inside the mesoporous channels. However, the distribution of immobilized functional groups was still under investigation.

Table 1. Michael addition reaction of β -nitrostyrene and diethyl malonate catalyzed by MSN catalysts.

Catalysts ^a	Yield (%) ^b	TON ^c
DMAP/FPUP-MSN	78.0	4.1
DMAP/PUP-MSN	65.9	4.4
DMAP/UP-MSN	34.1	1.7
DMAP-MSN+FPUP-MSN ^d	26.7	1.3
DMAP-MSN+ PUP-MSN	17.6	0.9
DMAP-MSN	26.9	0.7
FPUP-MSN	6.2	-
PUP-MSN	0.0	-

^a. Reaction condition: β -nitrostyrene/diethyl malonate=1/5, catalyst 50.0 mg in 0.5 mL toluene at room temperature for 20 h. ^b. Isolated yield. ^c. TON = mmol product/ mmol of DMAP functional group in the catalyst during 20 h reaction time. ^d. Physical mixture of corresponding monofunctionalized MSN catalysts.

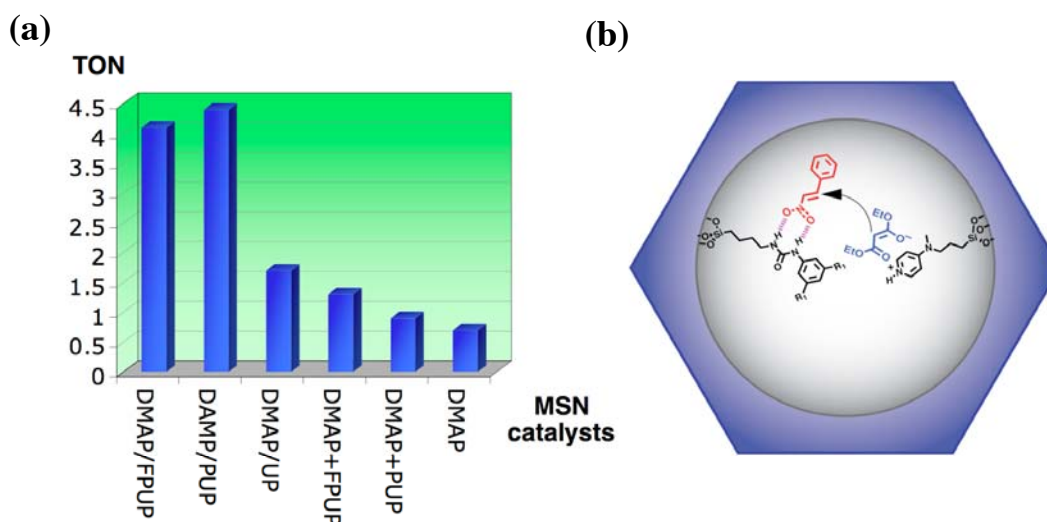


Figure 3. (a) Diagram showing the TONs for the Michael addition reaction with various MSN catalysts. (b) Schematic representation of dual activation of cooperative bifunctional acid and base MSN catalyst.

Conclusion

In conclusion, we demonstrated the catalytic ability of bifunctionalized MSN catalyst could be fine-tuned by manipulating the combination of bifunctional groups. By introducing urea functional group with superior hydrogen bonding ability, we were able to increase the reactivity performance of heterogeneous MSN catalysts up to sixth fold. We believe this novel heterogeneous catalysis design could apply for other mesoporous metal oxide such as TiO_2 or ZrO_2 , which led to more reactive and selective heterogeneous catalysts.

References

- (1) Wharton, C. W. *Comprehensive Biological Catalysis*; Academic Press, London, 1998; Vol. 1.
- (2) White, A. J.; Wharton, C. W. *Biochem. J.* **1990**, *270*, 627-37.
- (3) Huh, S.; Chen, H.-T.; Wiench, J. W.; Pruski, M.; Lin, V. S. Y. *Angew. Chem. Int. Ed.* **2005**, *44*, 1826-1830.
- (4) Alauzun, J.; Mehdi, A.; Reye, C.; Corriu, R. J. P. *J. Am. Chem. Soc.* **2006**, *128*, 8718-8719.
- (5) Zeidan, R. K.; Hwang, S.-J.; Davis, M. E. *Angew. Chem. Int. Ed.* **2006**, *45*, 6332-6335.
- (6) Chen, H.-T.; Huh, S.; Wiench, J. W.; Pruski, M.; Lin, V. S. Y. *J. Am. Chem. Soc.* **2005**, *127*, 13305-13311.
- (7) Chen, H.-T.; Trewyn, B. G.; Rajeev, K.; Wiench, J. W.; Pruski, M.; Lin, V. S. Y.
- (8) Wittkopp, A.; Schreiner, P. R. *Chem. Eur. J.* **2003**, *9*, 407-414.

- (9) Schreiner, P. R. *Chem. Soc. Rev.* **2003**, *32*, 289-296.
- (10) Huh, S.; Chen, H.-T.; Wiench, J. W.; Pruski, M.; Lin, V. S. Y. *J. Am. Chem. Soc.* **2004**, *126*, 1010-1011.
- (11) Huh, S.; Wiench, J. W.; Trewyn, B. G.; Song, S.; Pruski, M.; Lin, V. S. Y. *Chem. Commun.* **2003**, 2364-2365.
- (12) Huh, S.; Wiench, J. W.; Yoo, J.-C.; Pruski, M.; Lin, V. S. Y. *Chem. Mater.* **2003**, *15*, 4247-4256.
- (13) Okino, T.; Hoashi, Y.; Takemoto, Y. *J. Am. Chem. Soc.* **2003**, *125*, 12672-12673.
- (14) Okino, T.; Hoashi, Y.; Furukawa, T.; Xu, X.; Takemoto, Y. *J. Am. Chem. Soc.* **2005**, *127*, 119-125.
- (15) McCooey, S. H.; Connon, S. J. *Angew. Chem. Int. Ed.* **2005**, *44*, 6367-6370.
- (16) Connon, S. J. *Chem. Eur. J.* **2006**, *12*, 5419-5427.
- (17) Taylor, M. S.; Jacobsen, E. N. *Angew. Chem. Int. Ed.* **2006**, *45*, 1520-1543.

Appendix

Experimental section

All reagents and chemicals were used as received from commercial vendors without any further purification. Toluene was dried over CaH_2 and distilled before use. All three organic trialkoxysilanes, 4-[N-[3-(triethoxysilyl)propyl]-N-methyl-amino]pyridine (DMAP-TES), 3-[3-(3,5-dinitrofluoromethyl phenyl)-ureido]-propyl triethoxysilane (FPUP-TES), and 3-(3-phenyl ureido) propyl trimethoxysilane (PUP-TMS), were prepared according to our previous reports. The preparative thin-layer chromatography plate (silica gel with UV254, 1000 μ) was purchased from Analtech, Inc.

General synthesis of acid and base bifunctional MSN material

A solution of cetyltrimethylammonium bromide (CTAB) (1.0 g, 2.75 mmol), 2.0M NaOH(aq) (3.5 ml, 7.0 mmol) in 480 ml H_2O was stirred at 80°C for 30 min. A solution of 4-[N-[3-(triethoxysilyl)propyl]-N-methyl-amino]pyridine (DMAP-TES) (448.3 mg, 1.435 mmol), corresponding urea organic trialkoxysilane (1.435 mmol) in 2 ml MeOH and tetraethoxysilane (TEOS) (5 ml, 22.42 mmol) were added to the surfactant solution sequentially via syringes. The resulting mixture was stirred at 80°C for 2 h to yield a white solid as synthesized MSN. The as synthesized material was isolated by filtration, washed by copious amounts of H_2O and MeOH, and then drying in vacuo. The surfactant removal was performed by acid extraction. In a typical method, as-made MSN (1.0 g) was stirred in a 100 ml methanolic solution of concentrated hydrochloric acid (0.6 ml) at 60°C for 3 h. The resulting extracted MSN was obtained by filtration, washing by H_2O and MeOH, and dried in vacuo.

General procedure of Michael addition reaction

A mixture of β -nitrostyrene (28.0 mg, 0.188 mmol) and bifunctional MSN catalyst (50.0 mg) was charged to a screw-capped test tube. A solution of diethyl malonate (0.057 ml, 0.38 mmol) in 1 ml dry toluene was introduced to the test tube via syringe. The resultant solution was stirred in the room temperature for 24 h. After removing solid catalyst by filtration, the filtrate was concentrated to obtain an oily yellowish crude. The crude was further purified by preparative thin-layer chromatography with eluent (Ether/Hexane = 5/1) to yield the Michael addition product. The ^1H and ^{13}C NMR spectra of the product were found identical with reported data.¹³⁻¹⁵

Table S1. Textual properties of bifunctional MSN catalysts.

MSNs	S_{BET} (m^2/g) ^a	V_{p} (cm^3/g) ^a	W_{BJH} (nm) ^a
DMAP/FPUP	619.0	0.51	2.3
DMAP/PUP	929.1	0.69	2.7
DMAP/UP	738.4	0.53	2.6

^a The BET surface area (S_{BET}), the mesopore volume (V_{p}), and the mean mesopore width (W_{BJH}) were obtained from the nitrogen adsorption/desorption data. ^b The d_{100} numbers represent the d -spacing corresponding to the main (100) XRD peak. The unit cell size (a_0) is calculated from the d_{100} data using $a_0 = 2d_{100}/3^{1/2}$. The pore wall thickness ($d_{\text{pore wall}} = a_0 - W_{\text{BJH}}$).

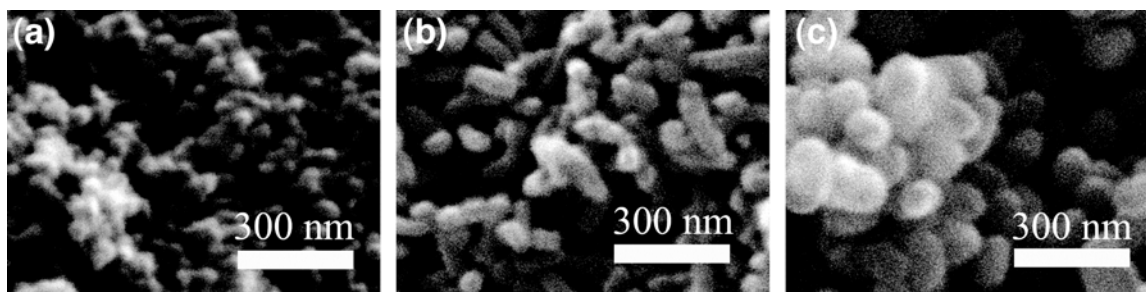


Figure S1. SEM micrographs of DMAP/FPUP-MSN (a), DMAP/PUP-MSN (b), and DMAP/UP-MSN (c).

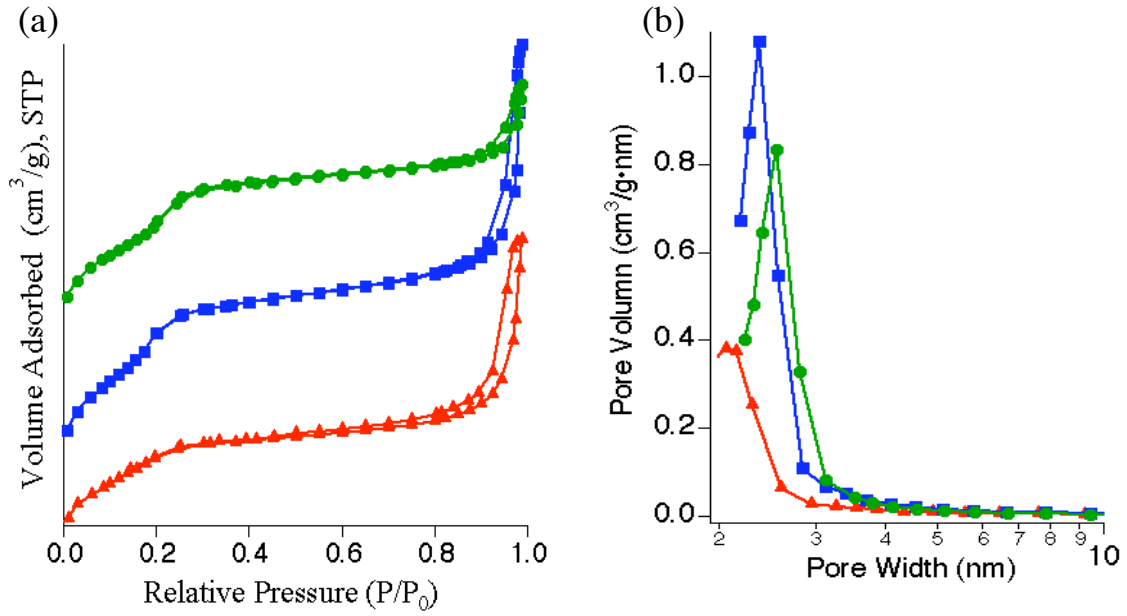


Figure S2. BET isotherm diagram (a) and BJH pore size distribution (b) of DMAP/FPUP-MSN (red), DMAP/PUP-MSN (blue), and DMAP/UP-MSN (green).

CHAPTER 5. SYNTHESIS AND CHARACTERIZATION OF CONJUGATED POLY(*p*-PHENYLENE ETHYNYLENE)- ENCAPSULATED MESOPOROUS SILICA NANOCOMPOSITE MATERIALS (PPE-MSN)

A manuscript in preparation and to be submitted to *Chemical Communication*

Hung-Ting Chen, Jerzy W. Wiench, Marek Pruski, and Victor S.-Y. Lin

Abstract

We developed a new synthetic method for the immobilization of transition metal complex on the interior surface of mesoporous silica nanosphere (MSN) material. As a proof of principle, we synthesized a novel Pd(II)-functionalized mesoporous silica nanosphere (Pd-MSN) material by using a radical coupling reaction between a Pd (II) complex **1** and our previously reported thiol-functionalized mesoporous silica nanosphere (MSN-SH). The resultant Pd-MSN material remained regular hexagonally-packed mesopore structure and spherical particle morphology with Pd(II) catalytic sites evenly distributed inside the mesoporous channels. We demonstrated that the Pd-MSN material could efficiently catalyze a Sonogashira cross-coupling-based polymerization of various 1,4-dialkoxy-2,5-diiodobenzenes with 1,4-diethynylbenzene. In contrast to the same poly(*p*-phenylene ethynylene) (PPE) polymers synthesized in homogeneous solutions, the PPE-MSN composite materials exhibited unprecedented large Stoke's shifts and bathochromic shifts in their fluorescence emission bands.

Introduction

Several recent reports have demonstrated that highly conjugated conducting polymers encapsulated within the structural ordered mesoporous silica materials exhibited interesting photophysical and electronic properties, which could lead to further developments of new optical and electronic nanodevices.¹⁻⁹ In particular, the regular hexagonal mesoporous structures of the MCM-41 silica matrix have been shown to be able to protect these molecular wires from oxidation, while providing a well-aligned one-dimensional channel-like structure for directional polymer growth. Our group have reported on the synthesis of a poly(phenylene butadiynylene) encapsulated inside of a MCM-41 type, copper-functionalized mesoporous silica nanoparticle (PPB-MSN) material.⁷ To apply this synthetic strategy to other π -conjugated conducting polymers, the development of a universal synthetic method is necessary for immobilizing diverse transition metal complexes on the surface of interior mesoporous channels of MSNs.

Immobilization of transitional metal complexes on the mesoporous silica surface is of enormous interest to many research groups worldwide because of the possible benefits of enhancing the catalytic reactivity of these complexes and obtaining high degrees of recyclability. Among all transition metal complexes, palladium-based transition metal complexes are perhaps the most widely used catalysts. Pd (II) complex functionalized mesoporous silicas have been synthesized previously by preparing simple organic ligand tethered MCM-41 materials such as amine or thiol functionalities through a post-grafting method, followed by an impregnation with a Pd (II) precursor solution.¹⁰⁻¹⁴ However, the grafting method usually resulted in an inhomogeneous distribution of catalytic sites on the

solid surface, and the positive charges of the Pd precursors often induced a non-specific adsorption with both the immobilized ligands and the anionic silicate surface.¹⁵ This inhomogeneous spatial distribution of catalysts on the silica walls has been attributed to the inefficient encapsulation of conducting polymers inside the pores of many mesoporous silica materials.⁷ Furthermore, most Pd (II) complexes were not stable enough against acid- or base-induced oxidation in the condensation reaction of silicate for the synthesis of mesoporous silica materials. To circumvent these problems, we have developed a new synthetic approach to prepare Pd (II) functionalized mesoporous silica nanosphere (Pd-MSN) catalyst by coupling Pd (II) complex precursor contained a pendent double bond with a thiol functionalized mesoporous silica nanosphere (MSN-SH) synthesized through co-condensation method via a radical reaction. Given that most immobilized thiol functional groups are located inside the mesoporous channels of MSNs and the Pd (II) complex precursors only react with the surface tethered thiol groups, this synthetic approach could ensure a homogeneous spatial distribution of Pd (II) catalytic sites, located on the interior pore surface.

Experimental Section

All reagents and chemicals were used as received from commercial vendors without any further purification. The bidentate phosphine ligand was synthesized according to the literature preparation.¹⁶ Thiol functionalized MSN (MSN-SH) was prepared based on our previous report.¹⁷⁻²³ The loading amount of thiol functional group in the MSN-SH material calculated from the 2-Aldrithiol method was 0.7 mmol/g.^{22,23} The 1,4-dialkoxy-2,5-diiodobenzene monomers was synthesized according to a reported method.²⁴

Dichloromethane, chloroform, and toluene was dried over calcium hydride and distilled before use. Tetrahydrofuran was dried over sodium and distilled before use.

Preparation of bis(diphenylphosphinomethyl) allylamine palladium (II) dichloride (1): A solution of bis(acetonitrile) dichloropalladium (II) (0.16 g, 0.61 mmol) in dichloromethane (14 mL) was placed in a 100 mL two-necked round bottle flask equipped with an additional funnel. A solution of bis(diphenylphosphinomethyl) allylamine (0.28 g, 0.61 mmol) in dichloromethane (22 mL) was added to the palladium complex solution dropwisely. During the slow addition, the color of solution changed from orange to light yellow due to the ligand exchange process. After addition, the solution was stirred further for 1h at room temperature. The resultant solution was filtered through a short column of celite under the N₂ atmosphere, and reduced volume to 20 mL by rotary evaporator. Acetone (20 mL) was added to solution to crystallize product. The light yellow product was collected by filtration, followed by wash with copious amount of acetone. The Pd (II) complex was obtained after dried under vacuum (0.21 g, 54 %). ¹H NMR spectrum (400 MHz, CDCl₃) δ 7.88~7.82 (m, 8H), 7.81~7.36 (m, 12H), 5.48~5.61 (m, 1H), 5.20~5.11 (m, 2H), 3.35 (br s, 4H), 3.22 (d, J=9.2Hz, 2H); ³¹P NMR spectrum (160 MHz, CDCl₃) δ 8.56 (s).

Synthesis of Pd(II) functionalized mesoporous silica nanoaphere (Pd-MSN): A mixture of palladium complex **1** (0.16 g, 0.25 mmol), α,α'-azoisobutyronitrile (AIBN) (5.0 mg, 0.03 mmol), and MSN-SH (0.3g) was placed in a 25 mL two necked round-bottom flask equipped with a condenser. A deoxidized chloroform solution (10 mL) was injected to flask through syringe. The whole solution was allowed to stir at 80 °C for 2 d. The resultant

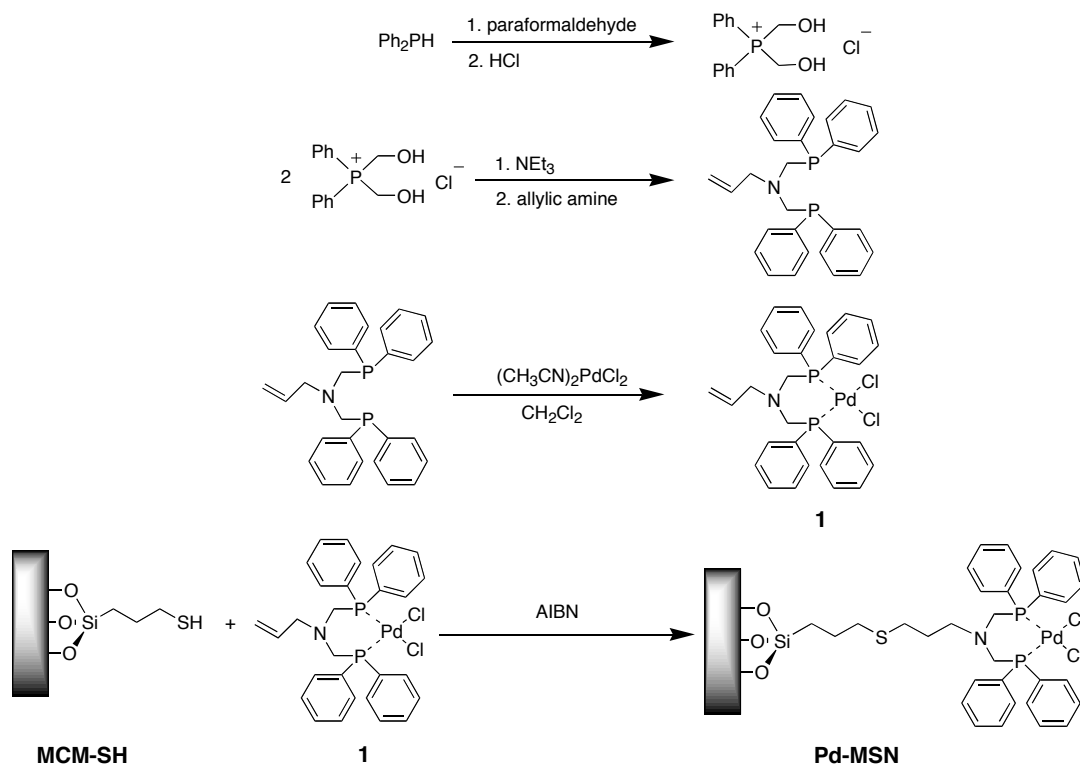
yellowish Pd-MSN material was obtained by filtration, followed by washing with copious amount of chloroform, and then dried under vacuo.

General procedure of fabrication of poly(*p*-phenylene ethynylene) encapsulated mesoporous silica nanosphere (PPE-MSN): A mixture of corresponded 1,4-dialkoxy-2,5-diiodobenzene (0.35 mmol), 1,4-diethynyl benzene (48.6 mg, 0.39 mmol), Pd-MSN (50.0 mg), and copper iodide (2.7 mg, 0.035 mmol) was placed in a 15 mL two-necked flask equipped with a condenser. A solution of diisopropylamine (3.9 mL) and toluene (6.0 mL) was added into flask, respectively. The resultant solution was polymerized at 50 °C for 3 d. The PPE-MSN composite material was obtained by filtration, followed by washing sequentially with copious amount of toluene and chloroform, and then dried under vacuo overnight.

Results and Discussion

The bis(diphenylphosphinomethyl) allylamine was first synthesized according to the literature procedure, as shown in Scheme 1.¹⁶ The Pd (II) complex precursor **1** was obtained by direct complexation of crude bidentate phosphine ligand in a dichloromethane solution of bis(acetonitrile) dichloropalladium (II), and purified by recrystallization. The precursor **1** was further fully characterized by ¹H NMR, ³¹P{¹H} NMR spectroscopy, and X-ray crystallography (see appendix). Only a single peak at 8.56 ppm was observed in the ³¹P{¹H} solution NMR spectrum, which indicated the mirror plane symmetry of compound **1**, and no oxidation happened during complexation with palladium metal.

Scheme 1.



A single crystal of compound **1** was grown from a dichloromethane/acetone mixed solvent, and its X-ray structure is shown in Figure 1. A dichloromethane solvent molecule was found present in the crystal structure of compound **1**. The X-ray structure of **1** exhibited a mirror plane symmetry, explained the single peak observed in the $^{31}\text{P}\{^1\text{H}\}$ NMR spectrum of compound **1**, and an anticipated square-planar geometry of palladium (II) metal with typical Pd-P bond lengths [Pd(1)-P(1) 2.2433(10)Å] and angles [P(1)-Pd(1)-P(1)#1 95.06(6)°].

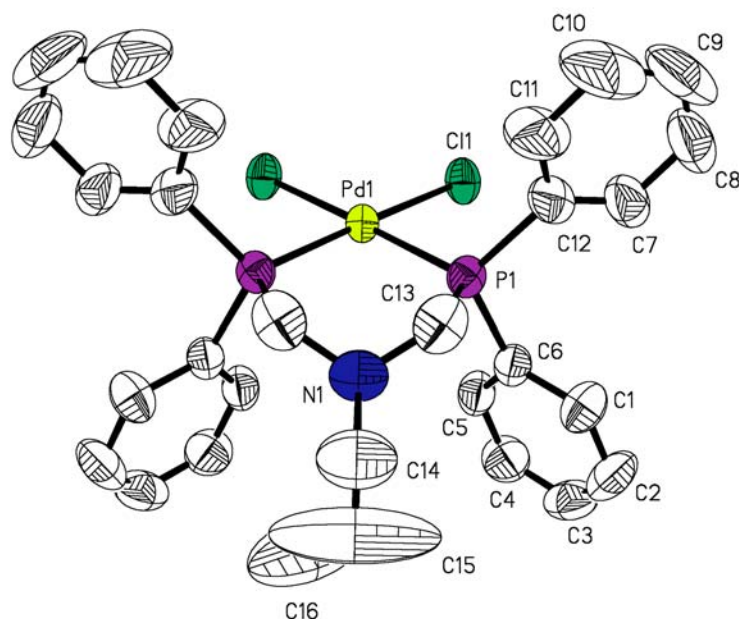


Figure 1. Molecular structure of compound **1**. All hydrogen atoms have been omitted for clarity. Thermal ellipsoid were drawn at the 50% probability level.

The palladium (II)-functionalized mesoporous silica nanoparticle (Pd-MSN) was synthesized through a radical coupling reaction with compound **1** and a pre-synthesized thiol functionalized MSN (MSN-SH) initiated by α,α' -azoisobutyronitrile (AIBN) in the refluxing chloroform solution for three days, as depicted in Scheme 1. The immobilization of palladium complex can be visualized by the pale yellow color of the resulting Pd-MSN material. The loading of palladium complex on the mesoporous silica surface was determined to be 0.66 mmol/g by measuring the amount of thiol groups in the MSN-SH and Pd-MSN.^{22,23} The Pd-MSN material preserved the spherical particle morphology of the MSN-SH as shown in the scanning electron microscopy (SEM) images (see appendix). Three distinct peaks, assigned as (100), (110), and (200), are clearly observed in the powder X-ray diffraction (XRD) spectrum of Pd-MSN as shown in Figure 2b, which indicated that the hexagonally packed mesoporous structure of the MSN-SH was not

distorted by the functionalization. The diminished high ordered diffraction (110) and (200) peaks of Pd-MSN observed in Figure 2b might be attributed to the incorporation of bulky Pd (II) complex inside the mesoporous channels. Further transmission electron microspectroscopy (TEM) analysis of Pd-MSN also confirmed the preservation of MCM-41 typed hexagonal mesopore structure as shown in Figure 3a. The N₂ sorption analysis of Pd-MSN exhibited a regular type IV BET isotherm without significant hysteresis, which implied that Pd (II) catalytic sites were evenly distributed on the silica walls (Figure 4). No bottlenecked mesopore structure, resulted from congregation of functional groups on the pore outlet, was observed by this functionalization method. However, the BET surface area and the BJH mean pore diameter slightly decreased due to the incorporation of relatively bulky Pd complex **1**. The ³¹P DPMAS solid-state NMR spectrum of Pd-MSN exhibited a broad single peak at 7.6 ppm close to the chemical shift of ³¹P{H} NMR spectrum of precursor **1**. No oxidation and ligand exchange was observed in the solid-state NMR spectrum of Pd-MSN. This result strongly suggested that the coordination environment of immobilized palladium catalytic site on the solid support remained intact during the radical coupling reaction.

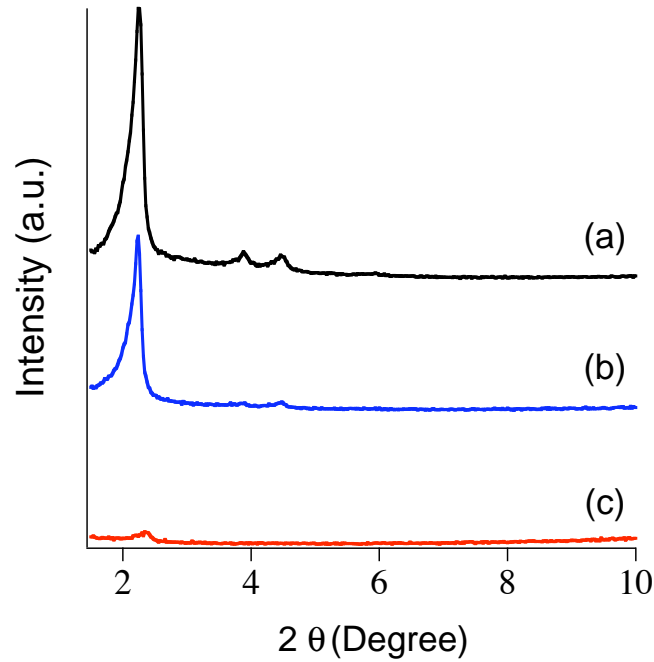


Figure 2. Powder X-ray diffraction (XRD) spectra of MSN-SH (a), Pd-MSN (b), and PPEC₆-MSN.

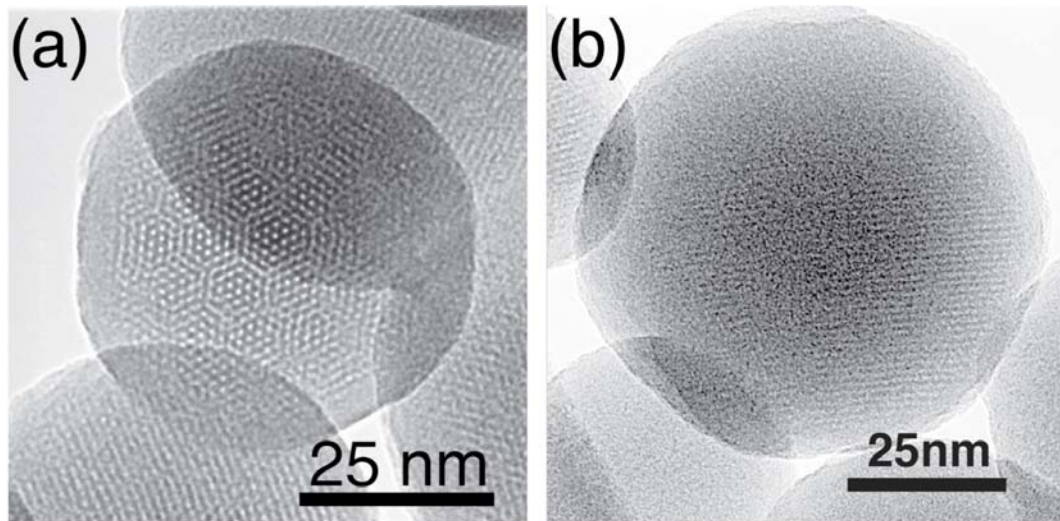


Figure 3. Transmission electron microscopy (TEM) micrographs of Pd-MSN (a) and PPEC₆-MSN (b), all scale bar = 25 nm.

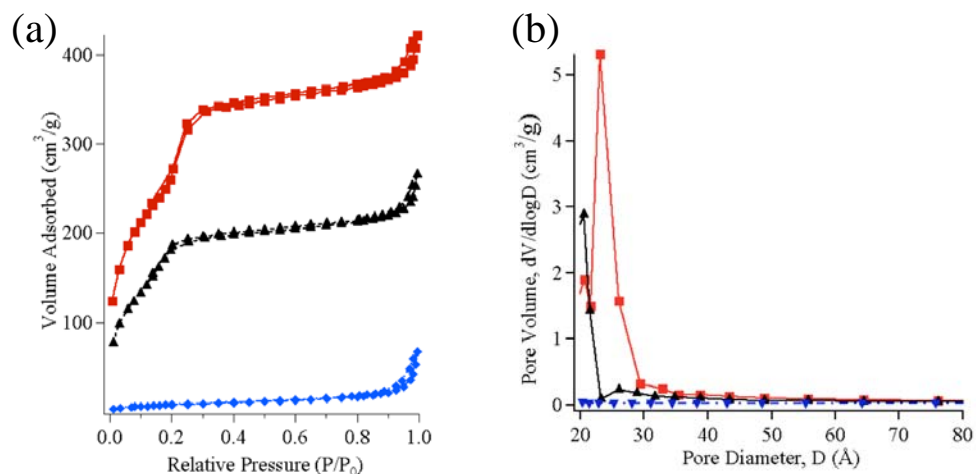


Figure 4. N₂ adsorption/desorption BET isotherms (a) and BJH pore size distribution (b) of MSN-SH (red), Pd-MSN (black), and PPEC₆-MSN (blue), respectively

The Pd-MSN material was further employed as a heterogeneous catalyst for the palladium-catalyzed Sonogashira coupling reaction of 1,4-diethynyl benzene and 2,5-dialkoxy-1,4-diiodobenzene. The resulting poly(phenylene ethynylene) (PPE) molecules are encapsulated inside the one dimensional hexagonal mesopores. Two alkoxy substituents were introduced to polymer main chains to increase the solubility of linear conjugated polymer, which allowed oligomers with sufficient solubility to suspend in the solution for further propagation of polymer chains. However, in the case of long alkoxy substituents, the resulting PPE polymer was too soluble to be trapped inside the mesopores. To circumvent this dilemma, we systematically investigated the influence of side chain based on the number of one alkoxy group. To simplify the nomenclature, a PPEC_n-MSN notation was used for representing a resulting PPE/silica nanocomposite material with n carbon numbers of alkoxy side chain. As depicted in Figure 5, the SEM micrograph of PPEC₄-MSN showed an agglomeration of silica nanospheres and insoluble polymer bundles, which originated from inefficient solubility of PPEC₄ polymers; whereas the SEM micrographs of nanocomposites of PPE polymer with longer side chain such as PPEC₆-MSN and PPEC₈-MSN clearly

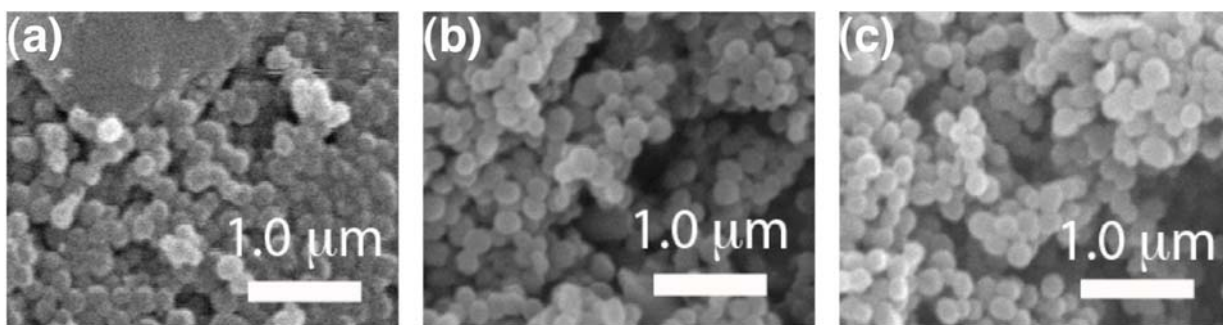


Figure 5. Scanning electron microscopy (SEM) images of PPEC₄-MSN (a), PPEC₆-MSN (b), and PPEC₈-MSN (c), all scale bar = 1.0 μm .

The fluorescence spectrum of PPEC₆-MSN exhibited an emission band centered at 546 nm. Compared to 1,4-diethynylbenzene, the fluorescence emission spectrum of PPEC₆-MSN showed a 243.5 nm bathochromic shift after 72h of refluxing in chloroform, whose profound red-shift indicated a large expansion of the π -conjugated of 1,4-diethynylbenzene due to the formation of PPE polymer. The wavelength of PPEC₆-MSN emission band was even higher than the corresponding un-encapsulated PPEC₆ polymer yielded in the same reaction condition by using compound **1** as catalyst, which could be attributed to certain degree of polymer alignment resulted in regularly one-dimensional parallel hexagonally packed mesoporous channels. A weak (100) peak without other high order diffraction peaks of powder XRD spectrum of PPEC₆-MSN was observed after polymerization as shown in Figure 2c. Given that the hexagonal mesoporous structure clearly displayed as the strips in the TEM micrograph of PPEC₆-MSN, this reduced diffraction pattern cannot due to the deterioration of silica framework during polymerization reaction (Figure 4b). The decrement of mesopore-oriented regularity could be rationalized by the intensity change of porous space, resulted from the pore filling effect of PPE conducted polymer. Similar results of pore filling phenomena in the PPEC₆-MSN were also observed in the N₂ sorption analysis, as

shown in Figure 5. The BET isotherm of PPEC₆-MSN turned into type I based on the IUPAC nomenclature, which was a characteristic of nonporous solid material. The BJH mean pore width of PPEC₆-MSN decreased below mesopore ranges (< 20Å). All experiment results demonstrated most mesoporous channels of PPEC₆-MSN was crammed by the conjugated PPEC₆ polymer.

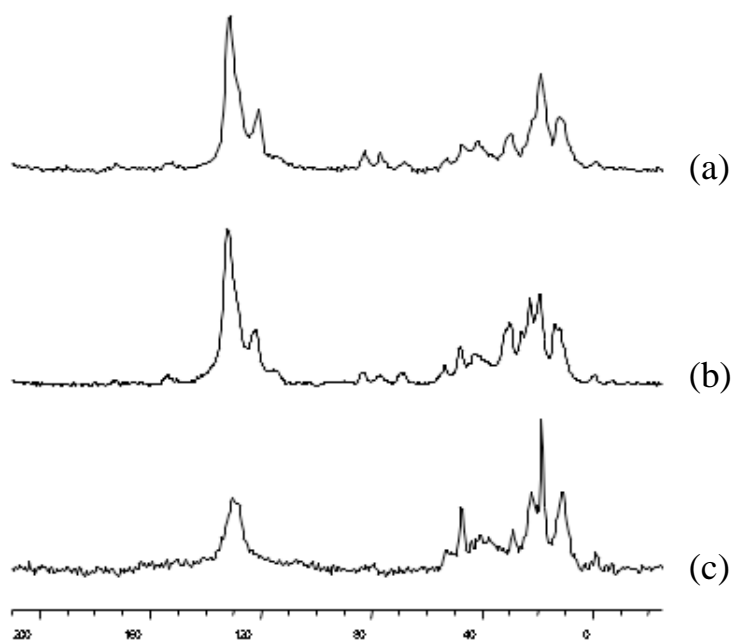


Figure 6. ¹³C CPMAS Spectrum of PPEC₄-MSN (a), PPEC₆-MSN (b), and PPEC₈-MSN (c).

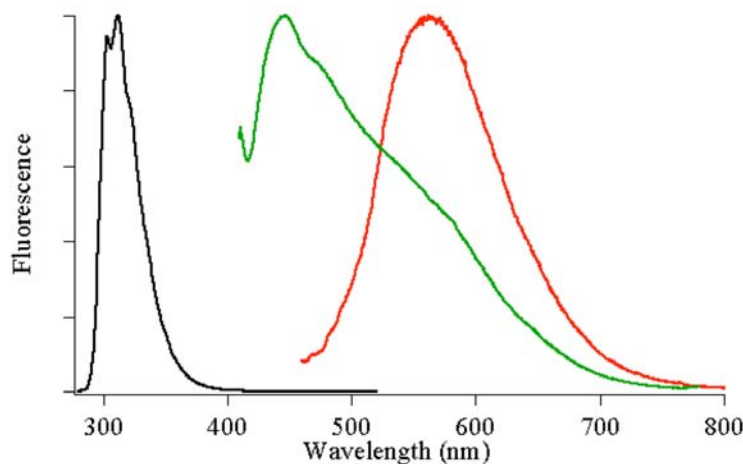


Figure 7. Normalized fluorescence emission spectra of 1,4-diethynylbenzene (black line), polymer-containing PPEC₆-MSN composite material (red line), and corresponding PPEC₆ polymer (green line) synthesized in the same condition by homogeneous catalyst after 72 h of polymerization.

Conclusion

In this paper, we developed a new synthetic approach for immobilization of palladium (II) complex on the surface of mesoporous silica by radical coupling reaction between Pd (II) complex precursor and pre-synthesized thiol functionalized MSN. The Pd-MSN showed spherical particle morphology and parallel hexagonally packed mesoporous channels with palladium catalytic sites homogeneously distributed inside the mesopore. Taking advantage of these parallel nanospace, an encapsulated conductive PPE polymer inside channels can be achieved by applying the Pd catalyzed Sonogashira coupling reaction. The PPE-MSN composite material exhibited an unprecedented large Stoke's shift and bathochromic shifts in their fluorescence emission bands. We envision further developing such polymer/silica nanocomposite material will lead to new optical and electronic nanodevices.

References

- (1) Clark Andrew, P. Z.; Shen, K.-F.; Rubin Yves, F.; Tolbert Sarah, H. *Nano Lett.* **2005**, *5*, 1647-52.
- (2) Nguyen, T.-Q.; Wu, J.; Doan, V.; Schwartz, B. J.; Tolbert, S. H. *Science* **2000**, *288*, 652-656.
- (3) Nguyen, T.-Q.; Wu, J.; Tolbert, S. H.; Schwartz, B. J. *Adv. Mater.* **2001**, *13*, 609-611.
- (4) Ryan, J. V.; Berry, A. D.; Anderson, M. L.; Long, J. W.; Stroud, R. M.; Cepak, V. M.; Browning, V. M.; Rollson, D. R.; Merzbacher, C. I. *Nature* **2000**, *406*, 169-172.
- (5) Wu, C.-G.; Bein, T. *Science* **1994**, *266*, 1013-15.

- (6) Wu, C. G.; Bein, T. *Science* **1994**, *264*, 1757-9.
- (7) Lin, V. S. Y.; Radu, D. R.; Han, M.-K.; Deng, W.; Kuroki, S.; Shanks, B. H.; Pruski, M. *J. Am. Chem. Soc.* **2002**, *124*, 9040-9041.
- (8) Coakley, K. M.; Liu, Y.; McGehee, M. D.; Frindell, K. L.; Stucky, G. D. *Adv. Funct. Mater.* **2003**, *13*, 301-306.
- (9) Lu, Y.; Yang, Y.; Sellinger, A.; Lu, M.; Huang, J.; Fan, H.; Haddad, R.; Lopez, G.; Burns, A. R.; Sasaki, D. Y.; Shelnutt, J.; Brinker, C. J. *Nature* **2001**, *410*, 913-917.
- (10) Crudden, C. M.; Sateesh, M.; Lewis, R. *J. Am. Chem. Soc.* **2005**, *127*, 10045-10050.
- (11) Karimi, B.; Zamani, A.; Clark, J. H. *Organometallics* **2005**, *24*, 4695-4698.
- (12) Clark, J. H.; Macquarrie, D. J.; Mubofu, E. B. *Green Chemistry* **2000**, *2*, 53-56.
- (13) Mehnert, C. P.; Weaver, D. W.; Ying, J. Y. *J. Am. Chem. Soc.* **1998**, *120*, 12289-12296.
- (14) Shimazu, S.; Baba, N.; Ichikuni, N.; Uematsu, T. *J. Mol. Catal. A: Chem.* **2002**, *182-183*, 343-350.
- (15) Quignard, F.; Larbot, S.; Goutodier, S.; Choplin, A. *J. Chem. Soc., Dalton Trans.* **2002**, 1147-1152.
- (16) Fawcett, J.; Hoye, P. A. T.; Kemmitt, R. D. W.; Law, D. J.; Russell, D. R. *J. Chem. Soc., Dalton Trans.* **1993**, 2563-8.
- (17) Chen, H.-T.; Huh, S.; Wiench, J. W.; Pruski, M.; Lin, V. S. Y. *J. Am. Chem. Soc.* **2005**, *127*, 13305-13311.
- (18) Huh, S.; Chen, H.-T.; Wiench, J. W.; Pruski, M.; Lin, V. S. Y. *J. Am. Chem. Soc.* **2004**, *126*, 1010-1011.

- (19) Huh, S.; Chen, H.-T.; Wiench, J. W.; Pruski, M.; Lin, V. S. Y. *Angew. Chem. Int. Ed.* **2005**, *44*, 1826-1830.
- (20) Huh, S.; Wiench, J. W.; Trewyn, B. G.; Song, S.; Pruski, M.; Lin, V. S. Y. *Chem. Commun.* **2003**, 2364-2365.
- (21) Huh, S.; Wiench, J. W.; Yoo, J.-C.; Pruski, M.; Lin, V. S. Y. *Chem. Mater.* **2003**, *15*, 4247-4256.
- (22) Lai, C.-Y.; Trewyn, B. G.; Jeftinija, D. M.; Jeftinija, K.; Xu, S.; Jeftinija, S.; Lin, V. S. Y. *J. Am. Chem. Soc.* **2003**, *125*, 4451-4459.
- (23) Radu, D. R.; Lai, C.-Y.; Huang, J.; Shu, X.; Lin, V. S. Y. *Chem. Commun.* **2005**, 1264-1266.
- (24) Wariishi, K.; Morishima, S.; Inagaki, Y. *Org. Process Res. Dev.* **2003**, *7*, 98-100.

Appendix

Figure S1. ^1H NMR spectrum of Pd (II) complex precursor **1**.

Figure S2. $^{31}\text{P}\{^1\text{H}\}$ NMR spectrum of Pd (II) complex precursor **1** (The x peaks represented side band).

Figure S3. ^{31}P DPMAS solid-state NMR spectrum of Pd-MSN.

Figure S4. SEM micrographs of Pd-MSN.

Figure S1.

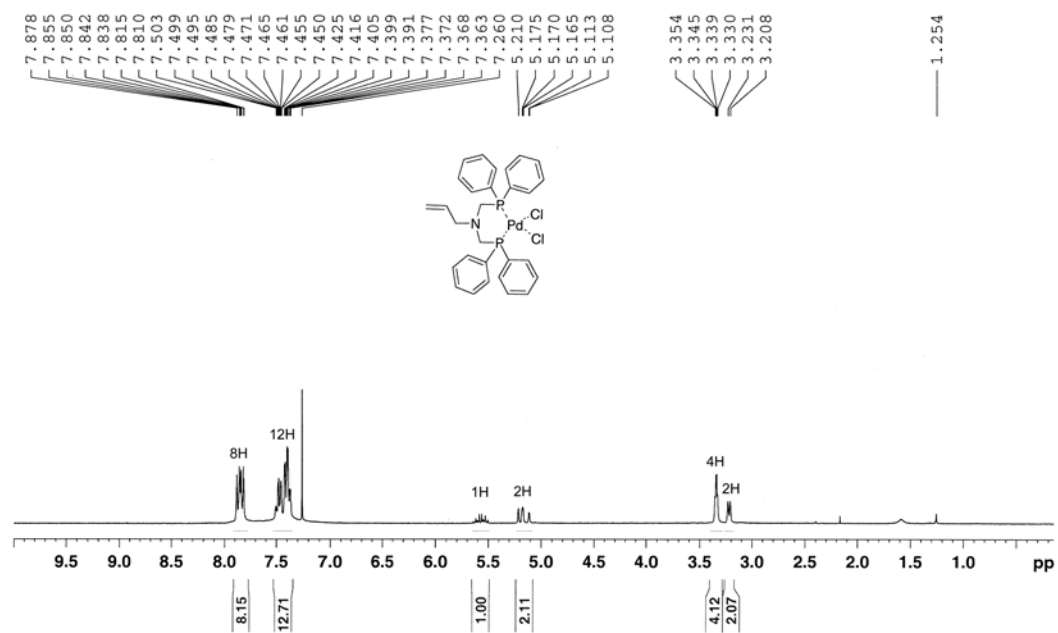


Figure S2.

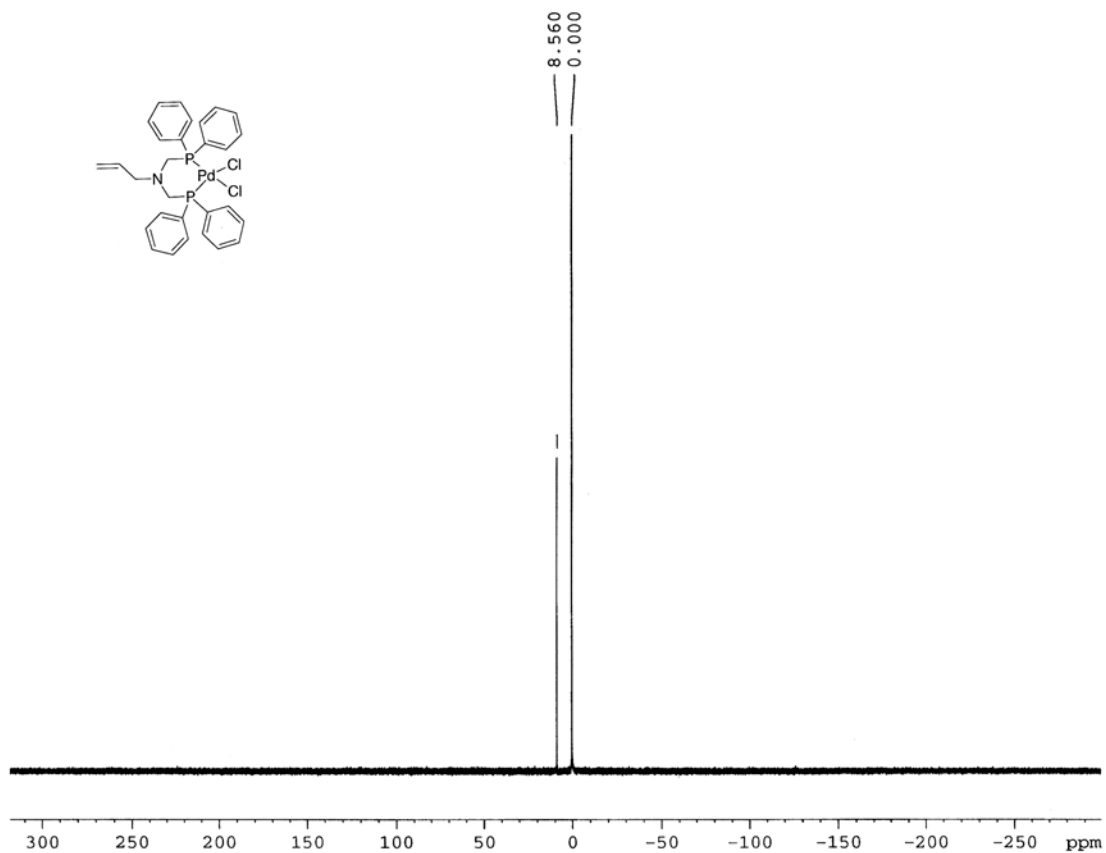


Figure S3.

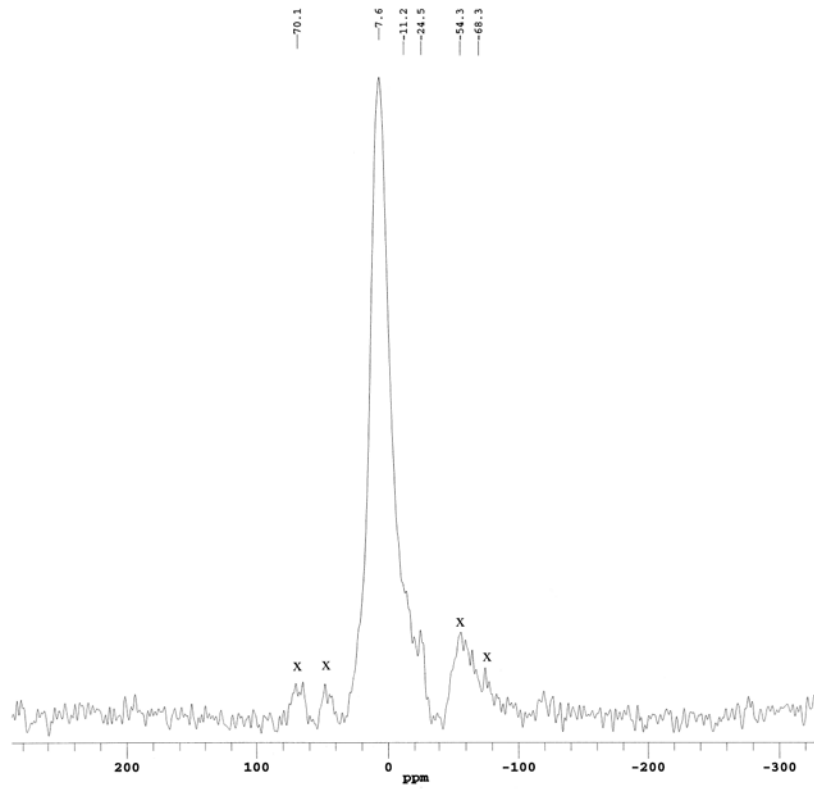
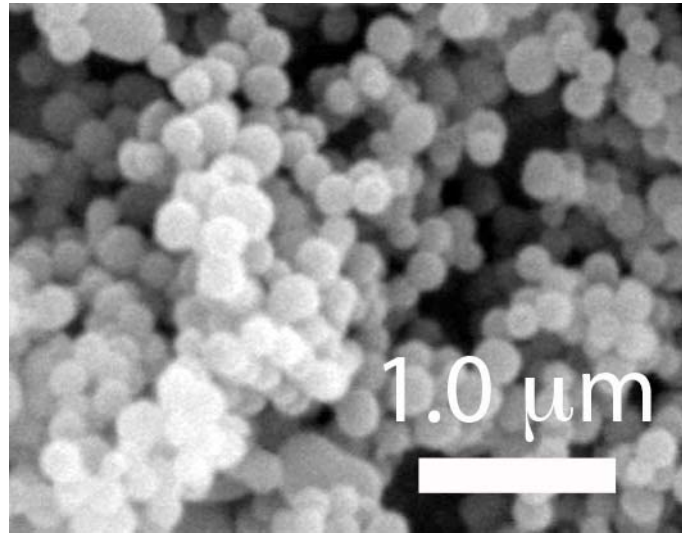


Figure S4.

X-ray crystallographic experimental section

Data collection

A yellow needle with approximate dimensions $0.28 \times 0.18 \times 0.16 \text{ mm}^3$ was selected under ambient conditions. The crystal was mounted and centered in the X-ray beam by using a video camera.

The crystal evaluation and data collection were performed at 293K on a Bruker CCD-1000 diffractometer with Mo K_{α} ($\lambda = 0.71073 \text{ \AA}$) radiation and the detector to crystal distance of 5.03 cm.

The initial cell constants were obtained from three series of ω scans at different starting angles. Each series consisted of 30 frames collected at intervals of 0.3° in a 10° range about ω with the exposure time of 10 seconds per frame. A total of 46 reflections was obtained. The reflections were successfully indexed by an automated indexing routine built in the SMART program. The final cell constants were calculated from a set of 1018 strong reflections from the actual data collection.

The data were collected using the full sphere routine. A total of 28850 data were harvested by collecting four sets of frames with 0.3° scans in ω with an exposure time 15 sec per frame. This dataset was corrected for Lorentz and polarization effects. The absorption correction was based on fitting a function to the empirical transmission surface as sampled by multiple equivalent measurements [1] using SADABS software [2].

Structure solution and refinement

The systematic absences in the diffraction data were consistent for the space groups *Pnma* [2] yielded chemically reasonable and computationally stable results of refinement.

The position of heavy atom was found by the Patterson method. The remaining atoms were located in an alternating series of least-squares cycles and difference Fourier maps. All non-hydrogen atoms were refined in full-matrix anisotropic approximation including atoms of solvent. All hydrogen atoms were placed in the structure factor calculation at idealized positions and were allowed to ride on the neighboring atoms with relative isotropic displacement coefficients. Final least-squares refinement of 187 parameters against 3403 independent reflections converged to R (based on F^2 for $I \geq 2\sigma$) and wR (based on F^2 for $I \geq 2\sigma$) of 0.048 and 0.121, respectively. The one molecule of CH_2Cl_2 solvent per each complex molecule was found. The asymmetric unit of orthorhombic cell includes a half of complex molecule (mirror plane symmetry) and 1 solvent molecule in a special position ($Z = 4$).

The ORTEP diagram was drawn at 50% probability level. H atoms were omitted for clarity. Only one of two equivalent positions for C15-C16 bond is shown.

References

- [1] Blessing, R.H. *Acta Cryst.* **1995**, *A51*, 33-38.
- [2] All software and sources of the scattering factors are contained in the SHELXTL (version 5.1) program library (G. Sheldrick, Bruker Analytical X-Ray Systems, Madison, WI).

Table S1. Crystal data and structure refinement for Pd (II) complex 1.

Identification code	Pd (II) complex 1
Empirical formula	C ₃₀ H ₃₁ Cl ₄ NP ₂ Pd
Formula weight	715.70
Temperature	298(2) K
Wavelength	0.71073 Å
Crystal system	Orthorhombic
Space group	Pnma
Unit cell dimensions	a = 22.561(3) Å, a = 90° b = 17.749(2) Å, b = 90° c = 8.0510(11) Å, c = 90°
Volume	3224.0(7) Å ³
Z	4
Density (calculated)	1.475 Mg/m ³
Absorption coefficient	1.027 mm ⁻¹
F(000)	1448
Crystal size	0.28 x 0.18 x 0.16 mm ³
Theta range for data collection	1.81 to 26.37°.
Index ranges	-28 ≤ h ≤ 27, -22 ≤ k ≤ 22, -10 ≤ l ≤ 10
Reflections collected	28850
Independent reflections	3403 [R(int) = 0.1965]
Completeness to theta = 26.37°	100.0 %
Absorption correction	Semi-empirical from equivalents
Max. and min. transmission	0.72 and 0.48
Refinement method	Full-matrix least-squares on F ²
Data / restraints / parameters	3403 / 0 / 187
Goodness-of-fit on F ²	0.926
Final R indices [I>2sigma(I)]	R1 = 0.0479, wR2 = 0.1212
R indices (all data)	R1 = 0.0606, wR2 = 0.1316
Largest diff. peak and hole	1.056 and -0.902 e.Å ⁻³

$$R1 = \sum ||F_o| - |F_c|| / \sum |F_o| \text{ and } wR2 = \{ \sum [w(F_o^2 - F_c^2)^2] / \sum [w(F_o^2)^2] \}^{1/2}$$

Table S2. Atomic coordinates ($\times 10^4$) and equivalent isotropic displacement parameters ($\text{\AA}^2 \times 10^3$) for Pd (II) complex **1**.

	x	y	z	U(eq) ^a
Pd(1)	1384(1)	2500	4741(1)	33(1)
C(1)	2521(2)	4513(3)	6789(6)	64(1)
C(2)	3067(3)	4821(3)	6417(7)	77(2)
C(3)	3410(3)	4526(4)	5179(7)	73(2)
C(4)	3204(2)	3926(3)	4288(7)	70(1)
C(5)	2657(2)	3614(2)	4629(5)	53(1)
C(6)	2312(2)	3897(2)	5898(5)	45(1)
C(7)	1093(3)	4846(3)	6031(8)	78(2)
C(8)	643(4)	5365(4)	6270(11)	114(3)
C(9)	154(4)	5174(7)	7173(13)	134(4)
C(10)	105(4)	4469(7)	7848(11)	130(4)
C(11)	549(3)	3956(4)	7602(8)	95(2)
C(12)	1051(2)	4144(3)	6715(6)	60(1)
C(13)	1776(2)	3176(3)	8661(5)	61(1)
C(14)	2557(6)	2500	10119(13)	118(4)
C(15)	3107(10)	2500	9900(30)	310(20)
C(16) ^b	3365(12)	2087(17)	8720(20)	210(19)
C(17)	9875(7)	2500	1443(17)	161(6)
Cl(1)	1172(1)	3457(1)	2802(1)	49(1)
Cl(2)	9498(3)	2500	-277(8)	222(3)
Cl(3)	9512(3)	2500	3295(8)	219(3)
N(1)	2133(3)	2500	8751(6)	62(2)
P(1)	1626(1)	3432(1)	6496(1)	41(1)

^a U(eq) is defined as one third of the trace of the orthogonalized U_{ij} tensor.

^b Atom C16 is disordered by mirror plane (two equivalent positions with occupancy factors 0.5).

CHAPTER 6. TEMPLATE REMOVAL AND THERMAL STABILITY OF ORGANICALLY FUNCTIONALIZED MESOPOROUS SILICA NANOPARTICLES

A paper published in *Chemistry of Material* **2006**, *18*, 4319-4327

Rajeev Kumar, Hung-Ting Chen, Juan L. V. Escoto, Victor S.-Y. Lin, and Marek Pruski

Abstract

The surfaces of organically functionalized, MCM-41-type mesoporous silica nanoparticle materials, prepared by a co-condensation method, were studied by solid-state nuclear magnetic resonance (NMR) spectroscopy following a series of heat treatments between 100 and 400 °C. The surfaces were functionalized with 2,2'-bipyridine, 4-dimethylaminopyridine and pentafluorobenzene. The ^{13}C and ^{29}Si NMR spectra of these materials showed that the structures and concentrations of these functional groups remained unaffected by the heat treatment. Furthermore, it has been demonstrated that the surfactant template, cetyltrimethylammonium bromide (CTAB), could be effectively removed from these materials by heat treatment, without disrupting the covalent bonds between the functional groups and the silica surface. The chemical accessibility and reactivity of the organic functionalities were also preserved after heating.

Introduction

Since the discovery of the M41S family of mesoporous materials by Mobil scientists in 1992,^{1,2} extensive studies have been performed by research groups worldwide on the synthesis and applications of these materials in the fields ranging from sorption, separation, sensor, delivery to electronics.³⁻⁸ Also, these materials provide uniform porous structures with high surface area and tunable morphology that are highly desirable for selective heterogeneous catalysis. The major challenge that hindered the utilization of mesoporous silica-based catalysts in industrial processes involved the synthetic methods for surface functionalization with control of spatial distribution and adequate thermal stability. Recently, significant progress in the area of functionalization of MCM and SBA types of mesoporous silicas with catalytically active organic groups has been demonstrated,^{3,9-15} which resulted in synthesis of efficient and highly selective catalysts for several industrially relevant reactions.¹⁶⁻¹⁸

Among the state-of-the-art methods for the surface functionalization of mesoporous silicas, the co-condensation of silicate with various organoalkoxysilanes has been shown to yield materials with a homogeneous spatial distribution of organic groups. To preserve the organic functional groups, the low-temperature processes, such as solvent extraction,^{19,20} have been widely used for template removal. These methods, on the other hand, often require the use of large volumes of organic solvents, and therefore cannot meet the economic and environmental constraints imposed by large-scale applications. Furthermore, several recent reports have indicated that the as-synthesized organically functionalized mesoporous silicas prepared by the solvent extraction methods lack the high hydrothermal stability that is

necessary for some industrially important processes.^{21,22} This has been attributed to the defect sites created during the synthesis and/or the template-removal process of these materials.

Recent studies on the hydrothermal treatments of several non-functionalized mesoporous silica materials have demonstrated that, by controlling the temperatures and moisture contents, these processes could not only effectively remove template molecules, but also “cure” the defects and strengthen the structure stability of the mesoporous silica framework.²²⁻²⁸ However, to the best of our knowledge, no studies has been reported on using these methods for the template removal of organically functionalized mesoporous silica materials prepared by the co-condensation method.

Herein, we report on a systematic investigation of the thermal treatments of three mesoporous silica nanoparticle (MSN) materials that are functionalized with 4,4'-di-[(*N*-propyl)aminocarbonyl]-2,2'-bipyridine (BPY), 3-(pentafluorophenyl)propyl (PFP), and 4-[(*N*-propyl-*N*-methyl-amino)pyridine (DMAP) groups. These MSNs were synthesized via the co-condensation method templated by CTAB surfactant micelles^{11,12,18,29,30} and characterized using a combination of solid-state NMR, X-ray diffraction, nitrogen adsorption and fluorescence spectroscopy. The different organic groups were chosen to represent the common metal-binding ligands, the Lewis acids, and the nucleophilic catalytic functionalities, respectively. The structures and concentrations of surfactant molecules and the functional groups were monitored following a series of thermal treatments between 100 and 400 °C. Our primary analytical tool was solid-state NMR spectroscopy, which has the outstanding applicability for silica surface characterization, especially in mesoporous materials.²⁹⁻³⁶ We have demonstrated that it is possible to efficiently remove the CTAB template molecules from the mesopores while fully preserving the chemical fidelity of the

organic functional groups. The chemical accessibility and catalytic reaction studies are fully consistent with spectroscopic characterization before and after the thermal treatments.

Experimental Section

Sample Synthesis. All reagents and chemicals were used as received from commercial vendors without any further purification. Cetyltrimethylammonium bromide (CTAB) and tetraethoxysilane (TEOS), and *cis*-bis(2,2'-bipyridine)dichlororuthenium(II) hydrate ($\text{Ru}(\text{bpy})_2\text{Cl}_2 \cdot x\text{H}_2\text{O}$) were purchased from Aldrich. 3-(Pentafluorophenyl)propyltrimethoxysilane (PFP-TMS) was purchased from Gelest. The DMAP-MSN material and the pertinent 4-[N-[3-(triethoxysilyl)propyl]-N-methylamino]pyridine (DMAP-TES) were synthesized according to the procedures described in our previous paper.¹⁸ The 2,2'-bipyridyl-4,4'-dicarboxylic acid was prepared based on a literature-reported procedure.³⁷ The non-functionalized MCM-41 silica and DMAP-MSN were synthesized following the procedures reported previously.¹⁸

Preparation of 4,4'-di-[N-[3-(trimethoxysilyl)propyl]aminocarbonyl]-2,2'-bipyridine (BPY-TMS): A solution of 2,2'-bipyridyl-4,4'-dicarboxylic acid (960 mg, 3.93 mmol) and excess thionyl chloride (20 mL) was refluxed for 3 h to yield the desired acid chloride. The reaction mixture was allowed to cool down to room temperature. The unreacted thionyl chloride was removed by the rotary evaporator. The resulting crude 2,2'-bipyridyl-4,4'-dicarboxylic acid chloride was re-dissolved in a solution of benzene (160 mL) and pyridine (1.0 mL), followed by the addition of 3-aminopropyl trimethoxysilane (1.5 mL, 8.5 mmol). The mixture was allowed to reflux for 12 h. The solid precipitate was formed and removed by filtration to yield a pink solution. The filtrate was centrifuged to separate

the pink impurity from the solution. The clear solution was decanted and concentrated in vacuo to give 788 mg (1.39 mmol, 35%) of BPY-TMS as a white solid powder. ^1H NMR (CDCl_3 , 300 MHz) δ 8.72 (d, 2H), 8.68 (s, 2H), 7.80 (d, 2H), 6.96 (s, 2H), 3.54 (s, 18H), 3.50 (m, 4H), 1.78 (m, 4H), 0.74 (t, 4H). ^{13}C NMR (CDCl_3 , 75 MHz) δ 165.7 (CONH), 156.2, 150.3, 143.4, 122.5, 117.7, 50.9, 42.7, 22.8, 6.9. IR (KBr): 3342 cm^{-1} , 3052 cm^{-1} , 1646 cm^{-1} , 1545 cm^{-1} , 1313 cm^{-1} , 1077 cm^{-1} . MS (EI) m/z : 567 $[\text{M}]^+$. HRMS calcd for $\text{C}_{24}\text{H}_{38}\text{N}_4\text{O}_8\text{Si}_2$ 566.2228, found 566.2235.

Synthesis of 2,2'-bipyridine-functionalized mesoporous silica nanoparticle (BPY-MSN) material: A mixture of CTAB (1.0 g, 2.75 mmol), 2.0 M of NaOH (aq) (3.5 mL, 7.0 mmol), and H_2O (480 g, 26.67 mol) was heated to 80 °C for 30 min. TEOS (5 mL, 22.4 mmol) was first introduced dropwise to the CTAB solution, followed by a slow addition of BPY-TMS (0.543 g, 0.958 mmol). The mixture was stirred vigorously at 80 °C for 2 h followed by a hot filtration of the solution to yield the crude BPY-MSN product (white solid). The as-synthesized material was washed with copious amount of water and methanol and then dried under vacuum. A surfactant-extracted BPY-MSN material was obtained by the acid extraction. In a typical procedure, as-synthesized BPY-MSN material (1.0 g) was treated with a methanolic solution (100 mL) of concentrated hydrochloric acid (1.0 mL) at reflux condition for 6 h, followed by the filtration, extensive wash with water and methanol, and dried under vacuum.

Synthesis of pentafluorobenzene-functionalized mesoporous silica nanoparticle (PFP-MSN) material: As mentioned above, a mixture of CTAB (1.0 g, 2.75 mmol), 2.0 M of NaOH (aq) (3.5 mL, 7.0 mmol), and H_2O (480 g, 26.67 mol) was heated to 80 °C for 30 min. Two alkoxy silanes, TEOS (5 mL, 22.4 mmol) and PFP-TMS (0.58 mL, 2.24 mmol),

were sequentially added to the surfactant solution via injection. White precipitate was observed within 30 sec upon mixing of the initial opaque emulsion. The mixture was stirred at 80 °C for 2 h, followed by a hot filtration to yield the as-synthesized PFP-MSN material. The material was washed extensively with copious amount of water and methanol and then dried under vacuum. The acid extraction of CTAB surfactant from as-made material was performed by the aforementioned experimental condition to obtain a surfactant-extracted PFP-MSN sample.

Heat Treatment. The as-synthesized and surfactant-extracted silicas in their initial state will be referred to as BPY-as-RT, BPY-ex-RT, DMAP-as-RT, etc., The first series of thermally treated samples, which we denote BPY-as-100, BPY-ex-100, DMAP-as-100 etc., was obtained by placing the materials in glass tubes and evacuating to 10^{-5} Torr overnight at temperature $T_c = 100$ °C. After the NMR measurements, the same samples were exposed to subsequent heat treatments at 150, 200, 225, 250, 282 and 350-400 °C, carried out for two hours under the same pressure of 10^{-5} Torr. Again, each thermal treatment was followed by an NMR analysis. The non-functionalized MCM-41 samples were treated only at 100 and 400 °C in as-synthesized state. In order to prevent rehydration, the samples were handled in a glove bag under dry nitrogen and measured in tightly capped MAS rotors.

Characterization of MSN materials. The particle morphology of MSNs was determined by scanning electron microscopy (SEM) with a JEOL 840A instrument. Powder XRD experiments were performed on a Scintag XDS 2000 diffractometer by scanning the 2θ angle between 1 and 10 degrees and using a Cu $K\alpha$ radiation source. The surface area and median pore diameter were determined by N_2 adsorption/desorption measurements in a

Micromeritics ASAP 2000 surface analyzer. Samples were prepared by degassing at 90 °C for 4 h before the measurements. The data were evaluated by Brunauer-Emmett-Teller (BET) and Barrett-Joyner-Halenda (BJH) methods to calculate the surface area and pore volumes/pore size distributions, respectively.

NMR. ^{13}C and ^{29}Si solid-state NMR experiments were performed on a Varian/Chemagnetics Infinity 400 spectrometer equipped with a 5 mm Chemagnetics magic angle spinning (MAS) probe operated at a rate of 10 kHz. The ^{13}C experiments, which used cross polarization (CP) from the nearby protons, were focused on monitoring the changes in the structure and concentration of molecules inside the mesopores as a function of T_c . During the CP period of 1.5 ms, the ^1H RF magnetic field $\nu_{\text{RF}}^{\text{H}}$ was ramped between 19 and 30 kHz using 1 kHz increments, whereas the ^{13}C RF field $\nu_{\text{RF}}^{\text{C}}$ was maintained at a constant level of 30 kHz. The magnetic fields $\nu_{\text{RF}}^{\text{H}}$ of 70 kHz and 50 kHz were used for initial excitation and during continuous wave decoupling, respectively. A total of 42 spectra were acquired (six samples treated at seven temperatures), each consisting of 12,000 scans, using a repetition time of 1.2 s. It is noted that direct polarization (DP), which is the preferred method in applications involving quantitative measurements, could not be used in this study due to prohibitively long relaxation delays, on the order of several minutes, associated with ^{13}C nuclei. The CPMAS NMR method, on the other hand, yielded spectra that are not quantitative because the observed ^{13}C magnetizations were influenced by site-dependent ^1H - ^{13}C distances, relaxation processes and molecular motions. However, we could still accurately monitor the relative changes in concentrations of functional groups as a function of T_c by acquiring each CPMAS NMR spectrum under identical conditions. To maximize the

accuracy, we have verified the magnitudes of the applied RF fields between the measurements within each series of spectra using a reference sample. The changes in mobility of chemisorbed species due to the reconstruction (dehydroxylation) of the silica surface at higher temperatures may be the main source of error in these measurements.

The ^{29}Si DPMAS NMR experiments were performed in order to compare the surface functionalities after the final treatment with those present in the starting samples. For each sample 300 scans were collected using ^1H TPPM decoupling³⁸ at $\nu_{\text{RF}}^{\text{H}} = 45$ kHz using a phase separation of 15° . The saturation recovery experiment showed that the values of T_1 relaxation times for the silicon groups varied between 30 and 60 s. Therefore, a pulse delay of 300 s was chosen to assure sufficient restoration of the initial ^{29}Si magnetization. All chemical shifts were referenced to SiMe_4 at 0 ppm.

The solution state spectra reported in this work were acquired on a Varian VRX-300 spectrometer.

Chemical Accessibility and Reactivity Test of BPY-MSNs. 50.0 mg of BPY-as-350 or BPY-ex-RT material was suspended in a 10 mL ethanol solution of *cis*-bis(2,2'-bipyridine)dichlororuthenium(II) hydrate (0.337 mM) and refluxed for 12 h. The supernatant was isolated by filtration and diluted with ethanol to 50 mL. The amount of unreacted $\text{Ru}(\text{bpy})_2\text{Cl}_2 \cdot x\text{H}_2\text{O}$ in the supernatant was determined by measuring the UV/Vis absorbance of the λ_{max} ($\epsilon = 3,199.1 \text{ cm}^{-1} \cdot \text{M}^{-1}$) at 365 nm in ethanol. The amount of chemically accessible 2,2'-bipyridine groups in BPY-as-350 and BPY-ex-RT was calculated by subtracting the amount of unreacted $\text{Ru}(\text{bpy})_2\text{Cl}_2 \cdot x\text{H}_2\text{O}$ from the initial concentration (0.337 mM). Also, the material obtained after reacting with $\text{Ru}(\text{bpy})_2\text{Cl}_2 \cdot x\text{H}_2\text{O}$ was carefully examined by

measuring fluorescence spectra of MSNs suspended in the ethanol solution. The spectra were taken using excitation at 450 nm, an average wavelength of MLCT band of a ruthenium (II) trispyridine complex.

In addition, we performed the Cu(II) adsorption capacity test on the same samples by following a literature-reported method.^{11,12,39} It was carried out by using 0.01 M $\text{Cu}(\text{NO}_3)_2 \cdot 2.5\text{H}_2\text{O}$ in 0.1 M tris(hydroxymethyl)aminomethane (trizma) solution and the contact time of 1 h. The amount of non-adsorbed Cu(II) ions in the filtrate was measured using UV/Vis spectrophotometer at $\lambda_{\text{max}} = 601$ nm.

Catalytic Reactivity Test of DMAP-as-400. A solution of 4-nitrobenzaldehyde (37.8 mg, 0.25 mmol) and DMAP-as-400 (50 mg, 0.075 mmol) in water/tetrahydrofuran (THF) (2mL, v/v = 1/3) was charged to a screw-capped test tube, followed by the addition of methyl vinyl ketone (41.0 μL , 0.5 mmol). The mixture was stirred at 50°C for 24 h. The catalyst was separated by filtration and washed with acetone. The filtrate was collected and concentrated in vacuo to yield a yellow liquid. The crude was purified by the chromatography with an eluent of ethyl acetate/hexane (v/v = 5/5) to yield 49.8 mg (0.225 mmol, 90%) of the purified product.

Results and Discussion

Solid-State NMR Characterization. The organically functionalized MSNs were thermally treated between 100 and 400 °C, as detailed in Section 2.2, and the resulting materials were analyzed by solid-state NMR spectroscopy. The ^{13}C CPMAS NMR spectra of functionalized samples showed that they contained the intended structures, i.e. the observed ^{13}C chemical shifts matched closely those in the solution NMR spectra of respective

functional groups. In Table 1 these structures are shown along with the site assignments, which will be further used in the discussion below. In order to separate the resonances representing functional groups from those due to CTAB, we measured the ^{13}C CPMAS NMR spectrum of a nonfunctionalized sample MCM-as-100, which is shown and assigned in Figure 1.

Table 1. ^{13}C Chemical Shifts, Spectral Assignments and Molecular Structures Identified in Functionalized MSN Materials. (Reprinted from *Chem. Mater.* Copyright 2006 American Chemical Society)

sample	spectral assignments ^a (δ_{C} given in ppm)	structure
BPY-MSN	C1: 14; C2: 24; C3: 44; C5: 167; C6: 143; C7: 121; C8: 149; C10: 157; C11: 123	
DMAP-MSN	C1: 11; C2: 23; C3: 55; C5: 36; C6: 155; C7,11: 108; C8,10: 151	
PFP-MSN	C1: 12; C2,3: 23; C4: 115; C5: 144; C6: 137; C7: 141; C8: 139; C9: 147	
MCM-as-100 (CTAB)	C1: 68; C2: 32; C3-14: 30; C15: 27; C16: 24; C17-19: 54	

^a As detailed in Sections 3.1.1-3.1.3, the observed species also included the methoxy groups (at 50 ppm), ethoxy groups (at 16 and 58 ppm), and the products of CTAB decomposition following Eqs (1) – (3).

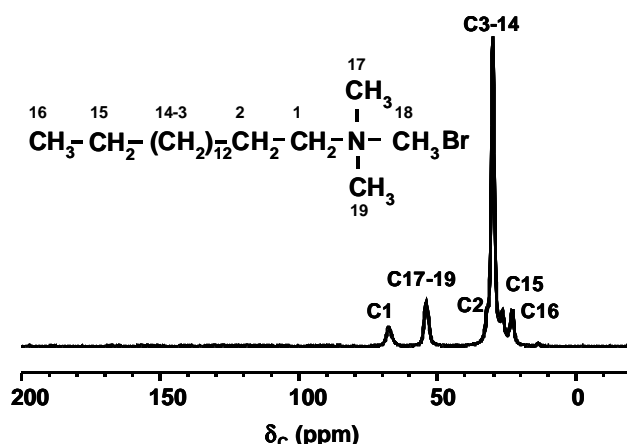
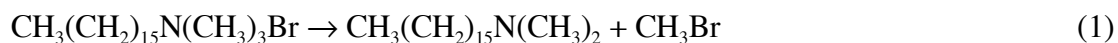


Figure 1. ^1H - ^{13}C CPMAS NMR spectrum of MCM-41-as-100. The resonances are assigned to CTAB, as shown. (Reprinted from *Chem. Mater.* Copyright 2006 American Chemical Society)

BPY-MSN. The ^{13}C CPMAS NMR spectra of BPY-as-100 to BPY-as-350 series of samples are shown in Figure 2a. The chemical shifts observed after the heat treatment at 100 °C (sample BPY-as-100, top spectrum) represent BPY and CTAB, as marked in the figure. The resonances representing BPY remained unaffected by the increased severity of heating, while those due to CTAB, which overwhelmed the top spectrum, rapidly declined in intensity with increasing T_c . Initially, at temperatures below 200 °C, CTAB's structure remained intact, as evidenced by resonances at 68 ppm (C1), 32 ppm (C2), 30 ppm (C3-14), 27 ppm (C15), 24 ppm (C16) and 54 ppm (C17-19), which are consistent with the ^{13}C CPMAS NMR spectrum of sample MCM-as-100 shown in Figure 1. However, in sample BPY-as-200 additional resonances appeared at 64 and 44 ppm, which at 225 °C took place of those representing C1 and C17-19 in CTAB. Their presence is due to carbons C1 and C17-C18 in *N,N*-dimethylhexadecylamine ($\text{CH}_3(\text{CH}_2)_{15}\text{N}(\text{CH}_3)_2$), which is a product of the decomposition of CTAB at 200 °C:



The resulting CH_3Br (boiling point = 4°C) is either evacuated or reacts with $\equiv\text{Si-OH}$ groups to form $\equiv\text{Si-OCH}_3$ and HBr according to:



The validity of reaction (1) was directly confirmed through the analysis of the liquid residue that condensed during the evacuation on the wall of the glass tube containing the sample. The solution ^{13}C NMR spectrum of this residue in CDCl_3 (spectrum S1a in appendix) is in exact agreement with the spectrum expected for $\text{CH}_3(\text{CH}_2)_{15}\text{N}(\text{CH}_3)_2$.^{40,41} In the case of reaction (2), HBr was most likely removed by evacuation, while the methoxy ($\equiv\text{Si-OCH}_3$) groups remained on the surface, as evidenced by the emergence of the resonance at 50 ppm in Figure 2a.

Thus, while CTAB does not exist in its intact form at $T_c \geq 200^\circ\text{C}$, the $\text{CH}_3(\text{CH}_2)_{15}\text{N}(\text{CH}_3)_2$ species persist inside some of the pores at a concentration level corresponding to about 5-10% of the initial CTAB concentration observed at $T_c = 100^\circ\text{C}$. This is illustrated in Figure 3a, which shows the sum of integrated intensities of all resonances representing CTAB and/or $\text{CH}_3(\text{CH}_2)_{15}\text{N}(\text{CH}_3)_2$ as a function of T_c . There are two possible explanations of this finding. The $\text{CH}_3(\text{CH}_2)_{15}\text{N}(\text{CH}_3)_2$ species may remain entrapped inside the silica matrix as a result of pore blockage during the heat treatment. The reduced pore volume per gram of materials after heating (see Section 3.3) agrees with this hypothesis. Alternatively, these observed signals could be attributed to the $\text{CH}_3(\text{CH}_2)_{15}\text{N}^+\text{H}(\text{CH}_3)_2$ species. As depicted in Eq. (2), HBr was generated from the reaction between CH_3Br and surface silanols. It is foreseeable that HBr could protonate $\text{CH}_3(\text{CH}_2)_{15}\text{N}(\text{CH}_3)_2$ to give rise to the cationic $\text{CH}_3(\text{CH}_2)_{15}\text{N}^+\text{H}(\text{CH}_3)_2$ species that electrostatically binds to the surface silicate

groups. Regardless of which scenario is operable, these residues did not affect the chemical properties of the organically functionalized BPY-MSNs, as detailed in Section 3.2.

We note that these results are consistent with our earlier solid-state NMR study of non-functionalized MCM-41 silica nanoparticles.²⁹ Indeed, by using one- and two-dimensional ^1H , ^{13}C and ^{29}Si experiments under 40 kHz MAS, we have demonstrated that the residual CTAB molecules, which were shown to remain inside the pores in the prone position along the channel walls, decomposed below 250 °C. Furthermore, the ^1H peak representing CTAB's head group ($\text{N}(\text{CH}_3)_3$) was reduced at a faster rate as a function of T_c than the lines representing the CH_2 groups and the tail group (CH_3).²⁹

The spectra of BPY-ex series (Figure 2b) demonstrate that CTAB was completely removed by acid extraction. Indeed, only the resonances representing BPY are observed within the entire temperature range $100 \leq T_c \leq 350$ °C. Also present in the spectra is a peak at around 50 ppm, which we attributed to the methoxy groups produced during washing.

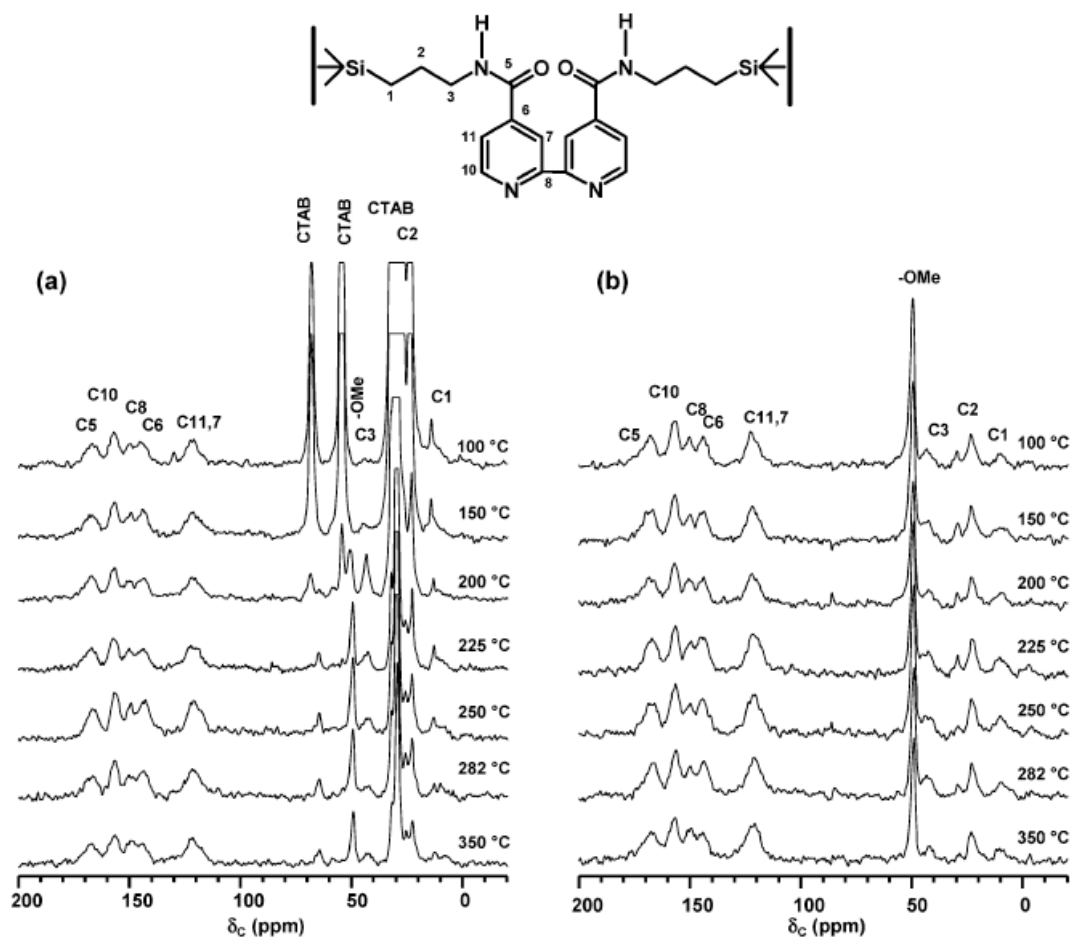


Figure 2. ^1H - ^{13}C CPMAS NMR spectra of (a) BPY-as and (b) BPY-ex series of samples following the heat treatment at $100\text{ }^\circ\text{C} \leq T_c \leq 350\text{ }^\circ\text{C}$. (Reprinted from *Chem. Mater.* Copyright 2006 American Chemical Society)

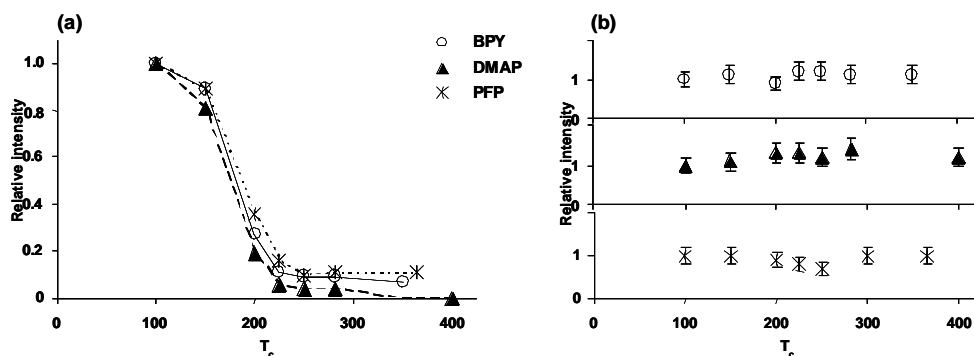


Figure 3. Concentrations of CTAB versus T_c in BPY-as, DMAP-as and PFP-as series of samples (a), and of the organic functional groups in the corresponding BPY-ex, DMAP-ex and PFP-ex samples (b). The experimental points represent integrated intensities of all ^{13}C resonances for each species. In the series of as-synthesized samples, the resonances

representing CTAB were deconvoluted from those due to the co-existing functional groups. (Reprinted from *Chem. Mater.* Copyright 2006 American Chemical Society)

Further analysis of the functionalization of silicas was made by ^{29}Si NMR, which provided quantitative measurements of the concentrations of carbon-silicon bonds on the silica surface. The ^{29}Si DPMAS spectra of samples BPY-as-100 and BPY-as-350 are shown in Figure 4. The functionalities of our interest, T^2 [$(\equiv\text{SiO})_2\text{Si}(\text{OH})\text{R}$] and T^3 [$(\equiv\text{SiO})_3\text{SiR}$], are well known to resonate at around -56 and -67 ppm, respectively. Their presence in both spectra explicitly confirms the existence of covalent linkages between silica surface and the organic groups in the entire T_c range. The resonance lines at around -92, -99 and -110 ppm represent silicon sites Q^2 [$(\equiv\text{SiO})_2\text{Si}(\text{OH})_2$], geminal silanol], Q^3 [$(\equiv\text{SiO})_3\text{SiOH}$], single silanol] and Q^4 [$(\equiv\text{SiO})_4\text{Si}$], siloxane], respectively.³⁶ The overall concentration ratio $T/Q = [(T^2+T^3)/(Q^2+Q^3+Q^4)]$, along with the average molecular formulae and the molecular concentrations of organic functionalities (in mmol/g), which were all calculated using the integrated intensities of the ^{29}Si NMR spectra, are listed in **Table 2**. The fact the T/Q ratio has remained essentially unchanged (within $\pm 5\%$) during the heat treatment, confirms that the BPY functional groups remain covalently bound to the silica surface. Remarkably, these functional groups persist on the surface in spite of considerable surface reconstruction due to dehydroxylation, which is evidenced by the decreased Q^3/Q^4 ratio.²⁹ These results were further corroborated by the analyses of chemical accessibility and reactivity of the bipyridine functional groups as described in Section 3.2.

In summary, the spectra of Figure 2 and the corresponding integrated intensities (Figure 3) showed that CTAB was efficiently removed during the heat treatment, whereas the structure and concentration of BPY functionalities remained intact as a function of T_c .

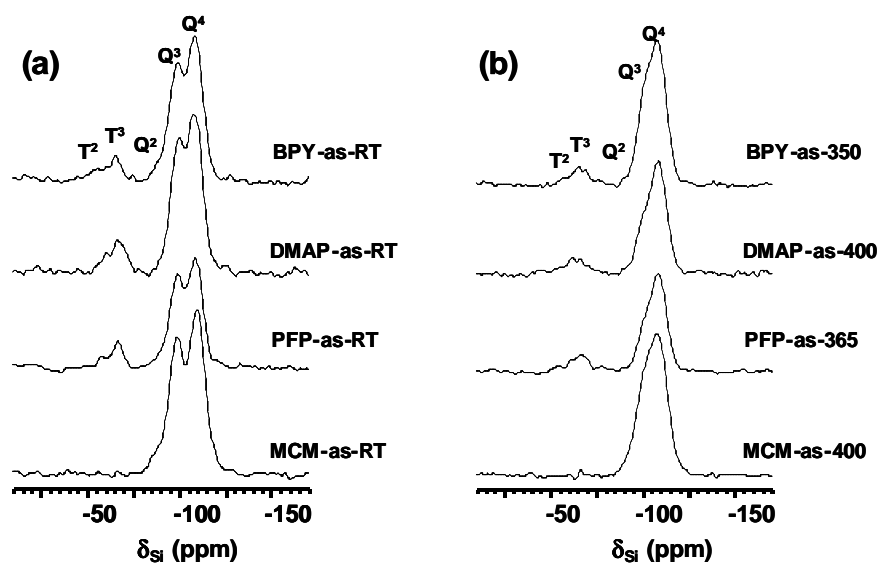


Figure 4. ^{29}Si DPMAS spectra of as-synthesized samples (a) prior and (b) after the heat treatment. Also shown are the corresponding spectra of non-functionalized samples MCM-41-as-RT and MCM-41-as-400. (Reprinted from *Chem. Mater.* Copyright 2006 American Chemical Society)

Table 2. Quantification of the Silicon Based on Deconvolution of ^{29}Si NMR Spectra of Figure 4. (Reprinted from *Chem. Mater.* Copyright 2006 American Chemical Society)

sample	T/Q ratio ^a	molecular formula (SiO_2) ₁₀₀ (H_2O) _m (R) _n	concentration of organic groups [mmol/g]
BPY-as-RT	0.12 (0.11)	(SiO_2) ₁₀₀ (H_2O) ₁₇ ($\text{C}_{18}\text{H}_{21}\text{N}_2\text{O}_2$) ₁₁	1.15
DMAP-as-RT	0.14 (0.14)	(SiO_2) ₁₀₀ (H_2O) _{16.5} ($\text{C}_9\text{H}_{14}\text{N}_2$) ₁₂	1.48
PFP-as-RT	0.13 (0.13)	(SiO_2) ₁₀₀ (H_2O) ₂₂ ($\text{C}_9\text{H}_7\text{F}_5$) ₁₂	1.54

^a Numbers in parenthesis correspond to samples calcined at highest temperatures, BP-as-350, DMAP-as-400 and PFP-as-365, respectively.

DMAP-MSN. The ^{13}C CPMAS NMR spectra of the DMAP-as series of samples are shown in Figure 5a and the observed carbon chemical shifts are assigned in Table 1 based on our recent report.¹⁸ At $T_c = 200$ °C we observed weak peaks at around 64, 44 and 50 ppm, which were earlier ascribed to $[\text{CH}_3(\text{CH}_2)_{15}\text{N}(\text{CH}_3)_2]$ and $\equiv\text{Si}-\text{OCH}_3$ species resulting from reactions (1) and (2). However, the removal of CTAB and $\text{CH}_3(\text{CH}_2)_{15}\text{N}(\text{CH}_3)_2$ from samples

functionalized with DMAP proceeded more rapidly than in the BPY-as series. The spectra of Figure 5a demonstrate that more than 90% of CTAB that was initially found in DMAP-as-100 was eliminated at $T_c = 225$ °C. At $T_c = 400$ °C, no detectable amount of the surfactant species was present, as further illustrated in Figure 3a. Again, our results show that DMAP functionalities appeared structurally intact during the heat treatment and maintained their initial concentration.

As in the case of BPY-MSNs, the spectra of DMAP-ex series of samples show that CTAB was completely removed by acid extraction (Figure 5b). However, two additional resonances were observed at around 58 and 16 ppm representing the ethoxy groups ($\equiv\text{Si-OCH}_2\text{CH}_3$), which were produced from DMAP precursor during DMAP-MSN preparation. The concentration of DMAP as a function of T_c is shown in Figure 3b. The T/Q ratios

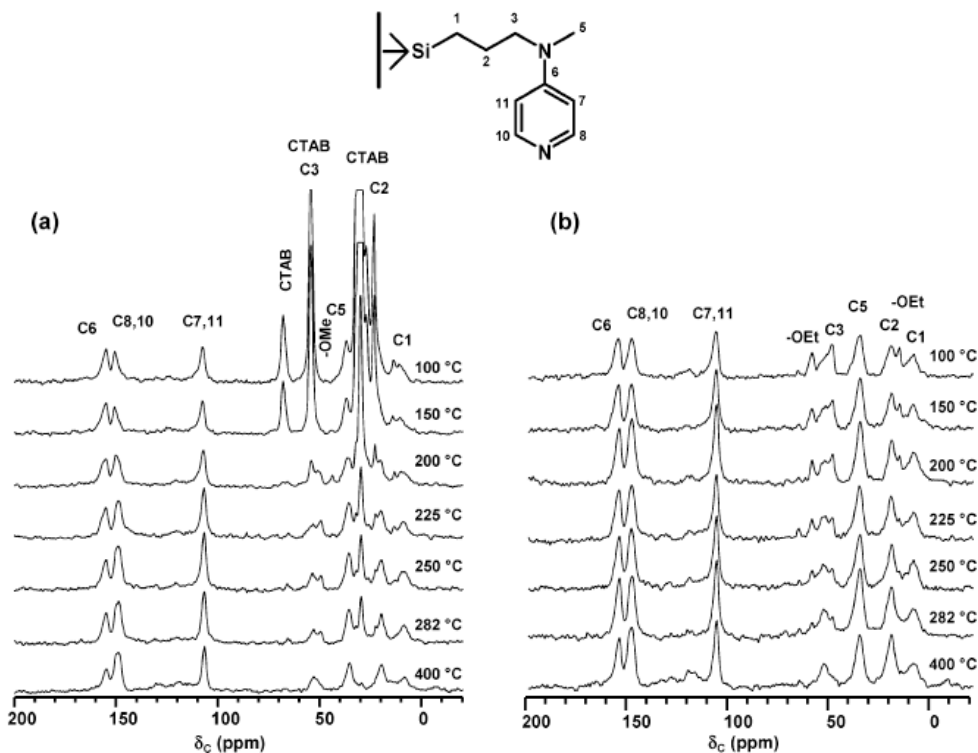
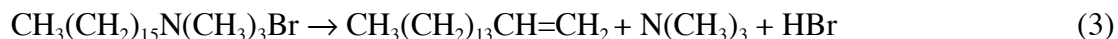


Figure 5. ^1H - ^{13}C CPMAS NMR spectra of (a) DMAP-as and (b) DMAP-ex series of samples following the thermal treatment at 100 °C $\leq T_c \leq 400$ °C. (Reprinted from *Chem. Mater.* Copyright 2006 American Chemical Society)

obtained from the ^{29}Si DPMAS spectra of samples DMAP-as-RT and DMAP-as-400 (Figure 4 and Table 2) are in good agreement, thereby conclusively confirming the thermal stability of the functional groups.

PFP-MSN. The ^{13}C CPMAS NMR spectra of the PFP-as samples are shown in Figure 6a. Again, the observed carbon chemical shifts (see Table 1) confirm the presence of PFP functional groups inside the pores. The thermal extraction of CTAB and the products of its decomposition proceeds similarly as in BPY-MSN and DMAP-MSN (see Figure 3a). The decomposition itself, however, follows two different routes. Here also at $T_c = 200\text{ }^\circ\text{C}$ we discerned peaks at around 64, 44 and 50 ppm, assigned to tertiary amine $[\text{CH}_3(\text{CH}_2)_{15}\text{N}(\text{CH}_3)_2]$ and $\equiv\text{Si}-\text{OCH}_3$ groups (see Eqs (1) and (2)). But the NMR analysis of liquid residue condensed during the evacuation at $T_c = 200\text{ }^\circ\text{C}$, showed that, in addition to the tertiary amine, resonances assigned to 1-hexadecene, $\text{CH}_3(\text{CH}_2)_{13}\text{CH}=\text{CH}_2$, were present (see spectrum S1(b) in appendix). This implies that some of the CTAB molecules followed another route,³⁵



In PFP-ex series, CTAB was completely removed by acid extraction, as well. The spectra of Figure 6b show only the resonances representing PFP and a peak around 50 ppm, assigned to the methoxy groups from PFP-TMS. The concentration of PFP in the extracted sample as a function of T_c is shown in Figure 3b. Here also the T/Q ratios obtained from the ^{29}Si DPMAS spectra of samples PFP-as-RT and PFP-as-365 remain in a very good agreement (see Figure 4 and Table 2). (This may not be immediately obvious in Figure 4;

note however that the intensity corresponding to Q^4 silicon sites increased considerably in sample PFP-as-365 at the expense of Q^3 .)

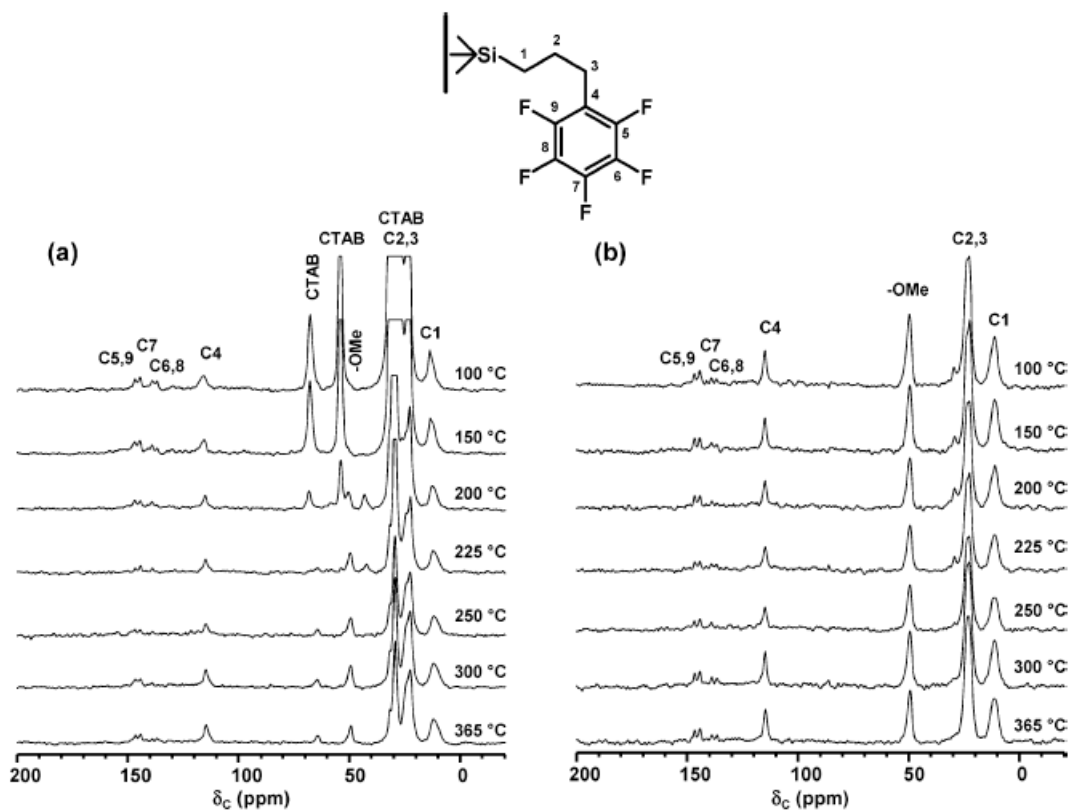
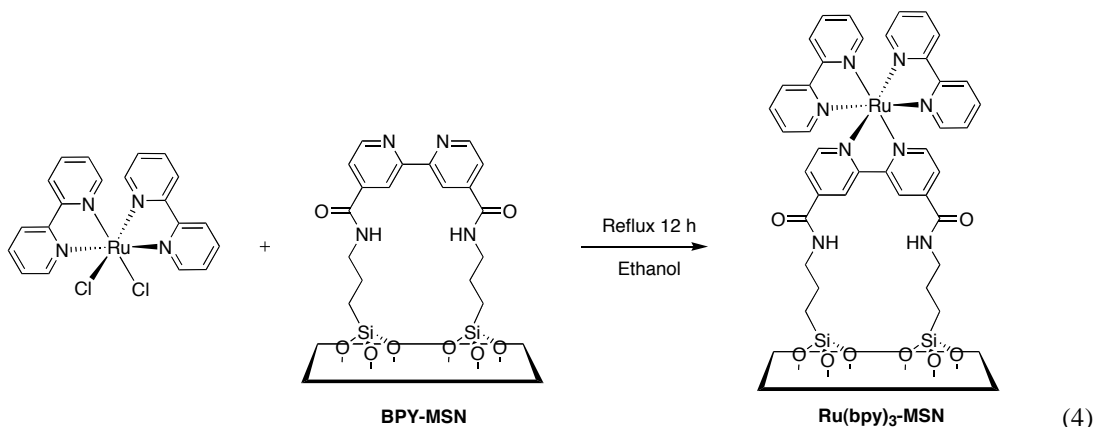


Figure 6. ^1H - ^{13}C CPMAS NMR spectra of (a) PFP-as and (b) PFP-ex series of samples following the thermal treatment at $100\text{ °C} \leq T_c \leq 365\text{ °C}$. (Reprinted from *Chem. Mater.* Copyright 2006 American Chemical Society)

Chemical Accessibility and Catalytic Reactivity of Functional Groups in the Calcined and Extracted MSNs. Based on the NMR results, it is plausible that some additional condensation of silica occurred in these MSNs during the heating process. The resulting structural changes could lead to the undesired entrapment of organic functional groups inside the silica matrices, which would lower the chemical accessibility of the thermally treated MSNs with respect to the MSNs prepared by the conventional acid extraction method.

We first compared the chemical accessibility of 2,2'-bipyridine moieties in the calcined sample BPY-as-350 and acid-extracted sample BPY-ex-RT, by treating both materials with excess $\text{Ru}(\text{bpy})_2\text{Cl}_2 \cdot x\text{H}_2\text{O}$ ethanol solution as shown in Eq. (4):

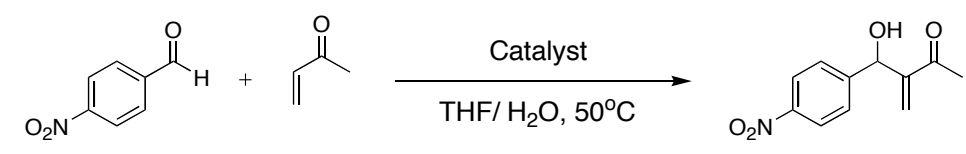


The quantity of chemically accessible bipyridine functional groups in the BPY-MSN was determined by analyzing the decrease of $\text{Ru}(\text{bpy})_2\text{Cl}_2 \cdot x\text{H}_2\text{O}$ in solution, as described in the experimental section. The obtained concentrations, 34.8 and 35.9 $\mu\text{mol/g}$ of 2,2'-bipyridine in the BPY-as-350 and BPY-ex-RT, respectively, were significantly higher than the amount of physisorbed complexes measured on pure inorganic MCM-41 (20.9 $\mu\text{mol/g}$). The fluorescence spectra of treated BPY-as-350 and BPY-ex-RT showed a broad emission band, centered at 630 nm, representing the $\text{Ru}(\text{bpy})_3$ complexes. As expected, no fluorescent emission was detected in the physisorbed sample of pure MCM-41 (see appendix). It is noted, however, that the concentrations of functional groups obtained by this method were about forty times lower than those measured by solid-state NMR (Table 2). A plausible explanation of this discrepancy is that $\text{Ru}(\text{bpy})_2\text{Cl}_2$ complexes are too large (1.15 nm) and too reactive to be used as a reliable probe of accessibility inside the pores with a diameter of about 2.5 nm (Table 4). Most likely, the complexation reaction which initiated near the pore

entrances produced sufficient local concentrations of $\text{Ru}(\text{bpy})_3$ complexes to inhibit further diffusion of $\text{Ru}(\text{bpy})_2\text{Cl}_2$ molecules into the channels. Therefore, we performed additional tests using a smaller molecule, $\text{Cu}(\text{NO}_3)_2$,^{11,12,39} which yielded the concentration of chemically accessible bpy groups of 0.28 mmol/g. This value, while still low, was exactly the same in BPY-as-350 and BPY-ex-RT samples. This strongly suggests that chemical properties of the organically functionalized MSNs obtained by our heating method remained unchanged.

To examine the catalytic reactivity after the heat treatment, a Baylis-Hillman reaction of 4-nitrobenzaldehyde and methyl vinyl ketone was conducted by using DMAP-MSNs as catalysts. As shown in the Table 3, the reaction catalyzed by DMAP-as-400 gave rise to 90 % yield, which was very similar with the yield obtained by the acid-extracted DMAP-ex-RT. This result confirmed that the chemical fidelity of the catalytic groups was indeed preserved in the calcined DMAP-MSN.

Table 3. Catalytic Reactivity of DMAP-MSNs.^a (Reprinted from *Chem. Mater.* Copyright 2006 American Chemical Society)



sample	yield (%) ^b
DMAP-as-400	90
DMAP-ex-RT	99 ^c

^a Reaction condition: 4-nitrobenzaldehyde (0.25 mmol), methyl vinyl ketone (0.5 mmol), and DMAP-MSN catalyst (50 mg, 30 mol%) in $\text{H}_2\text{O}/\text{THF}$ (2 mL, v/v = 1/3) at 50°C for 24 h; ^b isolated yield; ^c reference 18.

Textural Properties of the Calcined and Acid-Extracted MSNs. In addition to NMR, several structural characterization methods, including powder X-ray diffraction (PXRD), nitrogen adsorption/desorption experiment, and scanning electron microscopy

(SEM), were used to further examine the physical properties of the calcined and acid-extracted MSNs. The results were summarized in Table 4. As depicted in Figure 7, DMAP-MSN materials showed a disordered mesoporous structure as reported in our previous paper,¹⁸ whereas BPY-as-350 and PFP-as-365 materials exhibited the MCM-41 type, hexagonally packed mesopores, as indicated by (100), (110), and (200) peaks. The diffraction peaks of the calcined BPY-as-350 and PFP-as-365 were slightly shifted to a higher angle than those of the acid-extracted samples indicating the formation of a smaller unit cell (a_0). The measured BET surface areas of the calcined MSNs were lower than those of the acid-extracted samples. As shown in appendix, type IV isotherms of N₂ sorption were observed in the calcined MSN materials further confirming the cylindrical pore structures. The mean pore width of the calcined and acid-extracted MSNs, measured by BJH pore distribution, showed no significant difference. These results indicated that the calcined samples possess a thinner pore wall in comparison with those of the acid-extracted ones, which could be attributed to further condensation of silica framework during the heating process. It is finally noted that both the calcined and acid-extracted MSNs showed similar particle morphologies as depicted in the SEM micrographs (see appendix).

Table 4. Structural Properties of Mesoporous Silica Nanoparticles. (Reprinted from *Chem. Mater.* Copyright 2006 American Chemical Society)

samples	S_{BET} (m^2/g) ^a	V_{p} (cm^3/g) ^a	W_{BJH} (\AA) ^a	d_{100} (\AA) ^b	a_0 (\AA) ^b	$d_{\text{pore wall}}$ (\AA) ^b
BPY-as-350	734.8	0.54	2.5	37.1	42.9	17.9
BPY-ex-RT	861.1	0.80	2.4	40.5	46.8	22.8
DMAP-as-400	686.3	0.33	2.0	32.7	-	-
DMAP-ex-RT	834.5	0.39	2.0	32.2	-	-
PFP-as-365	854.0	0.59	2.6	37.8	43.6	17.6
PFP-ex-RT	993.1	0.75	2.7	40.5	46.8	19.8

^a The BET surface area (S_{BET}), the mesopore volume (V_{p}), and the mean mesopore width (W_{BJH}) were obtained from the nitrogen adsorption/desorption data. ^b The d_{100} numbers represent the d -spacing corresponding to the main (100) XRD peak. The unit cell size (a_0) is calculated from the d_{100} data using $a_0 = 2d_{100}/3^{1/2}$. The pore wall thickness ($d_{\text{pore wall}} = a_0 - W_{\text{BJH}}$).

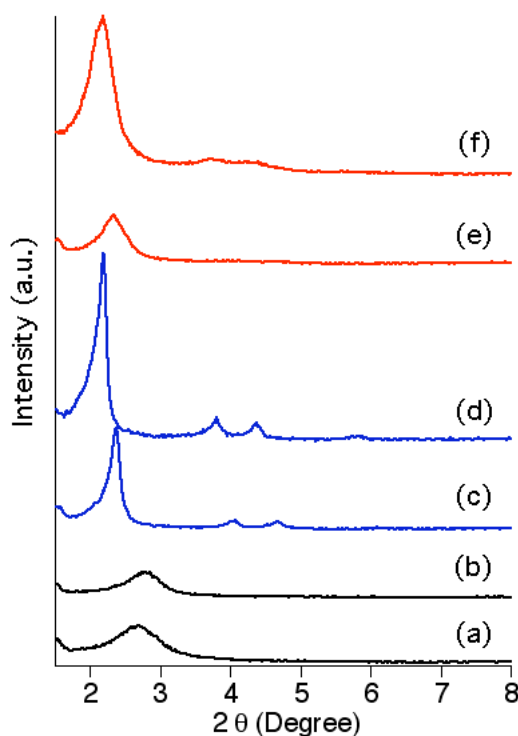


Figure 7. XRD spectra of (a) DMAP-as-400, (b) DMAP-ex-RT, (c) BPY-as-350, (d) BPY-ex-RT, (e) PFP-as-365, and (f) PFP-ex-RT. (Reprinted from *Chem. Mater.* Copyright 2006 American Chemical Society)

Conclusion

In summary, we have investigated the thermal stability of three types of organically functionalized mesoporous silica nanoparticles synthesized via the co-condensation method. The as-synthesized, surfactant-containing samples were thermally treated between 100 and 400 °C under vacuum and the resulting materials were analyzed by solid-state NMR spectroscopy. We have demonstrated that the CTAB template molecules could be effectively removed from the mesopores while fully preserving the chemical fidelity of the organic functional groups by controlling the temperature. The chemical accessibility and reactivity of the organic functionalities were also conserved after the heat treatments. We envision that this temperature-controlled heating process could be further developed into an economical and environmentally friendly method for surfactant-removal of various organically functionalized mesoporous silica materials.

Acknowledgments

The support for this research work at Ames Laboratory through the U.S. DOE, office of Basic Energy Sciences, through the Catalysis Science Grant No. AL-03-380-011 and under Contract W-7405-Eng-82 is gratefully acknowledged. The authors express appreciation to Dr. J. W. Wiench for his assistance with the experiments and helpful comments.

References

- (1) Kresge, C. T.; Leonowicz, M. E.; Roth, W. J.; Vartuli, J. C.; Beck, J. S. *Nature* **1992**, *359*, 710-12.
- (2) Beck, J. S.; Vartuli, J. C.; Roth, W. J.; Leonowicz, M. E.; Kresge, C. T.; Schmitt, K. D.; Chu, C. T. W.; Olson, D. H.; Sheppard, E. W.; et al. *J. Mater. Chem.* **1992**, *114*, 10834-43.
- (3) Corma, A. *Chem. Rev.* **1997**, *97*, 2373-2419.
- (4) Stein, A. *Adv. Mater.* **2003**, *15*, 763-775.
- (5) Lin, V. S. Y.; Lai, C.-Y.; Huang, J.; Song, S.-A.; Xu, S. *J. Am. Chem. Soc.* **2001**, *123*, 11510-11511.
- (6) Lai, C.-Y.; Trewyn, B. G.; Jeftinija, D. M.; Jeftinija, K.; Xu, S.; Jeftinija, S.; Lin, V. S. Y. *J. Am. Chem. Soc.* **2003**, *125*, 4451-4459.
- (7) Trewyn, B. G.; Whitman, C. M.; Lin, V. S. Y. *Nano Lett.* **2004**, *4*, 2139-2143.
- (8) Giri, S.; Trewyn, B. G.; Stellmaker, M. P.; Lin, V. S. Y. *Angew. Chem., Int. Ed. Engl.* **2005**, *44*, 5038-5044.
- (9) Stein, A.; Melde, B. J.; Schroden, R. C. *Adv. Mater.* **2000**, *12*, 1403-1419.
- (10) Clark James, H. *Acc. Chem. Res.* **2002**, *35*, 791-7.
- (11) Huh, S.; Wiench, J. W.; Yoo, J.-C.; Pruski, M.; Lin, V. S. Y. *Chem. Mater.* **2003**, *15*, 4247-4256.
- (12) Huh, S.; Wiench, J. W.; Trewyn, B. G.; Song, S.; Pruski, M.; Lin, V. S. Y. *Chem. Commun.* **2003**, 2364-2365.

- (13) Melero, J. A.; Stucky, G. D.; van Grieken, R.; Morales, G. *J. Mater. Chem.* **2002**, *12*, 1664-1670.
- (14) Hiyoshi, N.; Yogo, K.; Yashima, T. *Microporous Mesoporous Mater.* **2005**, *84*, 357-365.
- (15) Ford, D. M.; Simanek, E. E.; Shantz, D. F. *Nanotechnology* **2005**, *16*, 458-475.
- (16) Huh, S.; Chen, H.-T.; Wiench, J. W.; Pruski, M.; Lin, V. S. Y. *J. Am. Chem. Soc.* **2004**, *126*, 1010-1011.
- (17) Huh, S.; Chen, H.-T.; Wiench, J. W.; Pruski, M.; Lin, V. S. Y. *Angew. Chem., Int. Ed. Engl.* **2005**, *44*, 1826-1830.
- (18) Chen, H.-T.; Huh, S.; Wiench, J. W.; Pruski, M.; Lin, V. S. Y. *J. Am. Chem. Soc.* **2005**, *127*, 13305-13311.
- (19) Tanev, P. T.; Pinnavaia, T. J. *Chem. Mater.* **1996**, *8*, 2068-2079.
- (20) Zhao, X. S.; Lu, G. Q.; Whittaker, A. K.; Millar, G. J.; Zhu, H. Y. *J. Phys. Chem. B* **1997**, *101*, 6525-6531.
- (21) Igarashi, N.; Hashimoto, K.; Tatsumi, T. *J. Mater. Chem.* **2002**, *12*, 3631-3636.
- (22) Cassiers, K.; Linssen, T.; Mathieu, M.; Benjelloun, M.; Schrijnemakers, K.; Van Der Voort, P.; Cool, P.; Vansant, E. F. *Chem. Mater.* **2002**, *14*, 2317-2324.
- (23) Zhang, F.; Yan, Y.; Yang, H.; Meng, Y.; Yu, C.; Tu, B.; Zhao, D. *J. Phys. Chem. B* **2005**, *109*, 8723-8732.
- (24) Kim, J. M.; Jun, S.; Ryoo, R. *J. Phys. Chem. B* **1999**, *103*, 6200-6205.
- (25) Ryoo, R.; Jun, S. *J. Phys. Chem. B* **1997**, *101*, 317-320.
- (26) Kruk, M.; Jaroniec, M.; Sayari, A. *Microporous Mesoporous Mater.* **1999**, *27*, 217-229.

- (27) Igarashi, N.; Koyano, K. A.; Tanaka, Y.; Nakata, S.; Hashimoto, K.; Tatsumi, T. *Microporous Mesoporous Mater.* **2003**, *59*, 43-52.
- (28) Pauly, T. R.; Petkov, V.; Liu, Y.; Billinge, S. J. L.; Pinnavaia, T. J. *J. Am. Chem. Soc.* **2002**, *124*, 97-103.
- (29) Trebosc, J.; Wiench, J. W.; Huh, S.; Lin, V. S. Y.; Pruski, M. *J. Am. Chem. Soc.* **2005**, *127*, 3057-3068.
- (30) Trebosc, J.; Wiench, J. W.; Huh, S.; Lin, V. S. Y.; Pruski, M. *J. Am. Chem. Soc.* **2005**, *127*, 7587-7593.
- (31) Camus, L.; Goletto, V.; Maquet, J.; Gervais, C.; Bonhomme, C.; Babonneau, F.; Massiot, D. *J. Sol-Gel Sci. Technol.* **2003**, *26*, 311-314.
- (32) Shenderovich, I. G.; Buntkowsky, G.; Schreiber, A.; Gedat, E.; Sharif, S.; Albrecht, J.; Golubev, N. S.; Findenegg, G. H.; Limbach, H.-H. *J. Phys. Chem. B* **2003**, *107*, 11924-11939.
- (33) Christiansen, S. C.; Zhao, D.; Janicke, M. T.; Landry, C. C.; Stucky, G. D.; Chmelka, B. F. *J. Am. Chem. Soc.* **2001**, *123*, 4519-29.
- (34) Alam, T. M.; Fan, H. *Macromol. Chem. Phys.* **2003**, *204*, 2023-2030.
- (35) Hagaman, E. W.; Zhu, H.; Overbury, S. H.; Dai, S. *Langmuir* **2004**, *20*, 9577-9584.
- (36) Maciel, G. E. In *Encyclopedia of Nuclear Magnetic Resonance*; Grant, M. D., Harris, R. K., Eds.; John Wiley & Sons Ltd: Chichester, 1996; Vol. 7, p 4370.
- (37) Garelli, N.; Vierling, P. *J. Org. Chem.* **1992**, *57*, 3046-51.
- (38) Bennett, A. E.; Rienstra, C. M.; Auger, M.; Lakshmi, K. V.; Griffin, R. G. *J. Chem. Phys.* **1995**, *103*, 6951-58.

- (39) Burleigh, M. C.; Markowitz, M. A.; Spector, M. S.; Gaber, B. P. *Chem. Mater.* **2001**, *13*, 4760-4766.
- (40) Ganguly, S.; Roundhill, D. M. *Polyhedron* **1990**, *9*, 2517-26.
- (41) Ganguly, S.; Joslin, F. L.; Roundhill, D. M. *Inorg. Chem.* **1989**, *28*, 4562-4.

Appendix

Figure S1. (a) $^{13}\text{C}\{^1\text{H}\}$ NMR spectrum of the liquid residue (in CDCl_3) collected during thermal treatment of BPY-as and DMAP-as samples at 225 °C. The corresponding spectrum for PFP-as series is shown in figure (b).

Figure S2. BET isotherms of (a) DMAP-MSN, (b) BPY-MSN, and (c) PFP-MSN and BJH pore size distributions of (d) DMAP-MSN, (e) BPY-MSN, and (f) PFP-MSN.

Figure S3. SEM micrographs of SEM micrographs of (a) DMAP-as-400, (b) DMAP-ex-RT, (c) BPY-as-350, (d) BPY-ex-RT, (e) PFP-as-365, and (f) PFP-ex-RT, all the scalar bar = 2 mm.

Figure S4. Fluorescence spectra of BPY-MSNs, after treated with $\text{Ru}(\text{bpy})_2\text{Cl}_2$ solution, obtained by excited at 450 nm.

Figure S1.

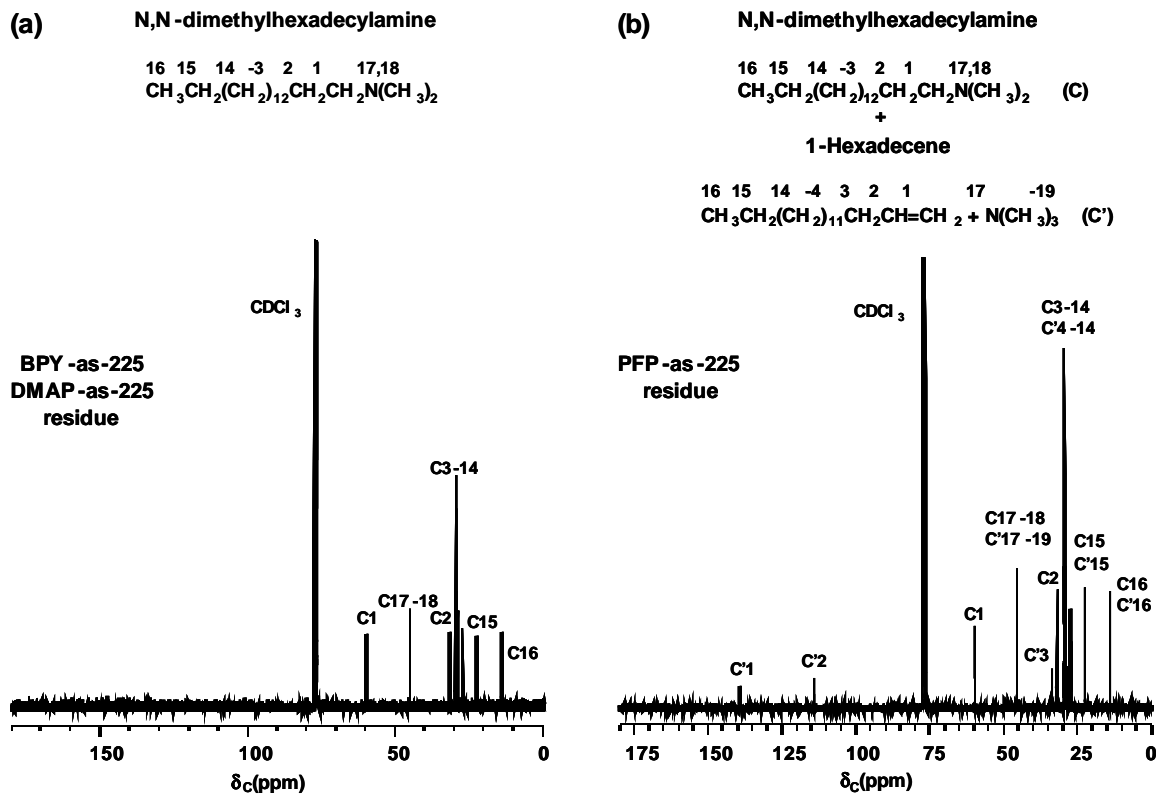


Figure S2.

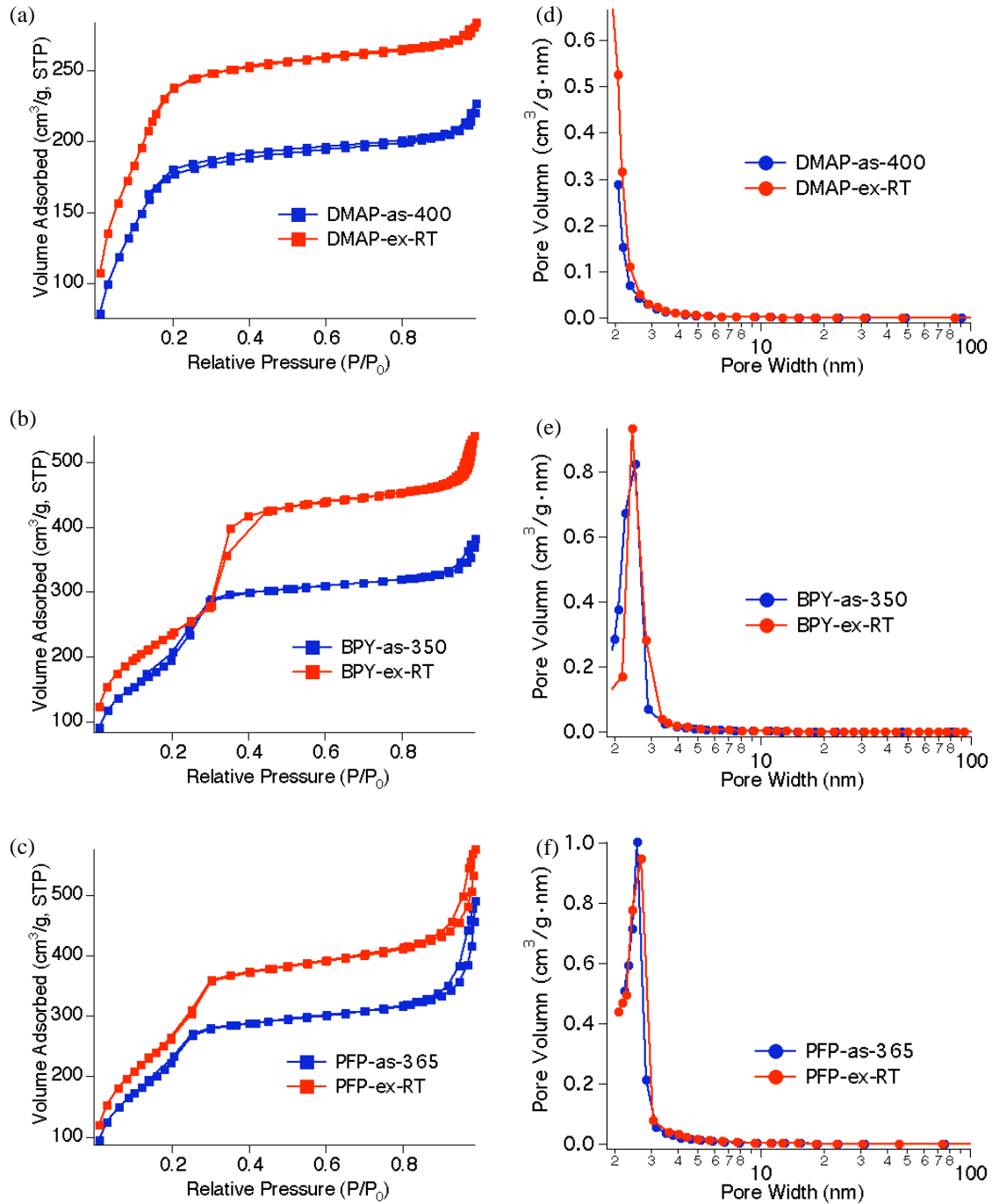


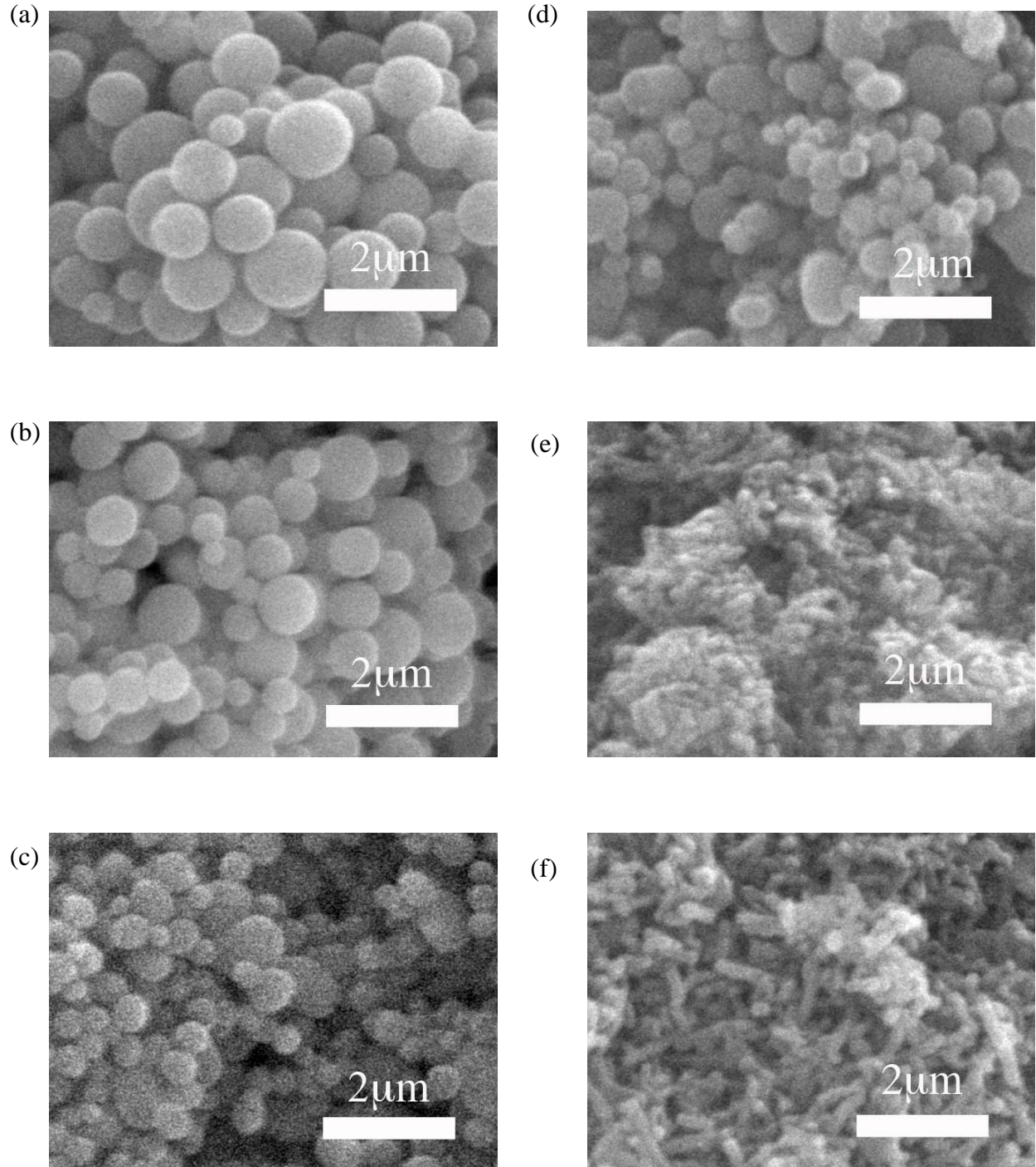
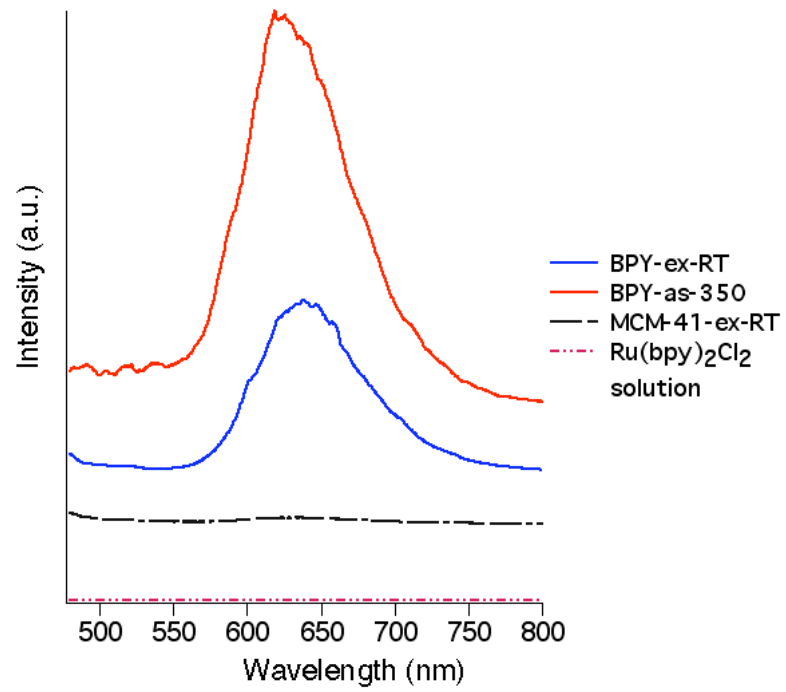
Figure S3.

Figure S4.



CHAPTER 7. GENERAL CONCLUSION

The field of functionalized mesoporous silica nanoparticles in the heterogeneous catalysis field grows vast and fast due to suitable developed functionalization methods and mature characterization techniques. High surface area, tunable particle morphology and pore diameter, and the robust inorganic silica framework of mesoporous silica provide many advantages for heterogeneous catalysis. In this dissertation, I utilized and expanded a co-condensation method developed in the Lin group to synthesize a series of mono- and bi-functionalized mesoporous silica nanoparticles and investigate their catalytic performance as well as recyclability.

First, I prepared a 4-dimethylaminopyridine functionalized mesoporous silica nanoparticle (DMAP-MSN) catalyst and successfully applied for several nucleophilic reactions, such as the Baylis-Hillman reaction, acylation, and silylation reactions. This heterogeneous MSN catalyst has been fully characterized by several techniques, including powder X-ray diffraction measurement, nitrogen adsorption/desorption analysis, scanning electron microscopy, transmission electron microscopy, and solid state NMR analysis. By taking advantage of the regular mesoporous structure and three-dimensional confined space, the inorganic mesoporous silica matrix was able to regulate the diffusion of substrates to reach the catalytic sites, giving rise to a superior selectivity compared to other heterogeneous catalyst systems as well as the homogeneous analog. DMAP-MSN also proved to be recyclable by simple filtration, at least up to ten times, without losing any reactivity. The DMAP-MSN is also proved for its stability by performing an acylation reaction for one

month. The resulting material maintained its reactivity after prolonged stirring. The turnover number obtained by this experiment was as high as 3341.

Utilizing a double hydrogen bonding ability of urea or thiourea organocatalysts, several urea or thiourea functionalized MSN catalysts, composed of 3-(3-phenyl ureido) propyl (PUP), 3-[3-(3,5-ditrifluoromethyl phenyl)-ureido)]-propyl (FPUP), and 3-(3-phenyl thioureido)]-propyl (TUP), and 3-[3-(3,5-ditrifluoromethyl phenyl)-thioureido)]-propyl (FTUP) functional groups, respectively, have been synthesized and fully characterized. These Lewis acid heterogeneous materials functioned as catalysts of Diels-Alder reaction for carbonyl activation. The Lewis acidity of the immobilized organic functional groups dominated the reactivity of those heterogeneous catalysts. Also, the reactivity of those MSN catalysts is even higher than the homogeneous analogs, by a six fold enhancement. This unique catalytic activity could be attributed to two reasons. First, anchoring the homogenous catalyst on the mesoporous silica support insulated each functional group, which avoids the formation of the self-assembled urea or thiourea network present in homogenous systems; second, a surface hydrogen bonding interaction between the surface silanols of the MSN framework and the tethered urea or thiourea functional groups are observed based on FT-IR studies. This interaction indeed enhanced Lewis acidity of the reaction center, resulting in a improvement in reactivity.

In addition, I also synthesized a series of bifunctional mesoporous silica nanoparticles with one common Lewis base, 4-dimethylaminopyridine (DMAP) and three different Lewis acid functionalities, 3-(3-phenyl ureido) propyl (PUP), 3-[3-(3,5-ditrifluoromethyl phenyl)-ureido)]-propyl (FPUP), and 3-ureido propyl (UP), respectively. All three DMAP/Urea-MSN exhibited a catalytic activity toward a Michael addition reaction of β -nitro styrene and

ethyl malonate. By incorporation of urea functional group, which enable to activate nitro group of electrophile through double hydrogen bonding, and DMAP functional group, which activated nucleophile through deprotonation, three bifunctionalized MSNs showed a cooperative effect in terms of reactivity due to the proximity of both acid and base sites immobilized inside the mesoporous channels. I also demonstrated that we could fine-tune the reactivity of the resulting bifunctional MSNs catalysts by simply manipulating the combination of immobilized acid or base sites.

Furthermore, utilizing radical addition reaction, I successfully coupled Pd(II) complex precursor and pre-synthesized thiol functionalized mesoporous silica nanoparticle material to yield Pd(II) functionalized mesoporous silica nanoparticle catalysts (Pd-MSN). This further chemical modification of functionalized mesoporous silica provided an efficient way to prepare a transition metal complex functionalized MSN with homogeneously distributed catalytic sites inside the pores, which is unable to be achieved by simple co-condensation methods due to the severe acidic or basic synthetic conditions involved in material preparation. The Pd-MSN material catalyzed a Sonogashira cross-coupling-based polymerization of various alkoxy-substituted 1,4-diethynylbenzene with 1,4-diiodobenzene. The resulting poly(*p*-phenylene ethynylene) (PPE) conjugated polymer was encapsulated inside the hexagonal mesoporous channel and grew in a well-aligned one-dimensional direction. In contrast to the same PPE polymers synthesized in homogeneous solutions, the PPE-MSN nanocomposite material exhibited interesting photophysical and electronic properties, which could lead to further developments of new optical and electronic nanodevices.

At last, I demonstrated that we could selectively remove the organic template, CTAB, from functionalized MSN materials without destroying immobilized functional groups by carefully controlling the calcinations temperature. This method not only provided an alternative approach, but also an economical and environmentally benign method to remove the organic surfactant from silica framework in the industrial scale, avoiding the use of huge amounts of alcohol.